Simulation and Mathematical Tools for Performance Analysis of Low-Complexity Receivers

by

Gautam Krishnakumar Deora

Thesis submitted to the Faculty of the
Virginia Polytechnic Institute and State University
in partial fulfillment of the requirements for the degree of
MASTER OF SCIENCE
in
Electrical Engineering

Approved:_____

_____
Dr. Annamalai Annamalai

_____
Dr. Jeffery H. Reed

_____
Dr. Luiz A. DaSilva

Keywords: Generalized Selection Combining, Satellite Digital Radio, GSC, SDARS, CDMA, Ultra-WideBand, UWB, Threshold GSC

January 2003
Blacksburg, Va

Simulation and Mathematical Tools for Performance Analysis of Low-Complexity Receivers

by

Gautam Krishnakumar Deora

Commitee Chairman: Dr. A. Annamalai

Bradley Department of Electrical Engineering

ABSTRACT

In recent years, research on the design and performance evaluation of suboptimal receiver implementations has received considerable attention owing to complexity in the realization of the optimal receiver algorithms over wireless channels. This thesis addresses the effects of using reduced complexity receivers for the Satellite Digital Audio Radio (SDAR), Code Division Multiple Access (CDMA) and UltraWideband (UWB) communications technologies.

A graphical-user-interface simulation tool has been developed to predict the link reliability performance of the SDAR services in the continental United States. Feasibility study of receiving both satellite and terrestrial repeater signals using a selection diversity (single antenna) receiver has also been performed.

The thesis also develops a general mathematical framework for studying the efficacy of a sub-optimal generalized selection combining (GSC) diversity receiver over generalized fading channel models. The GSC receiver adaptively combines a subset of M diversity paths with the highest instantaneous signal-to-noise ratios (SNR) out of the total L available diversity paths. The analytical framework is applicable for rake receiver designs in CDMA and UWB communications.

Acknowledgments

First and foremost, I would like to express my gratitude to my advisor, Dr. A. Annamalai for his infinite patience, guidance and constant encouragement. I have learned many things from Dr. Annamalai beyond what is reflected in this thesis, and I have enjoyed having him as a mentor and friend. I am thankful to Dr. J. Reed and Dr. L. DaSilva for their invaluable suggestions and discussions. I thank General Motors for sponsoring my research project at M.P.R.G. I am thankful to Mr. R. Riley, C. Dietrich and J. Loncoski for being ever-willing to offer their constructive suggestions (and criticisms).

I also wish to thank my fellow MPRGers Ramesh, Shakheela, Max, Vikash, Patrick, Raqib, Venkat and the MPRG staff for all their help and for making my stay at MPRG so wonderful - the memories of which shall remain with me forever. Thanks to Satya, Ajit, Vivek and Gaurav for being there whenever I needed them. They have been everything I could have ever hoped for from my friends.

Last, but the most of all, I would like to thank my parents and my uncle for teaching me the values of hardwork, sacrifices and perseverance.

Dedicated to

My uncle and parents.

List of Acronyms

ABER	Average Bit Error Rate
ASER	Average Symbol Error Rate
ASEP	Average Symbol Error Probability
AWGN	Additive White Gaussian Noise
BER	Bit Error Rate
BFSK	Binary Frequency Shift Keying
BPSK	Binary Phase Shift Keying
CDF	Cumulative Distribution Function
CDMA	Code Division Multiple Access
CEP	Conditional Error Probability
ConUS	Continental United States
DPSK	Differential Phase Shift Keying
DQPSK	Differential Quadrature Phase Shift Keying
EIRP	Effective Isotropic Radiated Power
EGC	Equal Gain Combining
FCC	Federal Communications Commission
FDMA	Frequency Division Multiple Access
FSK	Frequency Shift Keying
GIS	Geographic Information Systems
GSC	Generalized Selection Combining
IID	Independent and Identically Distributed
IND	Independent and Non-identically Distributed

MGF	Moment Generating Function
MRC	Maximal Ratio Combining
M-DPSK	*M*-ary Differential Phase Shift Keying
M-PSK	*M*-ary Coherent Phase Shift Keying
MRC	Maximum Ratio Combining
OFDM	Orthogonal Frequency Division Multiplexing
PDF	Probability Density Function
PSK	Phase Shift Keying
QPSK	Quadrature Phase Shift Keying
SC	Selection Combining
SDARS	Satellite Digital Audio Radio Service
SNR	Signal to Noise Ratio
TDMA	Time Division Multiplexing Access
T-GSC	Threshold Generalized Selection Combining
UMTS	Universal Mobile Telephone Service
UWB	Ultra-WideBand
WCDMA	Wideband CDMA

TABLE OF CONTENTS

LIST OF FIGURES

LIST OF TABLES

Chapter 1

Introduction

It would be an understatement to say that the wireless industry has grown at a phenomenal pace since the past decade. The thirst for entertainment and higher bandwidth has led to the evolution of the next generation wireless systems, and newer technologies are being deployed to provide the user with information and entertainment anywhere and anytime he desires. While the next generation systems based on the W-CDMA, OFDM and UWB concepts are projected to provide high data rates for both indoor and outdoor systems, new technologies like Satellite Digital Audio Radio Service (SDARS), already in service, are providing users with entertainment options like they have never experienced previously.

The fundamental constraints forseeable in all these technologies are high power requirements (leading to reduced battery life) and/or higher receiver costs due to large implementation complexities. This thesis demonstrates the effectiveness of simulation and mathematical tools in predicting system performance with low complexity, low cost receivers. It also emphasizes the utility of simulation tools to a system designer in making critical implementation decisions. The first part of the thesis investigates the effect of low complexity, low cost antenna configurations at the receiver on the SDAR system performance. The later part of the thesis deals with developing the mathematical framework for combating multipath fading and investigating the performance trade-off issues in the implementation of reduced complexity receivers in millimeter and UWB communications.

A brief review of SDARS and wideband systems such as CDMA/UWB is presented in Section 1.1. Section 1.2 discusses the motivation behind the thesis, with the contributions of the work listed in Section 1.3. An outline of the thesis is provided in Section 1.4.

1.1 Technology Review

1.1.1 Satellite Digital Radio

The gates for implementation of satellite digital audio services were opened by the FCC in 1992 by the allocation of 25 MHz in the 2.3 GHz band (S-Band). The 25 MHz bandwidth is split between the two service providers - Sirius Radio and XM radio, each of which provide around 100 digital radio channels all over the continental US (ConUS). The systems are also projected to provide future text-oriented services such as live stock quotes and weather information. Though the service providers are expecting to break even with an individual base of 4 million subscribers, the prospects of having around 20 million subscribers tuned in to satellite radio by 2005 estimated by some analysts provides an idea of the potential growth rates for satellite radio services.

The network of satellites and terrestrial repeaters enables satellite radio to provide the same radio channels all over the United States, yet at better sound quality compared to FM. The terrestrial repeaters capture the signals from the satellites and re-transmit them to provide the receiver with sufficiently high SNRs particularly in urban areas where the satellite signals may not be clear because of highrise buildings. Though Sirius Radio depends more on the network of 3 elliptically-oriented satellites in addition to the 100 repeaters for reliable service, XM relies on 2 geosynchronous satellites and a network of over 1500 terrestrial repeaters all over the country.

The in-built spatial, time and frequency diversities further ensure reliable performance of the system. The spatial and frequency diversity is obtained because of transmission from multiple satellites, each operating at different frequencies. The time diversity is obtained by transmitting the same content from the satellites, with a small time offset between the two signals. Since satellite radio is targeted primarily at highly mobile vehicle users, the receiver design is required to have high performance yet with significant cost constraints. The antenna design for the system is particularly challenging because of the need to have low-cost omni-directional antennas; the need for omni-directional antennas arises because of the difficulty in tracking the satellites with a directional antenna was used. The radio receiver currently employs dual antenna elements, one for the satellite

system and another for the terrestrial network.

1.1.2 Wideband Systems - CDMA/W-CDMA/UWB

Code Division Multiple Access (CDMA) or Wideband CDMA (W-CDMA) are considered to be wideband technologies based on the spread spectrum transmission scheme, where the each carrier in a W-CDMA system is spread over a wideband of 5 MHz. The relatively high bandwidths occupied by CDMA systems are responsible for the significant advantages of CDMA over traditional narrowband systems.

1. The spread of information over a very high bandwidth causes the CDMA signal to have power levels comparable to those of the noise floor. This guarantees high resistance to jamming and lower intercept probability.

2. The high bandwidth also ensures inherent resistance to multipath which causes significant signal attenuation in narrowband systems.

3. The soft handoff ensures that there are fewer "dropped" calls as the mobile moves from one cell to another.

4. The interference added by each user in the system can be considered as AWGN by the others. The whole system can therefore be designed using the average interference conditions. The ability to use the same set of frequencies within each cell results in an increase in the capacity of CDMA systems as compared to TDMA/FDMA systems.

One of the practical disadvantages of CDMA is its inability to provide good performance in indoor wireless communciation where the multipath delay spread is much smaller than the outdoor environment. This disadvantage can be overcome with the FCC ruling in February 2002 allowing the commercialization of the Ultra-WideBand (UWB) technology. UWB systems, like CDMA, are low-power systems resistant to jamming and interception. The main advantage of UWB lies in the fact that it has much higher bandwidths compared to the CDMA and is therefore able to resolve very small multipaths delays like those available in indoor environments.

The definition of UWB from the FCC ruling [1] can be stated as: "Any device where the fractional bandwidth is greater than 0.2 or occupies 500 MHz or more of spectrum. The formula proposed by the Commission for calculating fractional bandwidth is $2(f_H-f_L)/(f_H+f_L)$ where f_H is the upper frequency of the –10 dB emission point and f_L is the lower frequency of the –10 dB emission point. The center frequency of the transmission was defined as the average of the upper and lower –10 dB points, i.e., $(f_H+f_L)/2$."

Assuming a bandwidth of 1GHz for a UWB system, the minimum possible channel

resultion is 1 nsec. For an indoor channel with an average rms delay spread of 75 nsec, the number of resolvable multipaths are therefore as high as 75. The high bandwidths and the option of elimination of a carrier frequency are the two important characteristics which justify the use of UWB in various fields like imaging, surveillance and indoor communications. More details regarding the application of UWB to various applications and the frequency restrictions for those applications can be found in [1].

1.2 Motivation

The motivation for this thesis lies in designing simulation and mathematical tools that enable the system designer to make informed decisions on implementing low complexity, low cost receivers without a significant compromise in system performance.

One of the major factors that could determine the success of SDARS in the coming years is the measure of system reliability at different locations within the U.S. In the absence of any visual tool, identifying and taking measurements in regions suspected to experience poor performance can be a daunting task. Having a simulation tool that predicts the system performance in the form of contours on the US map and identifies the regions where performance measurements might need to be made could result in significant cost savings for the service providers.

One of the problems faced in the deployment of the SDARS system might be the non-uniformity of the antenna patterns at the radio receiver. The values for the receiver antenna gain may fall well below the minimum specified threshold gain values (resulting in nulls). This mismatch becomes particularly pronounced at lower elevation angles. In the absence of a tool that can accurately pinpoint the locations that are affected by these nulls, it is very difficult for the service provider to make decisions as to where to place the terrestrial repeaters so that the system performance improves. Given an antenna pattern, it would also be instructive to know the regions which are affected the most by the nulls with that antenna and also the reliability for these regions.

The radio receiver currently uses dual antenna elements, one for the satellite system and another for the terrestrial network. It might be possible to use a single antenna element for both terrestrial and satellite systems such that the single satellite antenna takes maximum advantage of the built-in satellite diversity. It would result in tremendous cost savings for the service providers if a single antenna element receiver could be used without significant degradation in system performance. The development of the General Motors (GM) simulation tool for SDAR has been greatly motivated by all of the above

reasons.

It is well-known that by using a rake receiver, the resolved multipaths in wideband systems such as CDMA can be exploited to reduce the fading effects on a signal. Thus, if a rake receiver has 5 fingers, we can combine the five multipaths using Maximum Ratio Combining (MRC) to give the best performance. However, it would be interesting to investigate the receiver performance if we implemented sub-optimal schemes and combined only the strongest 2, 3 or 4 fingers of the rake receiver out of the five available fingers (such receiver structures are termed as Generalized Selection Combining (GSC) receivers). The approach is significant since it encompasses the results for both Selection Combining (SC) and Maximum Ratio Combining (MRC), as elaborated in further chapters.

Though the above example depicts a CDMA system, the importance of developing the GSC framework can be particularly appreciated for UWB systems. As explained in Section 1.1.2, UWB systems are capable of resolving as many as 75-100 multipaths. Though it would be impratical to implement rake receivers with 75 fingers, it might be possible to capture significant percentage of energy using just 10-15 fingers (instead of 75) with the GSC receivers. Thus, the implementation complexity would be significantly reduced without much degradation in performance. The reduced number of fingers also ensures reduced power consumption at the receiver.

Unlike the wideband channels that result in frequency-selective channels, the GSC receiver structure can also be extended to analyze the performance of sub-optimal antenna arrays for narrowband, millimeter wave communication systems that are experience non-frequency selective (or flat) fading. Using spatial diversity helps in combating the performance degradation due to the flat fading channels. With frequencies as high as 60 GHz, the antenna elements can be placed at 2.5 mm ($\lambda/2$) without being correlated. Again, even though we have around 16 antenna elements in a space of 4 cm, we might be able to get performance comparable to MRC by combining much fewer antenna elements than the maximum available number of 16 elements.

The receiver performance is contingent to the fading conditions and also the type of modulation used. The motivation towards developing a unified framework that predicts the performance of GSC receivers in a myriad of fading conditions and for both coherent and noncoherent modulation schemes is central to the evolution of this thesis. Once the problem of performance of GSC receivers in independent and identically distributed (i.i.d) fading channels is tackled, the next level of motivation lies in evaluating the performance analysis of GSC receivers in independent and non-identical (i.n.d) fading chan-

nels. Though there has been an enormous amount of research in this area for the past 5-7 years, one of the motivations behind pursing this topic is to develop a framework that is comprehensive, yet simple and computationally efficient compared to all the ad-hoc approaches followed to date.

1.3 Contribution

The simulation tool developed for SDAR is probably among the first to provide a system-level performance analysis of the satellite radio systems. Though a lot of research dealing specifically with the antenna design for SDAR has been done previously, the effect of a particular antenna on the overall system performance and over areas as expansive as the North American subcontinent is presented for the first time for the SDAR system. The tool effectively demonstrates how the changes in the physical layers affect the higher layers metrics such as link reliability. The utility of the tool lies in the fact that it is able to predict the system performance all over the continental US (ConUS) by taking into account an extremely large number of factors such as the satellite (spatial) diversities, the antenna gain variations with elevation and azimuthal angles and the shadowing due to vegetation at lower elevation angles. With the system performance being a function of so many variables and in the absense of a simulation tool, it is a non-trivial task to identify the regions on ConUS experiencing poor performance from the SDAR system.

Much of the mathematical framework provided in Chapters 4-6 have been presented for the first time. The Moment Generating Function (MGF) expression developed in Chapter 4 to deal with the performance of the Generalized Selection Combining (GSC) receivers in a myriad of i.i.d. fading environments is the most concise result reported to date. Moreover, the results for the GSC receivers in Rician fading environments presented in Section 4.3.3 have never been reported in the literature before. Some of the results presented are extremely useful to the system designer and could not have been presented with the previous approaches used by researchers. The effectiveness and applicability of using the GSC receivers has been emphasized by presenting the performance of the GSC receivers in real world UMTS channels.

It is well known that the disadvantages in GSC(M,L) receiver can be overcome by using the Threshold GSC (T-GSC) framework. New expressions have been derived for performance prediction of T-GSC in Chapter 5. Developing upon the results presented in Chapter 4, some interesting observations can be made particularly with the mean combined SNR performance curves.

The assumption of having i.i.d. channels in the previous framework has been removed by proposing a novel approach to the performance analysis of GSC(M, L) receivers in independent, non-identical (i.n.d) channels in Chapter 6. The result initially obtained for Rayleigh fading i.n.d. channels have been extended to all of the commonly occurring fading environments.

Finally, the mathematical developments made in Chapters 4-6 have been integrated in a single GUI. The resultant software can be used either as a teaching aid or by system engineers to better understand the trade-off issues between performance and lower implementation complexity in GSC receivers.

1.4 Thesis Outline

This thesis consists of seven chapters. In Chapter 2, the large scale and small scale wireless channel models are described. While the link budget forms the backbone of satellite link design, the marginal moment generating function and the probability density function are the main statistics of interest for the small scale fading.

Chapter 3 is dedicated to the development of the simulation tool that predicts the performance of SDAR systems for the particular case of XM satellite radio. The system performance is evaluated using the link reliability metric which is dependent on the type of antenna used at the receiver.

Chapters 4-6 are devoted to the development of the mathematical framework; expressions have been derived for bit or symbol error probabilities, outage probabilities and mean output SNRs for coherent and noncoherent GSC receivers in a myriad of independent, identically distributed (i.i.d.) fading channels. Chapter 4 lays the fundamental framework for developing the simplified moment generating function for GSC receivers. The bit and symbol error performances for many modulation schemes in a Rician fading environment have been presented for the first time.

The expressions derived in Chapter 5 are used to obtain the error probabilities, outage probability and mean SNR performance curves for threshold GSC by expanding on the results obtained in chapter 4.

In Chapter 6, the performance curves of various modulation schemes in a variety of independent, non-identically distributed (i.n.d.) fading environments are presented by using a new approach from order statistics.

Finally, Chapter 7 presents the conclusions and suggestions for future work.

Chapter 2

Channel Models

2.1 Introduction

The performance of any wireless communication system is dictated to a large extent by the wireless channel. Depending on the receiver location and the environment in which it works, the wireless channel is subject to constant variations. This makes it impossible to select a single channel that would model all environmental conditions. It is because of the randomness in the radio channels that it is best to incorporate statistical tools to model the channel conditions. Another significant advantage that the statistical models have is flexibility, whereby by changing the statistical parameters, the same model can be used to mimic the channels under different conditions. The parameters for the statistical models at any location can be obtained from the measured data collected by others in areas similar to the location under consideration.

The instantaneous signal strength at a receiver can be predicted using the traditional large-scale and small-scale models, wherein the large-scale models predict the average received signal strength depending on the transmitter-receiver distance and the small-scale channel models represent the local variations and estimate the signal variations about the average signal strengths. The Rayleigh, Rician and Nakagami are some of the most common statistical models used to represent the small-scale fading phenomenon. The mean signal strengths (representing the large-scale fading effects) are predicted either by estimating the path-loss exponent through available measurements, or using empirical models

like the Hata, Okumora model for outdoor propagation modeling in cellular enviroments [2].

The lognormal model, in which the measured signal levels have a normal distribution about the mean received signal, are more applicable for emulating the large scale fading effects for satellite-mobile channels models. The normal deviation about the mean captures the random shadowing effects that occur because of the variation in the clutter surrounding a moving vehicle, though the mean signal strength at the vehicular receiver remains the same. Frameworks for modeling and simulating the satellite channel along with the time variations have been extensively reported in the literature. It is widely accepted that, while the lognormal-Rayleigh model accurately depicts the shadowed channel, a Rician channel model is more appropriate for the unshadowed channel.

Much of this chapter concentrates on presenting the fading statistics and simulated results for some of the channel models. Section 2.2 briefly discusses the different fading conditions while Section 2.3 presents the statistical parameters for the common small-scale fading channels. The simulation results and the satellite-mobile channel model are presented in Section 2.4.

2.2 Flat and Frequency Selective Fading

The comparison of the signal bandwidth with the channel bandwidth decides whether a channel is flat or frequency selective. For a signal that has bandwidth greater than the channel bandwidth, the channel is said to be frequency selective. For a frequency selective channel, the symbol duration is less than the multipath duration and hence the multipaths can be resolved in time. Rake receivers make it possible to take advantage of this resolution and thus obtain better performance for frequency selective channels.

A flat fading channel occurs for narrowband signals when the symbol duration is so large that there happens to be a lot of multipaths arriving at the receiver within the same symbol period thereby resulting in fading of the signal. Without the resolution in time, it is not possible to improve performance with the help of rake receivers. It is possible however to improve receiver performance in flat fading channels by including spatial diversity as will be shown in Chapter 4.

The fading conditions that the signal encounters with time or space diversities may not be same. The multipath/spatial signals may or may not experience identical channel

fading charateristics and may or may not be correlated. For this thesis, however, it is assumed that for systems deploying spatial diversity, the antenna spacing is greater than wavelength/2 so that the received signals are independent [3][4].

2.3 Statistical Representation of Fading Channels

The Probability Density Function (PDF), Cumulative Density Function (CDF) and Moment Generating Function (MGF) are the three most important statistics that can be used required to represent a channel model. The relation between the three are listed below.

The CDF of random variable $X(k)$ evaluated at any fixed value of x is defined as

$$F(x) = \text{Prob}[X(k) \le x]. \tag{2.1}$$

The PDF of $X(k)$ is obtained by differentiating $F(x)$ with respect to x, and is given as

$$p(x) = \frac{d}{dx}F(x). \tag{2.2}$$

Finally, the MGF is defined as

$$\phi(s) = \text{E}[e^{-sX}] = \int_{-\infty}^{\infty} e^{-sx}p(x)dx \tag{2.3}$$

where $\text{E}[X]$ is the expected value of $X(k)$. By definition, Eq. (2.3) is the Laplace transform of the PDF $p(x)$. Thus, using the Laplace transform of a derivative property, the MGF may alternatively be written in terms of the CDF:

$$\phi(s) = \int_{-\infty}^{\infty} e^{-sx}F'(x)dx = s\int_{-\infty}^{\infty} e^{-sx}F(x)dx - F(0)$$

where $F'(x)$ is the derivative of $F(x)$.

As will be seen in Chapter 4, the marginal MGF $\phi(s,x)$ is needed for simplistic representation of many expressions and is given as

$$\phi(s,x) = \int_{x}^{\infty} e^{-st}p(t)dt$$

It is trivial to note that $\phi(s)$ is a special case of $\phi(s,x)$.

In the following, we will summarize both $p(x)$ and $\phi(s,x)$ needed to represent different multipath fading environments.

A. Rayleigh Fading

Fading signal amplitudes in large cells (macro-cellular environments) in the absence of a direct line of sight component or tropospheric and ionospheric propagation based on reflection and refraction are usually modelled as Rayleigh random variables. The PDF of the instantaneous branch SNR therefore follows an exponential distribution and its marginal MGF is given by (2.5):

$$p(x) = \frac{1}{\Omega}\exp(-x/\Omega), x \geq 0 \tag{2.4}$$

$$\phi(s,x) = \frac{\exp[-x(s+1/\Omega)]}{1+s\Omega} \tag{2.5}$$

where $\Omega = E[X]$ denotes the average SNR/symbol/branch, as explained in chapter 4.

B. Rician Fading

In micro-cellular (e.g., urban and suburban land mobile radio communications) and pico-cellular (local area networks and indoor communications) environments, there usually exists a dominant line of sight path in addition to numerous diffused multipath components between the transmitter and receiver. Fading signal amplitudes in this case follow Rician distribution with the ratio between the specular and diffused components denoted by the Rice factor *K*. Then the PDF of instantaneous branch SNR follows a noncentral chi-square distribution (Eq. (2.6)) and the corresponding marginal MGF is given by (2.7):

$$p(x) = \frac{1+K}{\Omega}\exp\left[-K-\frac{(1+K)x}{\Omega}\right]I_0\left[2\sqrt{\frac{K(K+1)x}{\Omega}}\right], x \geq 0 \tag{2.6}$$

$$\phi(s,x) = \frac{1+K}{s\Omega+K+1}\exp\left[\frac{-sK\Omega}{s\Omega+K+1}\right]Q\left(\sqrt{\frac{2K(K+1)}{s\Omega+K+1}}, \sqrt{\frac{2(s\Omega+K+1)x}{\Omega}}\right) \tag{2.7}$$

where $Q(\sqrt{2a}, \sqrt{2b}) = \int_b^\infty \exp(-t-a)I_0(2\sqrt{at})dt$ is the first order Marcum Q-function, $I_0(.)$ is the modified Bessel function of the first kind and $K \geq 0$ is the Rice factor. For the limiting case of $K = 0$, the Rician distribution reduces to the Rayleigh distribution.

C. Nakagami-m Fading

Nakagami-m distribution with fading severity index $m \geq 1/2$ is a versatile statistical model because it can model fading amplitudes that experience either less or more severe

fading that that of Rayleigh variates. It sometimes fits experimental data (channel measurements in urban and indoor propagation environments) much better than Rayleigh or Rician distributions [5]-[6]. The model also includes the one-sided Gaussian ($m = 1/2$) and Rayleigh ($m = 1$) distributions as special instances, and closely approximates the Rician distribution via relationship $m = (K+1)^2/(2K+1)$ [7]. The instantaneous branch SNR is a Gamma variate (Eq. (2.8)) and its marginal MGF is given by (2.9):

$$p(x) = \frac{1}{\Gamma(m)}\left(\frac{m}{\Omega}\right)^m x^{m-1}\exp\left(\frac{-mx}{\Omega}\right), x \geq 0 \tag{2.8}$$

$$\phi(s,x) = \frac{1}{\Gamma(m)}\left(\frac{m}{m+s\Omega}\right)^m \Gamma[m, x(s+(m/\Omega))] \tag{2.9}$$

where $\Gamma(a,x) = \int_x^\infty \exp(-t)t^{a-1}dt$ denotes the complementary incomplete Gamma function and $m \geq 0.5$ is the fading severity index. If the fading index m assumes a positive integer value, (2.9) may be simplified as

$$\phi(s,x) = \left(\frac{m}{m+s\Omega}\right)^m \exp\left(-sx - \frac{mx}{\Omega}\right)\sum_{k=0}^{m-1}\frac{[x(s+m/\Omega)]^k}{k!} \tag{2.10}$$

D. Nakagami-q Fading

Fading signal amplitudes in satellite links that are subject to strong ionospheric scintillation tend to follow Nakagami-q distribution (also known as Hoyt distribution). In this case, the PDF of instantaneous branch SNR and its marginal MGF are given by (2.11) and (2.12) respectively:

$$p(x) = \frac{1}{\Omega\sqrt{1-b^2}}\exp\left[\frac{-x}{(1-b^2)\Omega}\right]I_0\left[\frac{bx}{(1-b^2)\Omega}\right], x \geq 0 \tag{2.11}$$

$$\phi(s,x) = \frac{1}{\sqrt{[s\Omega+1]^2 - [s\Omega b]^2}} - \frac{1}{s(1-b^2)\Omega+1}I_e\left[\frac{b}{s(1-b^2)\Omega+1}, \frac{x(1-b^2)\Omega}{s(1-b^2)\Omega+1}\right] \tag{2.12}$$

where $-1 \leq b = (1-q^2)/(1+q^2) \leq 1$, $0 \leq q_k \leq \infty$ is the fading parameter and Rice's I_e-function is related to the first-order Marcum Q-function as

$$I_e(V/U, U) = \frac{U}{W}[Q(\sqrt{U+W}, \sqrt{U-W}) - Q(\sqrt{U-W}, \sqrt{U+W})]$$

while $W = \sqrt{U^2 - V^2}$. The above model also includes the one-sided Gaussian ($b = 1$) and Rayleigh ($b = 0$) distributions as special instances.

2.4 Satellite-Mobile Channel Model

Figure 2.1 illustrates the simulation model presented in [8] for a land-mobile satellite channel. A good channel state implies an unshadowed channel in which there is a direct line of sight signal component available to the receiver in addition to the other diffused signals. The channel model for a good channel is therefore modeled based on the Rician distribution. The bad channel state represents the condition where in the land-mobile receiver does not "see" the satellite directly. In such cases, the channel is described by the Rayleigh/lognormal distribution which is often used for the terrestrial land mobile channel. μ represents the mean signal power level, which can be calculated based on the link budget calculation in [9], while σ represents the standard deviation about the mean.

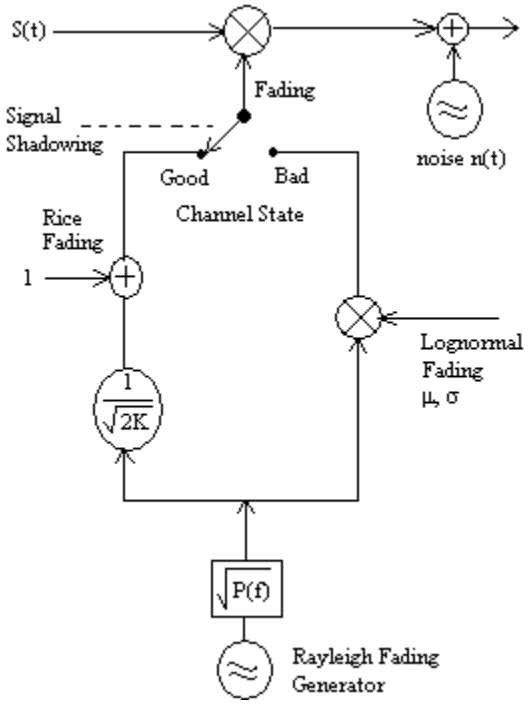

Figure 2.1 Simulation model for a land-mobile satellite channel [8].

The switching between the good and the bad channel states depends on the percentage of shadowing time A. The factors A, μ, σ and K for a particular region can be obtained

from previously recorded measurements in similar regions. The total PDF of the received signal based on the above model is given as

$$p(s) = (1-A)p_{Rice}(s) + A\int_0^{\infty} p_{Rayl}(s/s_0)p_{LN}(s_0)ds_0$$

The Rayleigh/Rician coefficients for the simulator can be generated by using either Jake's model or Clark and Gan's fading model [2]. Figure 2.2 and Figure 2.3 illustrate the channel gains for the Rayleigh and Rician fading channels for various scenarios. The histograms shown in Figure 2.2 closely match the PDF in [2]. The effects of varying the mobile speeds are clearly visible. At 50 m/sec, deep fades occur much more frequently than at 5 m/sec. The severity of fading increases significantly for the Rayleigh channel in comparison to the Rician channel (K = 4) because of the direct line of sight component in Rician channels.

2.5 Chapter Conclusion

In this chapter, we presented the statistical properties for a number of commonly useful channel models. The models and the matehematical relationships shall be extensively used in the development of the GSC receiver performance analysis in the subsequent chapters.

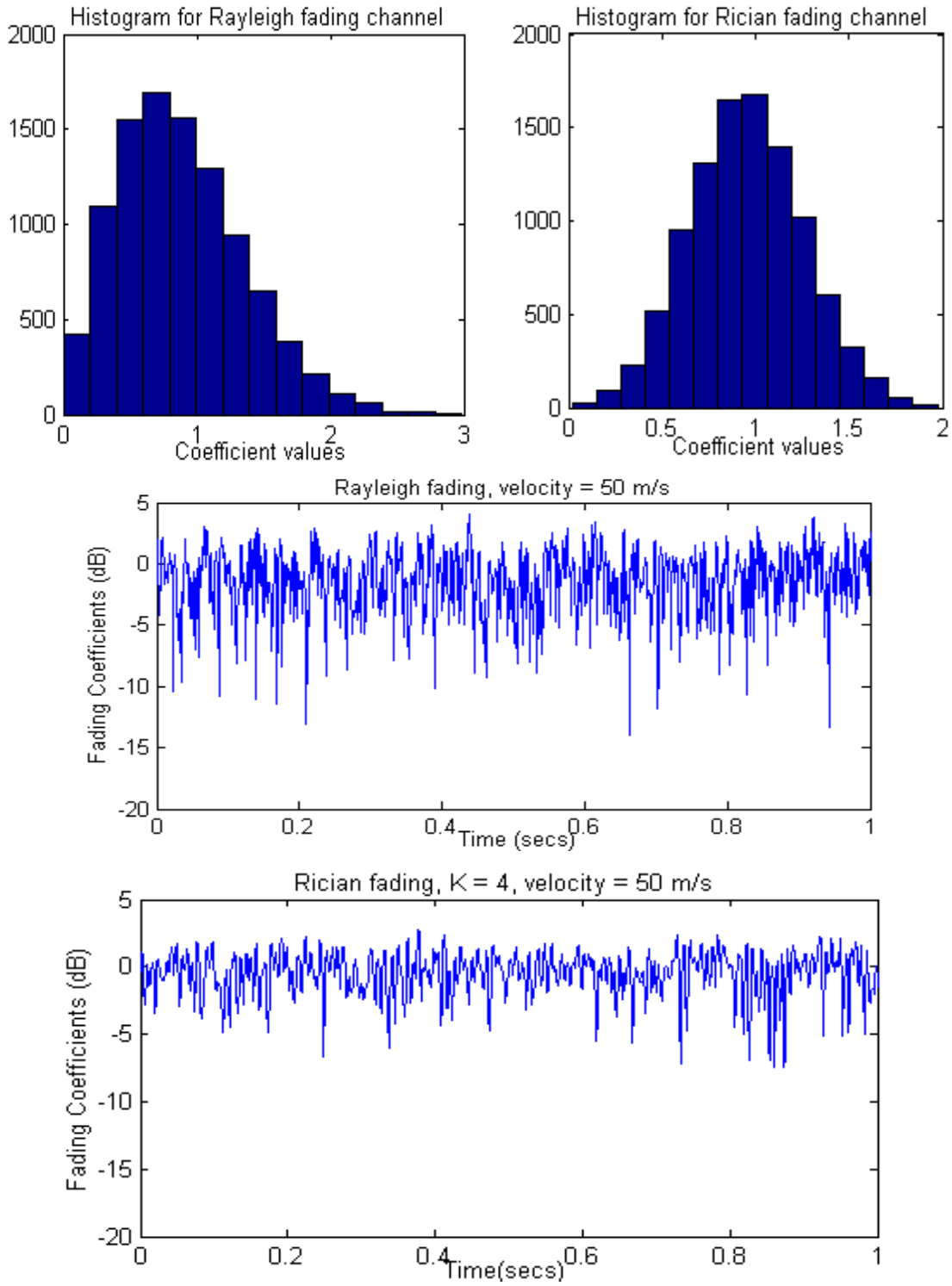

Figure 2.2 Histogram plots and fading coefficient variations for Rayleigh and Rician fading (K = 4) channels at high velocities of 50 m/s.

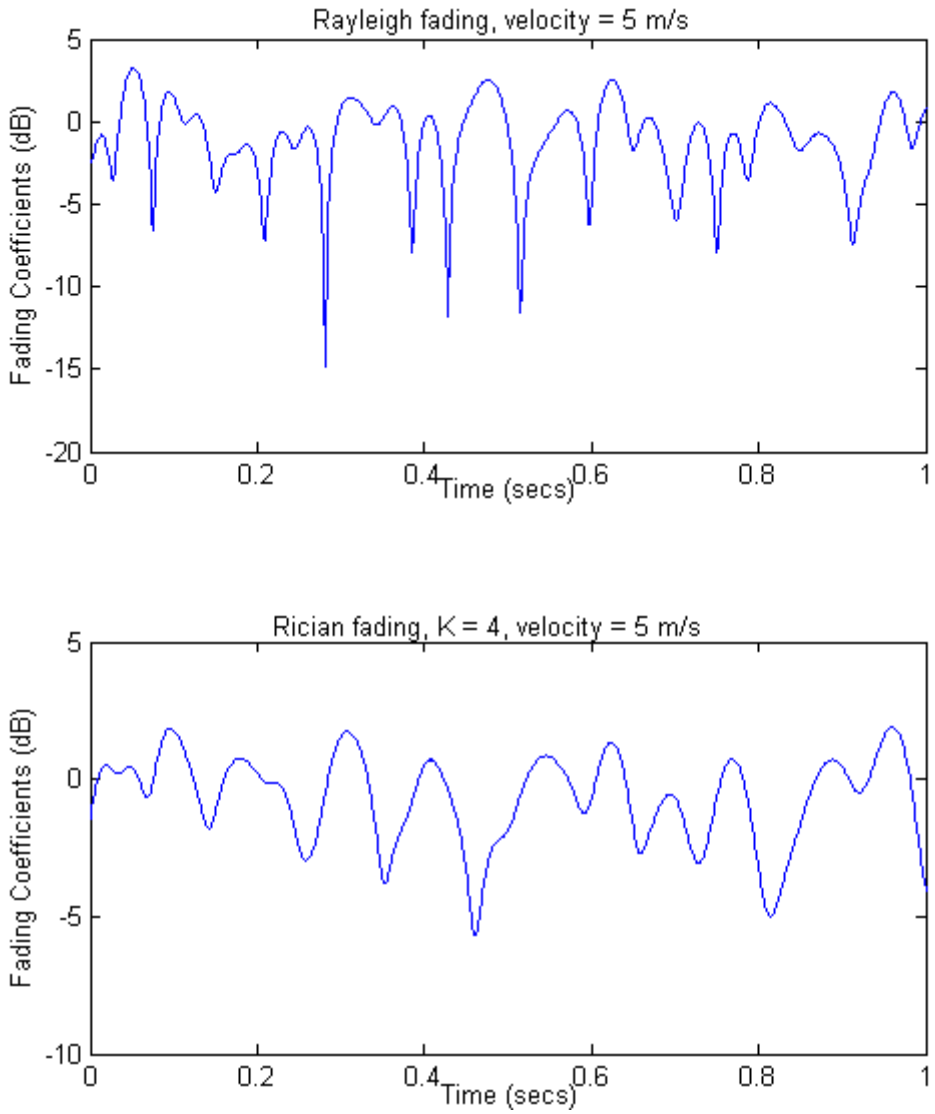

Figure 2.3 Fading coefficient variations for Rayleigh and Rician fading channels at low velocities of 5 m/s.

Chapter 3

SDAR Simulation Tool

3.1 Introduction

Recently there have been a number of publications in the area of Satellite Digital Audio Radio Service [10]-[14] explaining the system fundamentals and the types of antenna that can be used for improved performance of SDARS. In the absence of any simulation tool however, it would be difficult to provide a visual graphic of the system performance and pinpoint the areas on the continental United States (ConUS) that might be susceptible to below-par performance of the service. In addition, though antenna selection for SDARS has been a hot topic of research recently, there has not been much research to show how a particular antenna affects the system performance at the higher layers.

This chapter illustrates the usefulness of simulation tools for performance prediction of the SDARS system. Though the simulation tool can be used with for any of the SDAR systems with some modifications in software, the results presented in this chapter considers the test case of the XM satellite system. Sections 3.2-3.3 discuss the development of the simulation tool. Results predicting the link reliability for the XM satellite receiver (with an average antenna gain) are presented in section 3.4 and the areas where the performance might not meet the specifications are identified. Once the system performance is determined, the logical step of finding ways and means to reduce system cost follows. Section 3.5 discusses the utility of the simulation tool in helping the user (service provider) tp take decisions on the type of antenna to use so that the system cost may be reduced without compromising too much on the link reliability. The chapter ends with section 3.6 where we discuss some of the future possible improvements that can be incorporated in the simulator.

3.2 XM System Overview and Motivation for Tool Development

The XM Satellite system ensures reliable coverage by providing spatial, frequency and time diversities to all the receivers. Figure 3.1 gives a high level overview of the XM system architecture. Spatial (or satellite) diversity is provided by having two geostationary satellites Rock and Roll, located at 115 ^{o} W and 85^{o} W longitudes, respectively. The two satellites provide coverage all over ConUS with the Effective Isotropic Radiated Power (EIRP) for each satellite weighted towards the areas of higher populations. Frequency and time diversity is achieved by having both satellites transfer the same content at different frequencies and with a small time lag of 4-5 seconds.

In addition to the two satellites, the terrestrial network of about 1500 repeaters ensure that adequate coverage is provided in the urban areas where the two satellites may not be visible to the SDAR receivers because of high buildings. To decide the locations where the repeaters are to be placed, the service providers need to know the areas where link reliability is not good for the satellite network. In the absence of any simulation tool, the only way service providers currently use is to evaluate the performance of the system by taking measurement at specific areas which they think (from prior experience) might be susceptible to poor performance. Significant cost reduction can result if a tool is developed to pinpoint the locations on ConUS where link reliability might be low, and thus help the service provider in making important decisions regarding where measurements need to be taken and if and where more repeaters are to be placed.

Unlike many wireless systems in which the antennas are designed more as an afterthought, a lot of attention has been paid to the antenna design for the XM system. These low-cost antennas need to work well in highly mobile environments such as fast moving cars. Though a uniform antenna gain is ideal, for all practical purposes, the gain for a particular antenna is a function of the elevation and the azimuthal angles. As will be shown in section 3.3.2, a variance of even 1-2 dB in the receiver antenna gain can make a significant difference in the link reliability. The XM receiver utilizes two passive elements, one for the satellite and the other for the terrestrial repeaters. One area worth investigating is the possibility of using a single element for both satellite and terrestrial networks. A single antenna element would rely mostly on the signal from the two satellites and would result

in major cost saving for the service providers. A major motivation for creating the simulation tool was to predict the link reliability obtained by using the single element and whether that link reliability is sufficient to do away with the second antenna element (which is used mainly for the terrestrial repeaters).

Though the repeaters are installed to ensure enhanced link reliability, the XM system coverage depends mainly on the two satellites. The simulation tool discussed in the following sections discusses the reliability with only the satellite links and does not consider the performance improvement obtained with the additional repeaters.

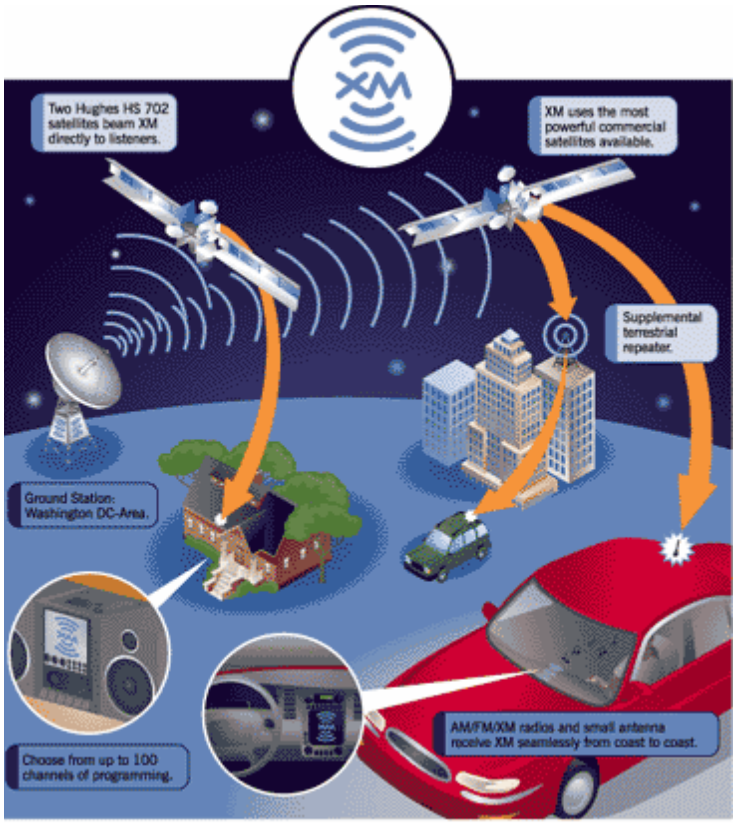

Figure 3.1 XM satellite system overview (courtesy [15]).

3.3 Evolution of Simulator Tool

The link reliability, which is the single major metric used by the simulation tool to measure the satellite link performance for the XM system, is obtained from a dual mapping - first, a mapping from the satellite signal EIRP to link margin and then a mapping from link margin to the reliability.

3.3.1 Mapping of EIRP to Link Margin

The mapping from the EIRP to link margin is obtained from the link budget calculations for the satellite link. In that sense, the mapping can be considered as a large scale propagation effect where the decrease in the satellite signal strength can be attributed to the path loss from the satellite to the mobile ground units. Table 3.1 illustrates the sample calculations for a sample EIRP value. The complete EIRP contours can be developed based on either the measured EIRP values at 55 locations all over the ConUS specified in the XM specifications or from other independent measurements. For our sample calculations, the receiver antenna is assumed to have an average gain of 2 dBi. Once the SNR at the receiver is calculated, the final link margin value is obtained by subtracting a figure of 8.5 dB from the received SNR. A SNR of 8.5 dB is sufficient to achieve Bit Error Rates (BER) of 10^{-2}, which are acceptable for the SDARS system.

Description	Symbol	Value
Receiver North Latitude	Le	25.75 degrees
Receiver West Longitude	le	80.2 degrees
Satellite North Latitude	Ls	0 degrees
Satellite West Longitude	ls	115 degrees
Central angle	γ	42.3 degrees
Elevation angle	El	41.2 degrees
Satellite Orbit Radius	Rs	4.22×10^7 meters
Distance between Satellite and receiver	D	3.78×10^7 meters
Satellite EIRP	EIRP	61 dBW = 1.26×10^6 W
Power Flux density at earth's surface	F[4 KHz]	-128.2 dBW/m2/4KHz
Receiving antenna gain	G(θ)	2 dBi

Table 3.1. SNR and Link Margin calculations for a sample case.

Description	Symbol	Value
System center frequency	Fc	2.333865 GHz
Receiving antenna effective aperture	Ae	-26.8 dBm2
Received power = Ae + F	Pr	-128.3 DBW
System Noise Temperature (faded)	Ts	280 K = 24.5 DBK
System bandwidth	BW	1.84 MHz
Boltzmann's constant	K	-228.6 dBW/K/Hz
System Noise Power (faded)	N	-141.5 dBW
Received SNR	SNR	13.1 dB
Minimum BER for acceptable sound quality	BERmin	0.01
Minimum SNR for acceptable BER	SNRmin	8.5 dB
Link Margin	LM	4.6 dB

Table 3.1. SNR and Link Margin calculations for a sample case.

The expressions used to derive the central angle, elevation angle, flux density, the received power and the elevation angles were obtained from [9].

3.3.2 Mapping of Link Margin to Reliability

The number of parameters that must be considered for the link margin to reliability mapping makes it more complex than the previous mapping. Even though we know the link margin at any given location in ConUS, the mapping of link margin to reliability is a function of the elevation angles and the propagation environment at that location.

1. Elevation angles: The elevation angle is defined as the angle measured upward from the horizon to the direction aimed towards the satellite from that point. For the XM system with two geosynchronous satellites, a region may have a high elevation angle with respect to one satellite and a lower elevation angle with the other. As illustrated in Figure 3.2, the lower elevation angles are subject to higher blockage and therefore a lower link reliability. The elevation angles formed by a location with the two satellites are therefore an important parameter in the prediction of the overall link reliability.

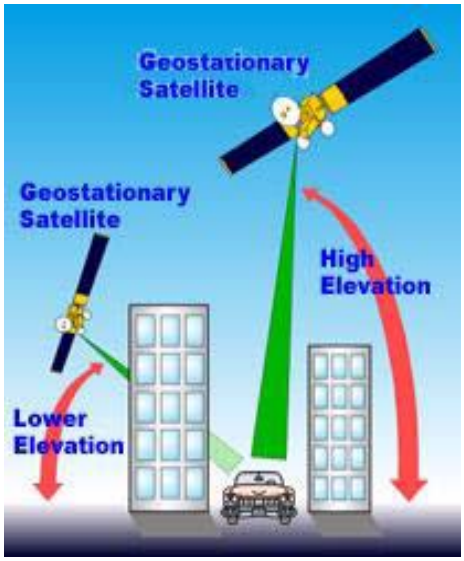

Figure 3.2 Effect of elevation angles (courtesy [16]).

2. Propagation Environment: Natural terrain such as high mountains or dense vegetation adjacent to the roads is another important source of signal blockage. Factors such as the height of the vegetation, the type of vegetation and the frequency of the signal are all important factors in evaluating the reliability of the satellite link. With so many local variations, it is very difficult and impractical to predict the link reliability for each place individually. The best approach, therefore, is to model the propagation environment collectively by using an empirical statistical model obtained from measurements at frequencies as close to the 2.3 GHz frequencies used by XM system as possible. Though the statistical model used does not provide any details regarding the average fade duration and the level crossing rate, it can be used to obtain relatively accurate first–order statistics.

For lack of adequate measurements in the 2.3 GHz region, the statistical model used to map the link margin to the link reliability for our system is based on the CCIR recommendations [17] in which the measurements were obtained at 860 MHz and 1.55 GHz. For urban areas, the statistical model is given by [17]:

$$M = 17.8 + 1.93f - 0.052\delta + K\,(7.6 + 0.053f + 0.04\,\delta)$$

while the statistical model for rural areas is given by [17]

$$M = 12.5 + 0.17f - 0.17\delta + K\,(6.4 - 1.19f - 0.05\,\delta)$$

where M is the link margin in dB, δ is the elevation angle, f is the carrier frequency (in

GHz) and K is the factor used to estimate the percentage of locations for which a specified carrier power will be exceeded. The values of K are:
K (50 %) = 0, K (90 %) = 1.3, K (95 %) = 1.65, K (99 %) = 2.35.

The statistical model presented above can be pictorially represented by Figure 3.3 which illustrates the relation between the link margin in dB and the reliability as a function of the elevation angles.

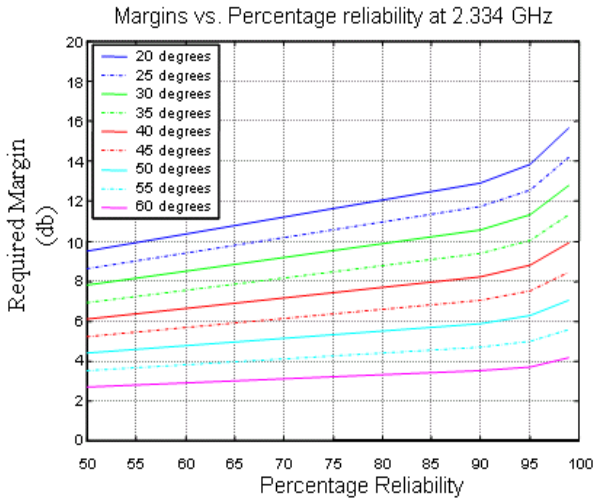

Figure 3.3 Required link margin versus percentage reliability for the statistical model

A prominent observation from Figure 3.3 is that a change in link margin of even 1-2 dB causes a significant change in the link reliability. Remembering that the link margin is a function of the antenna gain, this fact is particularly important while considering the system performance for a practical antenna where the antenna gains may fall well below the average antenna gain of 2 dB as specified by the standards.

3.4 System Performance with Average Antenna Gain

Figure 3.4 and Figure 3.5 show the link reliability contours over ConUS with and without the satellite diversities. The contours were obtained assuming the receivers to have an average antenna gain of 2 dBi. While it may be possible to have link reliability as low as 25-30 % with a single satellite, the dual satellite diversity ensures that reliability does not fall below 55%. The high EIRP values also ensure that the link reliability is as high as 95% over most of the United States and especially in most of the highly populated areas.

In addition to the reliability plots, the tool also provides the capability to display the EIRP contours, the link margin contours and the elevation angles input by the user.

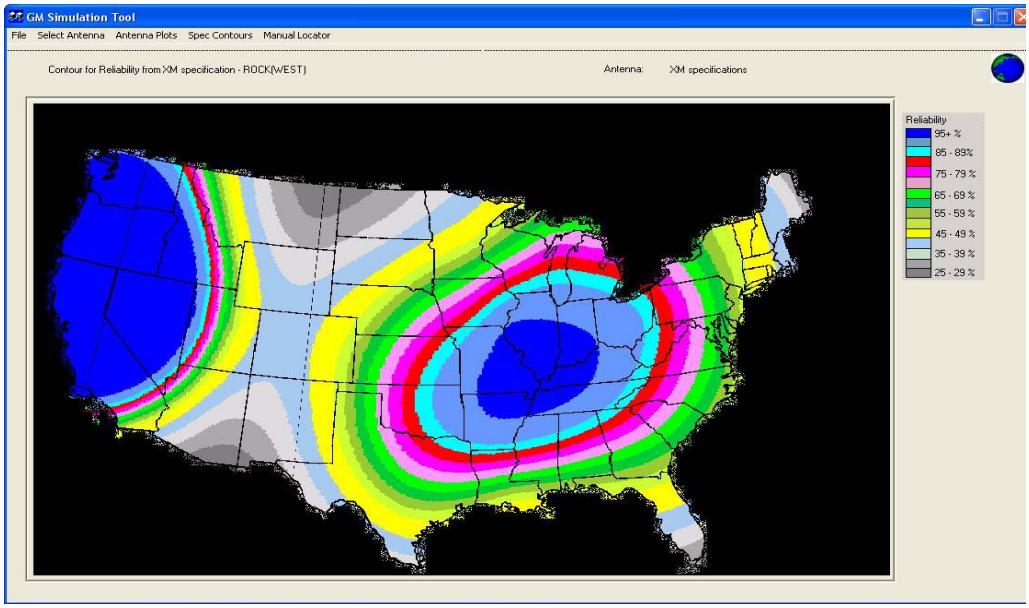

Figure 3.4 Link reliability contour with only Rock satellite (no diveristy).

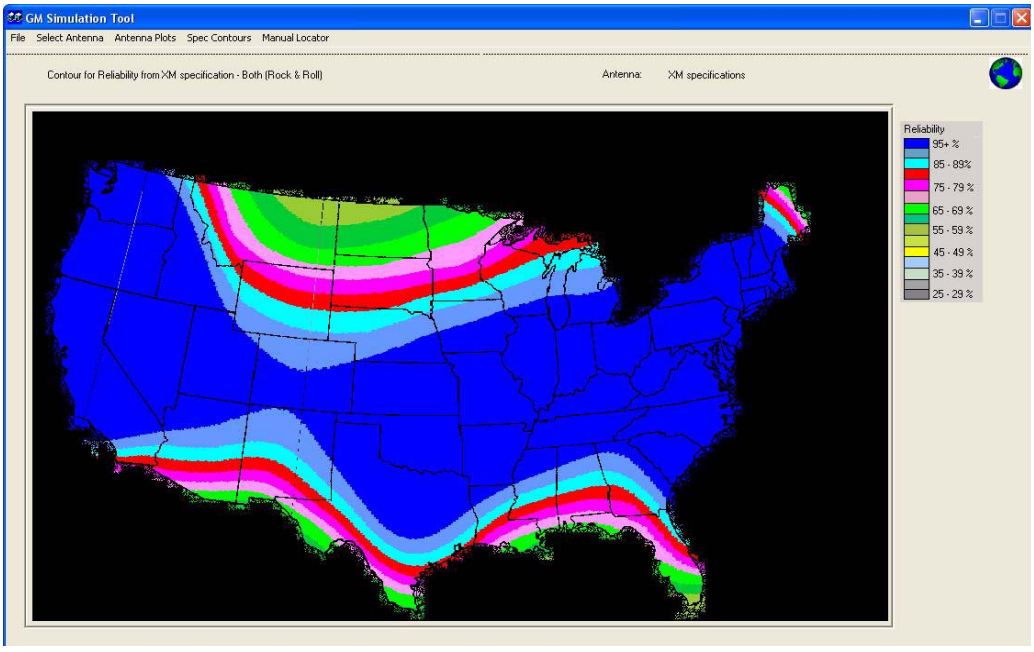

Figure 3.5 Link reliability contour with satellite diversity.

3.5 System Performance for Specific Practical Antennas

The results presented in section 3.4 assumed the antenna gain to be uniform over all the elevation (ϕ) and azimuthal angles (θ). However, the gain of practical antennas is far from uniform and differs widely from the specifications with changes in azimuthal and elevation angles. The results presented in this section identify the areas where the antenna gain might be below specifications for a given practical antenna. The simulation tool takes the measured gain patterns for an antenna as the input and provides the contours for the link reliability and % nulling time for the satellite signals.

3.5.1 Gain Patterns for a Practical Antenna

Figure 3.6 shows the 3-dimentional gain pattern for a real-world antenna. For an average specified antenna gain of 2 dBi, the performance is particularly poor at the lower elevation angles as indicated by the blue-colored regions. The blacked out areas in Figure 3.7 identify the azimuthal and elevation angles where the antenna gain does not meet the specifications. However, because of the spatial diversity created by using multiple satellites, not all the regions that have elevation angles identified in Figure 3.7 experience nulling of the satellite signals. The satellite signal is said to be "nulled" if the antenna gain is less than the average gain for a given set of (ϕ, θ), depending on where the receiver is on ConUS. The nulling of the satellite signals can be best explained by an illustrative example.

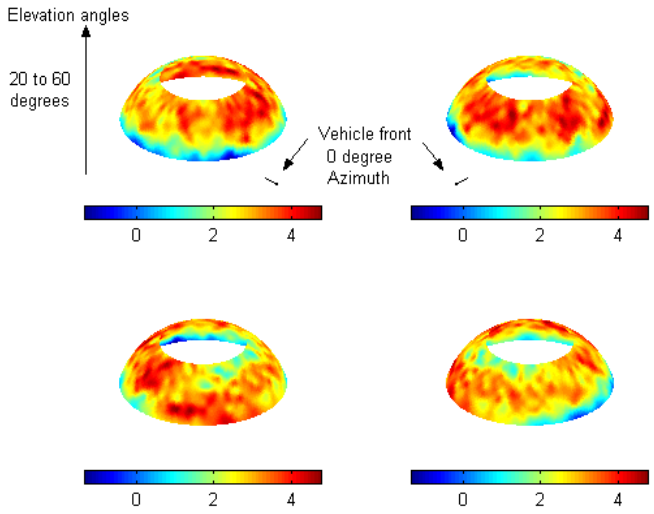

Figure 3.6 Four-sided 3-dimentional antenna gain pattern of a practical antenna.

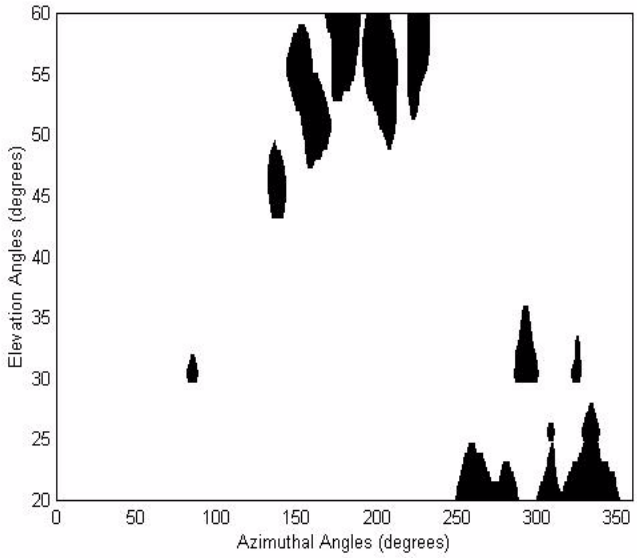

Figure 3.7 Plot identifying the elevation and azimuthal angles where the antenna gain is below specifications.

Depending on its location, each area on ConUS forms two elevation angles, one with each of the two satellites. The two satellite signals arriving at the radio receiver therefore see two separate antenna gains $G(\phi, \theta)$, one for each set of (ϕ, θ) values. It may now be possible that, because of the different angles of arrivals of the two signals, either one or both the signals may be nulled. Also note that even though (ϕ) remains the same for a given location, (θ) (and therefore $G(\phi, \theta)$) is a function of the direction of travel of the vehicle. Figure 3.8a, b illustrate the antenna gains and the angles of arrivals of the satellite signals for a particular location. Thus, while both the signals are nulled in Figure 3.8a, changing the direction of travel of the vehicle removes the nulling in Figure 3.8b. Similarly, it may be possible that only the strongest satellite signal is nulled while the weaker signal is good for a specific scenario and vice versa. When the strongest signal is good, the nulling of a weaker signal does not contribute significantly to the reduction of the overall system performance. Hence, the results presented lay emphasis on only the simultaneous nulling and nulling of the stronger satellite signals. The direction of the vehicle motion was assumed to be uniformly distributed for the development of the simulation tool.

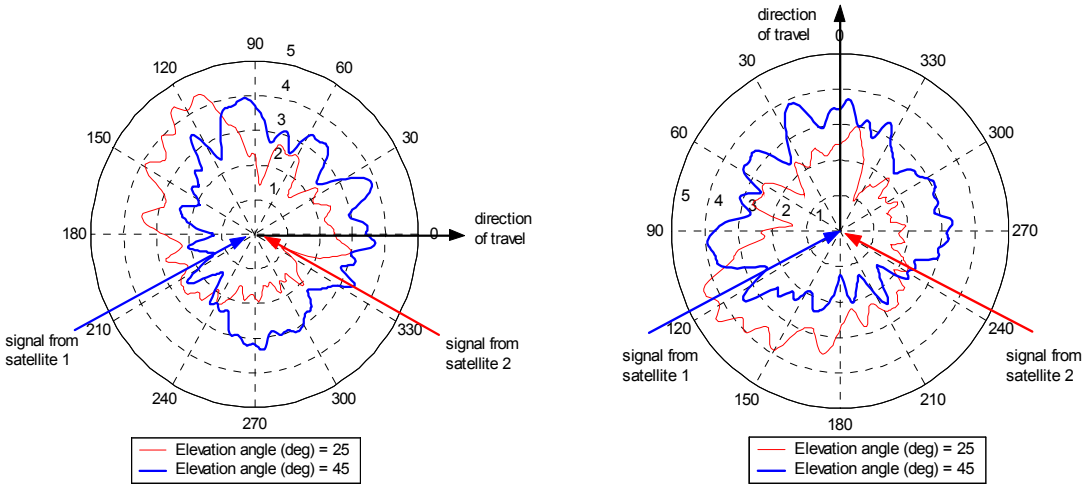

(a) (b)

Figure 3.8 Two-dimentional plots illustrating the effect of changes in the direction of travel on the nulling of the satellite signals.

3.5.2 Results with practical antenna

Knowing only the regions where the satellite signals may be nulled is not sufficient. Once the regions have been identified, it is important to know the duration and the depth of the nulls. Some nulls may be very small or occuring for a short duration and thus may not significantly impact the system performance. The simulation tool therefore not only provides the contours for the reliability but also provides the percentage nulling time at the locations susceptible to bad performance because of sub-spec antenna performance.

Figure 3.9 identifies the regions where the signals from both the satellites are nulled simultaneously and plots the reliability for those locations. We note that the link reliability is still greater than 95% for some the regions identified as nulled, indicating that the antenna gain for those regions were marginally below the specification values. Comparing Figure 3.5 and Figure 3.9, we note that at the southern tip of Texas, the link reliability with the practical antenna is about 10 % less than the reliability with the average antenna gain of 2 dBi. Figure 3.10 shows the contour for the percentage nulling time for the simultaneously nulled satellite signals. Using the simualtion tool, it is possible to obtain similar contours for the case where only the strongest signal is nulled.

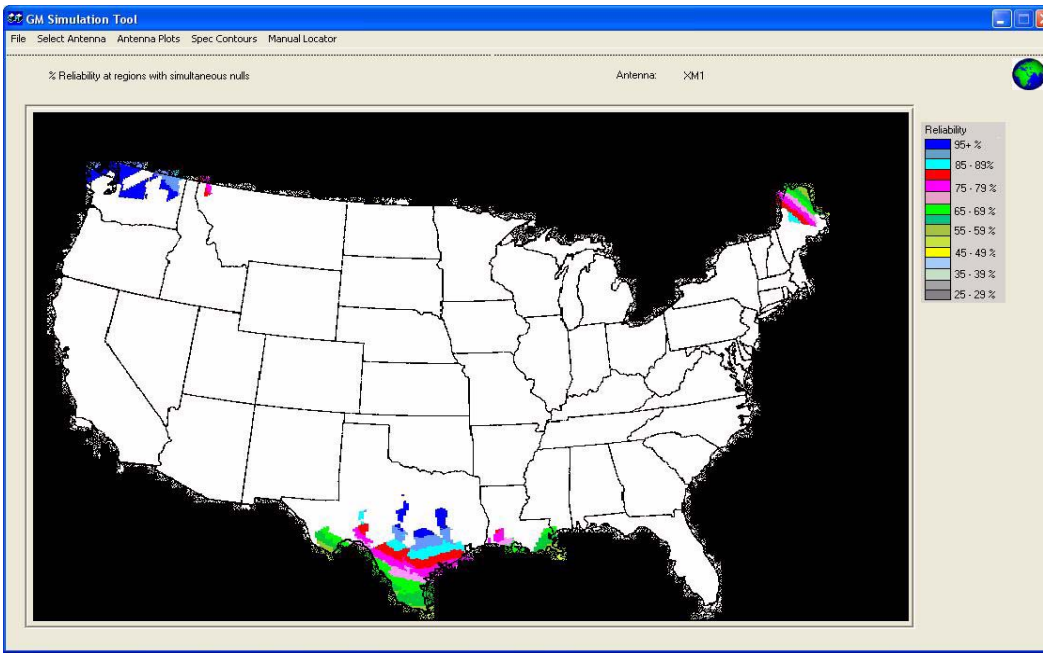

Figure 3.9 Contour for link reliability identifying locations with simultaneous nulls for a practical antenna.

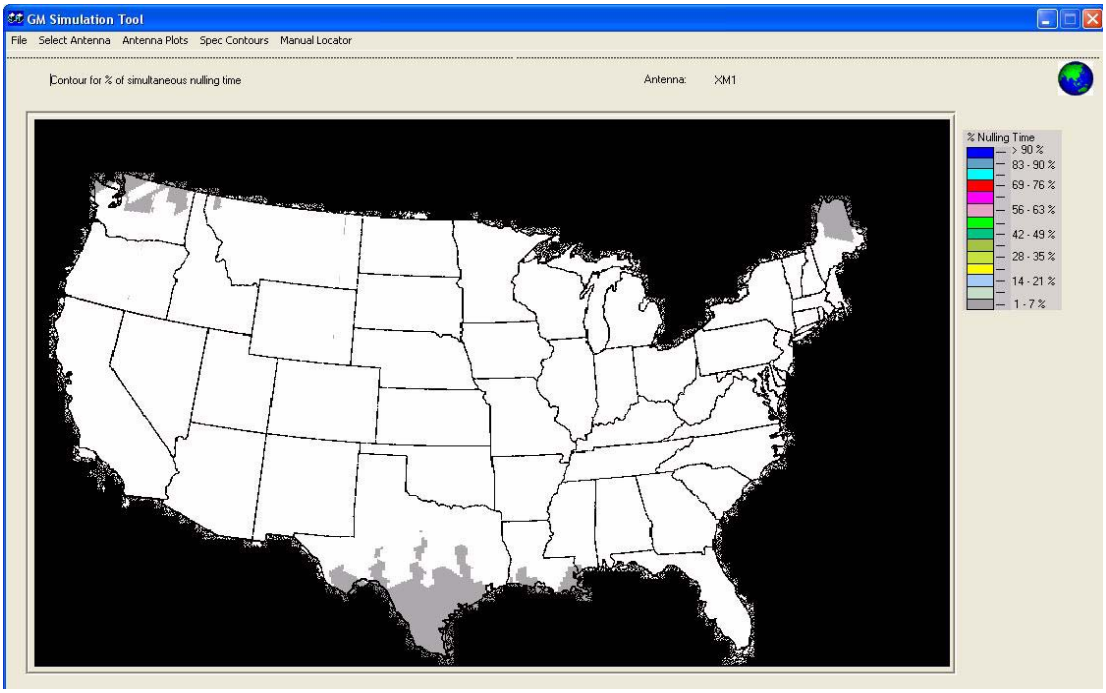

Figure 3.10 Contour for % nulling time at locations susceptible to simultaneous nulling.

As mentioned earlier, one of the motivations for the development of the simulation tool is to investigate whether it is possible to use a single antenna element for both the terrestrial and satellite systems. The tool has the capability of allowing the user to enter the measured gain patterns for new antennas. By comparing the performances of the various antennas, the user can select the satellite antenna that gives minimum simultaneous signal nulling. A good satellite antenna will reduce the dependence on the second antenna which is used for receiving terrestrial signals.

In addition to the above mentioned plots, contours for the elevation angles, EIRP and link margins can also be obtained using the tool. The tool has the capability to print any of the contours.

3.6 Chapter Conclusion

We conclude this chapter by re-stating some of the assumptions made in the development of the tool and elaborating on the future developments that are possible in the tool.

The simulation tool is based on a simple statistical model that incorporates only the first order statistics of the channel. The performance prediction by this model is therefore is a bit more pessimistic than in practice. The simulation tool does not take into consideration the error-correction coding schemes built into the system, nor does it account for the performance gains obtained because of the inbuilt frequency and time diversities in the system. Even with all these shortcomings, this simulation tool can be used to get a good high level understanding of the system performance. Useful insights are obtained regarding the areas susceptible to poor performance and the suitability of a particular antenna. As stated earlier, it is possible to use this tool to investigate whether it may be possible to use a single antenna element for both the satellite and the terrestrial repeater networks instead of two separate elements.

The simulation tool can be used as a framework to develop future software for GIS systems helpful in evaluating the system performance at the higher layers. As part of the future work, it may be possible to make some measurements and provide a mapping between the received SNR and BER. This might be interesting from a research point of view because the simulation tool would then be able to illustrate how the performance of a particular antenna (essentially a physical layer device), would map to the BER and the frame error rate.

Chapter 4

Error Probability Analysis for Generalized Selection Diversity Systems

4.1 Introduction

A Generalized Selection Combining (GSC) scheme aims at mitigating the detrimental small scale fading effects experienced in wireless channels. The technique takes advantage of the spatial diversity in the signal reception and applies an optimal linear combining rule to a subset of the "strongest" available diversity paths. It is possible to use this suboptimal technique without significant degradation in receiver performance, yet at a reduced receiver complexity and lower costs (i.e., fewer electronics and lower power consumption).

Figure 4.1 is a diagramatic representation of the receiver structure for millimeter wave communication systems where the GSC framework can be used for signal reception. The mean SNR/symbol for each branch γ_k is different for the signals arriving at each of the antenna elements. The reduction in the implementation complexity of $\mathrm{GSC}(M, L)$ is obtained by combining only the strongest M out of the L available branches. The importance of performance analyses of coherent and noncoherent GSC receivers from a theoretical viewpoint is therefore emminent by noting that $\mathrm{GSC}(1, L)$ and $\mathrm{GSC}(L, L)$ are simply the classical selection combining and maximal-ratio combining (coherent detection) or post-detection equal-gain combining (noncoherent detection) receivers that form the upper and lower performance bounds, respectively.

Previous studies on GSC have been limited to only Rayleigh [18]-[26] and Nakagami-m channels [27]-[32]. While the Rayleigh model may be appropriate for macro-cells,

it is customary to model the fading signal amplitudes in micro-cellular and pico-cellular environments as Rician distributed as discussed in Chapter 2. The appropriateness of this model has been validated by numerous field measurements. Moreover, Stein [34] and several other researchers have shown that the Nakagami-m approximation for a Rician random variable suggested by Nakagami [35] tends to overestimate the receiver performance particularly at large SNRs owing to the fact that the tails of the Rician and its Nakagami-m approximation distributions do not fit very closely.

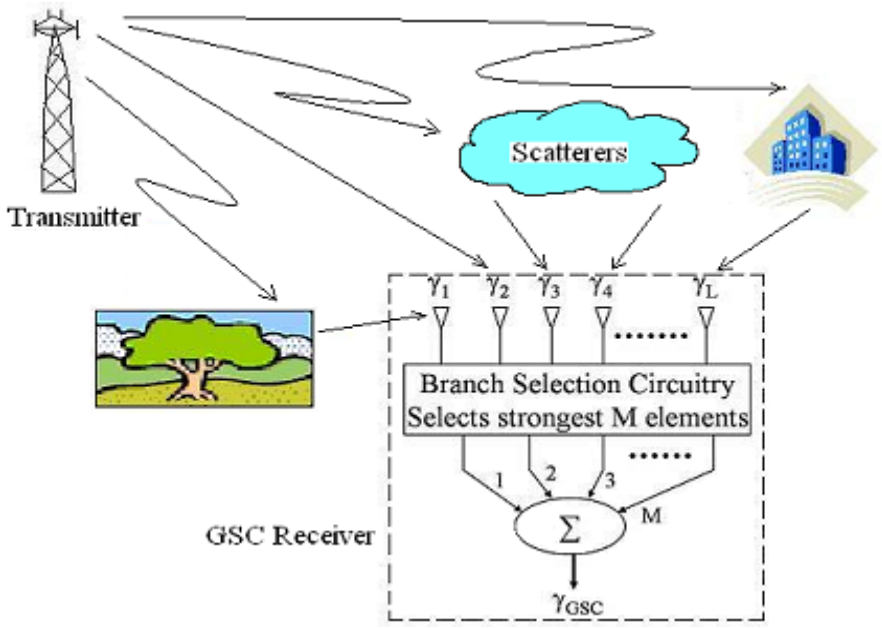

Figure 4.1 High-level diagramatic representation of a GSC receiver used for millimeter wave communications.

Despite the above reasons, performance analyses of both coherent and noncoherent GSC(M, L) receivers in Rician multipath fading channels are not available in the literature. Moreover, to date, there has not been a single unified approach that coherently deals with all the commonly used fading channels. The primary difficulty stems from the fact that the ordered SNRs γ_k (obtained after rearranging the SNRs of all the L diversity branches, $\gamma_1, \gamma_2, \ldots, \gamma_L$, in descending order such that $\gamma_1 \geq \gamma_2 \geq \ldots \geq \gamma_L$), are necessarily dependent because of the inequalities among them. Consequently, finding the moment

generating function (MGF) of a linear sum of ordered random variables $\gamma_{gsc} = \sum_{k=1}^{M} \gamma_k$ (i.e., GSC output SNR) is generally much more difficult than for the unordered random variables. In the past, numerous ad-hoc attempts have been made to compute the MGF of ordered exponential [18]-[20] and Gamma variates [29]-[32], resulting in various complicated formulas. Furthermore, the existing mathematical approaches do not lend themselves to the performance evaluation of GSC receivers in Rician channels easily. As such, one of the motivations behind this work is to report the development of a novel mathematical framework that can facilitate the problem of analyzing the GSC receiver performance with independent and identically distributed (i.i.d) diversity branches in a variety of fading environments, including the Rician fading model. An attractive feature of our approach is that the MGF of $\mathrm{GSC}(M, L)$ output SNR for all common fading channel models as well as for all combinations of M and L values can be simply expressed in terms of only a single finite-range integral whose integrand is composed of tabulated functions. For the special cases of Rayleigh and Nakagami-m fading, this integral may be further simplified into a closed-form expression. Utilizing these MGFs, we then compute several important performance metrics of coherent and noncoherent GSC receiver structures, including the average bit or symbol error probability with different binary and M-ary modulation schemes, outage rate of error probability and mean combined SNR at the GSC receiver output.

The chapter is organized as follows. Section 4.2 derives the MGF, Probability Density Function (PDF) and the Cumulative Distribution Function (CDF) of γ_{gsc} with the assumption of i.i.d diversity paths. The outage probability, used as one of the receiver performance metric, is also discussed. In Section 4.3, we utilize the MGF to unify the error probability analysis for a wide range of digital modulation schemes in conjunction with coherent and noncoherent (quadratic) $\mathrm{GSC}(M, L)$ receivers. An analytical expression for computing the mean combined SNR at the GSC receiver output is presented in Section 4.4. Finally, the major results are summarized in Section 4.5.

4.2 GSC(*M*,*L*) Combiner Output Statistics

In this section, we will derive analytical expressions for the $\mathrm{GSC}(M, L)$ combiner output statistics by modeling the branch amplitudes as i.i.d Rayleigh, Rician, Nakagami-m or

Nakagami-q random variables. These expressions can be applied directly for computing the Average Bit Error Rate (ABER) or the Average Symbol Error Rate (ASER), and outage probability for different modulation schemes.

From [36], we know that when M strongest diversity branches are selected from a total of L available i.i.d diversity branches the joint PDF is given by

$$p_{\gamma_{(1)}, \ldots, \gamma_{(M)}}(x_1, \ldots, x_M) = M!\binom{L}{M}[F(x_M)]^{L-M}\prod_{k=1}^{M} p(x_k) \tag{4.1}$$

where $x_1 \geq \ldots \geq x_M \geq 0$, $p(.)$ and $F(.)$ correspond to the PDF and CDF, respectively, of the SNR for a single channel reception (no-diversity case). As mentioned earlier, the symbol error rates and other combiner characteristics are a function of the MGF. Recognizing that the MGF of the combiner's output SNR $\phi_\gamma(.)$ is the key to the unified analysis of many modulation/detection schemes over wireless channels, our immediate intention will be to derive the desired MGF first. Let $\gamma = \gamma_{\text{gsc}} = \sum_{k=1}^{M} \gamma_k$ denote the hybrid combiner output SNR. Then, the MGF of γ_{gsc} may be computed as [33]

$$\begin{aligned}\phi_\gamma(s) &= \int_0^\infty \int_0^{\gamma_1} \ldots \int_0^{\gamma_{M-1}} e^{-s\sum_{k=1}^{M}\gamma_k} p_{\gamma_1, \ldots, \gamma_M}(\gamma_1, \ldots, \gamma_M) d\gamma_M \ldots d\gamma_2 d\gamma_1 \\ &= M!\binom{L}{M}\int_0^\infty e^{-s\gamma_M} p(\gamma_M)[F(\gamma_M)]^{L-M} \underbrace{\int_{\gamma_M}^\infty e^{-s\gamma_{M-1}} p(\gamma_{M-1}) \ldots \int_{\gamma_2}^\infty e^{-s\gamma_1} p(\gamma_1) d\gamma_1 \ldots d\gamma_{M-1} d\gamma_M}_{(M-1)\text{-fold integral}}\end{aligned} \tag{4.2}$$

From Appendix, we know that Eq. (4.2) can be re-written very concisely as

$$\phi_\gamma(s) = M\binom{L}{M}\int_0^\infty e^{-sx} p(x)[F(x)]^{L-M}[\phi(s,x)]^{M-1} dx \tag{4.3}$$

where $\phi(s,x) = \int_x^\infty e^{-st} p(t) dt$ denotes the marginal MGF of SNR of a single diversity branch and $F(x) = 1 - \phi(0,x)$. If $\phi(s,x)$ can be evaluated in closed-form, then it is apparent from Eq. (4.3) that the computational complexity of $\phi_\gamma(.)$ involves only one-fold integration (instead of an M-fold integration as in the case of (4.2)) because the integrand can be evaluated term by term for different x. Fortunately, as shown in chapter 2, closed-form solutions for $\phi(s,x)$ are available for all the statistical channel models that are typically

used to characterize the variations in the received signal power over wireless channels. The net result is a considerable reduction in computational complexity of $\phi_\gamma(.)$. Eq. (4.3) can be further operated on to obtain closed form expressions for the MGF for Rayleigh and Nakagami-m fading channels [42]. This development is interesting in view of the general belief that the closed form solution for $\mathrm{GSC}(M, L)$ receivers in a Nakagami-m fading channel with an arbitrary value of m is ordinarily unobtainable [29].

For the purpose of numerical computations, it is much more desirable to rewrite Eq. (4.3) as

$$\phi_\gamma(s) = M\binom{L}{M}\int_0^{\pi/2} e^{-s\tan\theta} p(\tan\theta)[1-\phi(0,\tan\theta)]^{L-M}[\phi(s,\tan\theta)]^{M-1}\sec^2\theta d\theta \tag{4.4}$$

since Eq. (4.4) has finite integration limits. Besides, Eq. (4.3) and/or Eq. (4.4) can be evaluated very efficiently using a Gauss-Chebychev Quadrature (GCQ) method. From this viewpoint, Eq. (4.4) will yield significant improvement over [31] in terms of computational complexity for the specific case of i.i.d Nakagami-m channels because the latter involves an *M*-dimensional GCQ sum, whereas in our case we need to compute only a one-dimensional GCQ sum.

The PDF of GSC output SNR can be evaluated as [37]

$$p_\gamma(x) \cong \frac{4}{T}\sum_{\substack{n=1 \\ n \text{ odd}}}^{\infty} \mathrm{Real}\left[\phi_\gamma\left(\frac{-j2\pi n}{T}\right)\exp\left(\frac{-j2\pi nx}{T}\right)\right] \tag{4.5}$$

where $j = \sqrt{-1}$ and the coefficient T selected is sufficiently large such that $Pr(x > T) \le \varepsilon$, and ε can be set to a very small value. The above PDF may also be used for ABER or ASER analysis of coherent, differentially coherent and noncoherent digital modulation schemes in conjunction with $\mathrm{GSC}(M, L)$ receiver.

The knowledge of the CDF of γ_{gsc} is also of interest because the outage probability P_{out} of GSC diversity systems can be expressed in terms of this metric alone. P_{out} is defined as the probability that the instantaneous symbol error rate of the system will exceed a specified value (say P_e^*). The outage probability criterion and the higher-order statistics of output SNR are often used as comparative performance measures of diversity

systems in wireless (fading) channels. Numerical computation based on ([33], eq. (14)) indicates that the Fourier series converge slowly at low values of $F_\gamma(x)$, we therefore exploit the Laplace inversion method suggested in [38] to compute the CDF of γ_{gsc}, viz.,

$$F_\gamma(x) \cong 2^{1-C} e^{A/2} \sum_{c=0}^{C} \binom{C}{c} \sum_{b=0}^{c+B} (-1)^b \alpha_b \text{Real}\left[\phi_\gamma\left(\frac{A + j2\pi b}{2x}\right) / (A + j2\pi b)\right] \tag{4.6}$$

where $\alpha_0 = 0.5$, $\alpha_b = 1$ for any $b \geq 1$ and the constants A, B and C are arbitrarily chosen to be 30, 18 and 24 respectively, yield an accuracy of at least 10^{-13}.

Eq. (4.6) can be used to predict the efficacy of a GSC diversity receiver on the outage probability metric, viz., $P_{out} = F_\gamma(\gamma^*)$ where γ^* is the threshold SNR. Given a digital modulation scheme with conditional error probability $P_s(\gamma)$, γ^* is obtained by solving $P_s(\gamma^*) = P_e^*$. Closed-form solutions for γ^* are available for several common modulation schemes and these are summarized in Table 4.1 [33]. For example, if $P_e^* = 10^{-3}$ is specified, $P_{out} = F_\gamma(4.77)$ because $\gamma^* = [\text{erfc}^{-1}(2 \times 10^{-3})]^2 = 4.77$ for BPSK modulation scheme. Similarly, for QPSK or square 4-QAM, $P_{out} = F_\gamma(10.83)$. Figure 4.2 depicts the CDF curves as a function of normalized mean SNR/symbol/branch Ω/γ^* for GSC(M, 5) receiver in a Rician channel ($K = 3$). Using these curves, it is possible to determine the mean SNR/symbol/branch to satisfy an outage requirement when a GSC(M, 5) receiver is employed. For instance, if $P_{out} = 10^{-2}$ is specified, then the mean SNR/symbol/branch requirement for BPSK modulation may be estimated as $\Omega = 4.77(10^{-0.21}) = 4.69\text{dB}$ (interpolated from Figure 4.2) assuming that $M = 3$ and $L = 5$. If QPSK is used rather than BPSK, then $\Omega = 10.83(10^{-0.21}) = 8.25\text{dB}$. Thus, to achieve the same outage probability, QPSK modulation requires approximately 3.56 dB higher mean SNR/symbol/branch compared to BPSK for GSC(3, 5) at Rice factor $K = 3$. While higher order alphabets allow higher data transmission rates, the increased bandwidth efficiency is attained at the expense of increasing the mean SNR/symbol/branch requirement (to compensate for denser signalling constellation). It is also apparent from Figure 4.2 that the relative diversity improvement diminishes with increasing M.

Table 4.1 Threshold SNR/symbol γ^* in closed-form for several common modulation schemes.

Modulation/ Detection	Conditional Error Probability $P_s(\gamma)$	Threshold SNR/symbol γ^*
BPSK	$\frac{1}{2}erfc(\sqrt{\gamma})$	$[erfc^{-1}(2P_e^*)]^2$
CFSK	$\frac{1}{2}erfc\left(\sqrt{\frac{\gamma}{2}}\right)$	$2[erfc^{-1}(2P_e^*)]^2$
NCFSK	$\frac{1}{2}\exp\left(-\frac{\gamma}{2}\right)$	$-2\ln(2P_e^*)$
DPSK	$\frac{1}{2}\exp(-\gamma)$	$-\ln(2P_e^*)$
QPSK	$erfc(\sqrt{\gamma/2})-\frac{1}{4}erfc^2(\sqrt{\gamma/2})$	$2\{erfc^{-1}[2(1-\sqrt{1-P_e^*})]\}^2$
M_c - QAM	$2q\cdot erfc(\sqrt{a})-(q^2\cdot erfc^2\sqrt{a})$ where, $q = 1-1/(\sqrt{M_c})$, $a = \frac{3\gamma}{2(M_c-1)}$	$\frac{2(M_c-1)}{3}\left[erfc^{-1}\left(\frac{1-\sqrt{1-P_e^*}}{1-1/(\sqrt{M_c})}\right)\right]^2$
MSK	$erfc(\sqrt{\gamma/2})-\frac{1}{4}erfc^2(\sqrt{\gamma/2})$	$[erfc^{-1}(1-\sqrt{1-2P_e^*})]^2$

4.3 ASER Analysis

In this section, we derive the ASER expressions for a multitude of digital modulation schemes in conjunction with coherent and noncoherent GSC receiver structures for i.i.d paths using Eq. (4.4). The advantage of using Eq. (4.4) is that the final ASER expression will be in the form of a finite-range integral whose integrand is composed of only the MGF of the GSC output SNR, $\phi_\gamma(.)$. Several examples are provided next to highlight the utility of the MGF and PDF of γ_{gsc} in the ASER analysis. If the branches are coherently combined before signal detection, then we refer the diversity combining scheme as coherent GSC. In noncoherent GSC, noncoherent combining (i.e., post-detection equal-gain combining) of diversity branches is implemented after the signal detection.

4.3.1 Coherent GSC Receivers

Using the MGF approach [25][32], the ASER of a myriad of modulation schemes can be obtained by using the generalized expressions stated below.

A. BPSK, CFSK, QPSK and Mc-PSK

$$\overline{P_s} = \frac{1}{\pi}\int_0^{\theta_H} \phi_\gamma\left(\frac{\zeta}{\sin^2\theta}\right) d\theta$$

where M_c denotes the alphabet size of M-ary signal constellations and $\phi_\gamma(.)$ is defined in Eq. (4.4). The coefficients θ_H and ζ for the different modulation schemes are listed below.

Modulation	BPSK	CFSK	QPSK	M_c-PSK
θ_H	$\pi/2$	$\pi/2$	$3\pi/4$	$\pi - \pi/M_c$
ζ	1	$1/2$	$1/2$	$\sin^2(\pi/M_c)$

B. M_c **-** QAM, QPSK and DE-BPSK (differentially encoded BPSK)

$$\overline{P_s} = \frac{a}{\pi}\int_0^{\pi/2} \phi_\gamma\left[\frac{c}{\sin^2\theta}\right] d\theta - \frac{b}{\pi}\int_0^{\pi/4} \phi_\gamma\left[\frac{c}{\sin^2\theta}\right] d\theta \qquad (4.7)$$

The coefficients a,b,c are again given by the following table.

Modulation	M_c **- QAM**	QPSK	DE-BPSK
a	$4(1 - 1/\sqrt{M_c})$	2	2
b	$4(1 - 1/\sqrt{M_c})^2$	1	2
c	$1.5/(M_c - 1)$	1/2	1

Although the coherent GSC receiver is typically employed for coherent modulation/ detection schemes (i.e., channel estimates are required for coherent diversity combining implementation), the analysis of noncoherent modulation schemes with coherent GSC receivers are also of interest because they provide a lower bound on the error rates with noncoherent GSC receivers. This is particularly useful if the Conditional Error Probability (CEP) for the multichannel quadratic receivers are not known or are in a complicated form. For instance, the ASER of M-ary DPSK with coherent GSC receiver is given by

$$\overline{P_s} = \frac{1}{\pi}\int_0^{\pi-\frac{\pi}{M_c}} \phi_\gamma\left[\frac{\sin^2(\pi/M_c)}{1+\cos(\pi/M_c)\cos\theta}\right] d\theta \tag{4.8}$$

For the special case of binary DPSK ($M_c = 2$), Eq. (4.8) simplifies to $\overline{P_b} = \phi_\gamma(1)/2$.

Using the procedure above, it is also possible to write down the generalized ASER formulas for other modulation schemes [32].

4.3.2 Noncoherent GSC Receivers

Since square-law detection (also known as post-detection equal-gain combining) circumvents the need to co-phase and weight the diversity branches, the multichannel quadratic receiver has a simple implementation and suitable for use in noncoherent and differentially coherent communication systems [19]. The ABER of DPSK, BFSK and π/4-DQPSK with noncoherent $\mathrm{GSC}(M, L)$ receiver may be computed using [39]

$$\overline{P_b} = \frac{1}{(1+\eta)^{2M-1}2\pi}\int_0^{2\pi} \frac{g(\theta)}{1-2\beta\cos\theta+\beta^2}\phi_\gamma\left[\frac{b^2}{2}(1-2\beta\cos\theta+\beta^2)\right] d\theta \tag{4.9}$$

where $0^+ < \beta = a/b < 1$,

$$g(\theta) = \sum_{k=0}^{2M-1}\binom{2M-1}{k}\beta^{k+1-M}\eta^k\{\cos[(k-M+1)\theta]-\beta\cos[(k-M)\theta]\} \tag{4.10}$$

and the values for constants a, b and η for the three different modulation schemes are summarized in the Table 4.2 below.

Table 4.2 Modulation related parameters for several noncoherent and differentially coherent communication systems.

Modulation	***a***	***b***	η
DPSK	0	$\sqrt{2}$	1
BFSK	0	1	1
π/4-DQPSK	$\sqrt{2-\sqrt{2}}$	$\sqrt{2+\sqrt{2}}$	1

Note that as $\beta \to 0$, Eq. (4.9) assumes an indeterminate form but its limit converge smoothly to the exact ABER. Thus, the ABER of DPSK and BFSK can be computed using Eq. (4.9) with good accuracy by setting $a = 10^{-3}$ instead of zero. Alternatively, one

may utilize Eq. (4.5) to average over the CEP of an M-order post-detection equal-gain combining (EGC) to yield an infinite series expression for the ABER:

$$\overline{P_b} \cong \frac{4}{T} \sum_{\substack{n=1 \\ n \text{ odd}}}^{\infty} \text{Real}\left[\phi_\gamma\left(\frac{-j2\pi n}{T}\right) G_\gamma\left(\frac{2\pi n}{T}\right)\right] \tag{4.11}$$

where $G_\gamma(\omega) = \text{FT}[P_b(\gamma)] = \int_0^\infty P_b(\gamma) e^{-j\omega\gamma} d\gamma$. Recognizing that the exact CEP of an M-order post-detection EGC for DPSK and BFSK is simply

$$P_b(\gamma) = \frac{1}{2^{2M-1}} \sum_{k=1}^{M} \binom{2M-1}{M-k} \frac{\Gamma(k, g\gamma)}{\Gamma(k)} \tag{4.12}$$

where $g = 1$ for DPSK and $g = 1/2$ for BFSK, we obtain

$$G_\gamma(\omega) = \frac{1}{2^{2M-1}(j\omega)} \sum_{k=1}^{M} \binom{2M-1}{M-k} \left[1 - \left(\frac{g}{g+j\omega}\right)^k\right] \tag{4.13}$$

This approach may be extended to other digital modulation schemes, the details of which can be found in [40][42].

4.3.3 Numerical Examples

Figure 4.3 shows the average bit error rate performance for BPSK modulation with a receiver in a Rician fading environment (Rice factor $K = 3.5$). All the performance curves are upper and lower bounded by $\text{GSC}(1, 5)$ and $\text{GSC}(5, 5)$, which correspond to the Selection Diversity (SD) and the Maximal-Ratio Combining (MRC) schemes respectively. Moreover, the performance curve for $\text{GSC}(M, 5)$ quickly move towards the MRC case as M is increased gradually (the gap between the curves gets closer). For example, at the ABER of 10^{-5}, the diversity gains for $\text{GSC}(2, 5)$ and $\text{GSC}(3, 5)$ are approximately 2.6 dB and 3.8 dB respectively, with respect to the SD receiver. It is also observed that these gains remain almost constant particularly at the low error rates.

In Figure 4.4 and Figure 4.5, we illustrate the effect of fade distributions on the error probability performance of QPSK and DPSK modulation schemes in conjunction with a coherent GSC receiver. Even though the ASER decreases as the channel condition

improves, the slope of the curves (i.e., rate of decay) in Figure 4.4 is a function of the number of diversity paths combined at the receiver. The diversity improvement observed from Figure 4.4 is attributed to the following two factors: (i) statistical gain realized by ordering and choosing the strongest branch SNRs; (ii) total energy captured by combining additional diversity paths. The former depends on both the fading parameter K and the difference between L and M, while the latter is dictated only by the number of combined diversity paths M. Looking at the trends in Figure 4.4, we may conclude that factor (i) has a stronger influence in severe fading conditions, while factor (ii) is predominant in a less severely faded environments (i.e., the ABER curve for $\mathrm{GSC}(1, 5)$ becomes almost flat for $K > 6$). While $\mathrm{GSC}(M, 5)$ with a moderate M value (say, $M = 3$) yields comparable performance with that of MRC in severely faded wireless channels (e.g., $K = 0$), the discrepancy between them gets larger as the Rice factor increases (see Figure 4.4). Thus, it is highly desirable to combine more diversity paths to improve the overall receiver performance when strong specular components are available. It is apparent from Figure 4.5 that the effect of fade distribution on ABER performance becomes more pronounced as Ω increases.

Figure 4.6 depicts the ABER variation for BPSK modulation as a function of diversity order L. It is evident that increasing L also translates into a considerable improvement in the receiver performance. However, the relative improvement with higher order diversities declines because the the probability of deep fades decreases with increasing M and/or L. Figure 4.6 may also be used to investigate the benefits/trade-off between various combinations of L and M in a receiver design. For example, the ABER performance obtained with selection combining with $L = 10$ may be realized using diversity orders as low as $\mathrm{GSC}(2, 5)$ or even $\mathrm{GSC}(3, 4)$, given that the mean SNR/bit/branch $\Omega = 10$ dB.

The error performance of $\pi/4$-DQPSK in conjunction with coherent and noncoherent $\mathrm{GSC}(M, 5)$ receiver structures in a Rician fading environment ($K = 2.5$) are illustrated in Figure 4.7. The ABER of $\pi/4$-DQPSK with coherent GSC receiver may be computed as [43]

$$\overline{P_b} = \frac{1}{2\pi}\int_0^{\pi} \phi_\gamma\left(\frac{2}{2-\sqrt{2}\cos\theta}\right) d\theta \tag{4.14}$$

and the ABER with noncoherent GSC receiver is given by Eq. (4.9).

For the special case of selection diversity, both predetection combining and post-detection combining perform identically. The difference between the coherent GSC and noncoherent GSC gets larger as M increases. For small and moderate M values, however, noncoherent GSC is attractive owing to its simple implementation and also because it yields comparable performance with that of the coherent GSC receiver. We also observe that for a fixed M value, the ABER performance with noncoherent GSC asymptotically approaches the ABER performance with coherent GSC receiver (i.e., the gap between the curves gets smaller as the mean SNR/bit/branch Ω increases).

4.4 Mean Combined SNR

The mean combined SNR is another useful performance measure of diversity systems. Since the mean combined SNR $\bar{\gamma}_{\text{gsc}}$ is the first moment (mean) of the random variable γ_{gsc}, it can be determined by differentiating the MGF Eq. (4.3) with respect to s and then evaluating the derivative at $s = 0$:

$$\bar{\gamma}_{\text{gsc}} = \int_0^{\infty} \gamma p_\gamma(\gamma) d\gamma = -\frac{d}{ds}\phi_\gamma(s)\bigg|_{s=0} \tag{4.15}$$

However, it is much simpler to derive an expression for $\bar{\gamma}_{\text{gsc}}$ by computing the sum of the expected value of the individual ordered SNRs as

$$\bar{\gamma}_{\text{gsc}} = \sum_{k=1}^{M} \bar{\gamma}_{(k)} \tag{4.16}$$

and utilizing the density function of the the k-th strongest branch SNR $\gamma_{(k)}$ from a population of L i.i.d random variables $\gamma_1, \gamma_2, \ldots, \gamma_L$ given by [30]

$$p_k(x) = k\binom{L}{k}[F(x)]^{L-k}[1-F(x)]^{k-1}p(x) \tag{4.17}$$

Thus, we obtain

$$\bar{\gamma}_{\text{gsc}} = \sum_{k=1}^{M} k\binom{L}{k}\int_0^{\infty} x[F(x)]^{L-k}[1-F(x)]^{k-1}p(x)dx \tag{4.18}$$

which may be computed efficiently via Gauss-Legendre quadrature method. It should be stressed that Eq. (4.18) holds for all values of M, L as well as for different fading environments.

In Figure 4.8, the normalized mean combined SNR at the GSC output, $\bar{\gamma}_{gsc}/\Omega$, is plotted as a function of diversity order L for different M values. For a fixed M, we observe that $\bar{\gamma}_{gsc}/\Omega$ increases with increasing diversity order L. The rate at which the normalized mean output SNR increases declines gradually as $(L-M)$ increases, which is typical of selection diversity systems. Also, for a fixed value of L, $\bar{\gamma}_{gsc}/\Omega$ increases with M as expected. Comparing the two subplots of Figure 4.8, we note that the normalized mean combined SNR curve for a specified M and L becomes flatter as the channel experiences fewer deep fades (higher K values). This anomaly can be explained by considering the limiting case of an AWGN (non-fading) channel in which the mean combined SNR is independent of the diversity order L and depends only on M (the number of paths combined at the receiver). Thus, as the channel condition improves, the statistical gain realized by ordering and choosing the strongest branch SNRs goes on decreasing and the dominating factor is the total energy captured by combining additional diversity paths. From Figure 4.9, we observe that $\bar{\gamma}_{gsc}/\Omega = 5$ for $\mathrm{GSC}(5,5)$ and this value is independent of the fading severity index m of a Nakagami-m channel. This trend is in agreement with the well-known result $\bar{\gamma}_{mrc} = L\Omega$ for an MRC receiver with L i.i.d diversity branches. The dependence of $\bar{\gamma}_{gsc}/\Omega$ on the fading parameter becomes more pronounced as M decreases. We also found that the normalized mean output SNR asymptotically approaches M as the fading index gets very large (i.e., $\lim_{m\to\infty} \bar{\gamma}_{gsc}/\Omega = M$).

4.5 Chapter Conclusion

This part of the thesis investigates the performance of both coherent and noncoherent $\mathrm{GSC}(M,L)$ receiver with i.i.d diversity paths in Rician fading which heretofore had resisted solution in a simple form. Unified expressions for computing the MGF, PDF and CDF of GSC output SNR in a myriad of fading environments are also derived. The MGF and PDF of γ_{gsc} are used to facilitate an unified ASER analysis for different modulation/

detection schemes while the outage rate of error probability performance is predicted from the CDF expression. A concise analytical expression for the average combined SNR is also presented. Our mathematical framework for computing the MGF of γ_{gsc} has several advantages: (a) it treats all common fading channel models in a unified sense; (b) it leads to a much more elegant and computationally efficient expression for $\phi_{\gamma}(.)$ than those available in the literature; (c) it also holds for any combinations of *M* and *L* values and arbitrary fading parameters. The mathematical framework developed in this paper can be utilized in the design of several wireless systems of interest, such as the design of GSC antenna arrays for use in millimeter-wave and broadband indoor wireless communications and the development of a reduced-complexity rake receiver for use in wideband CDMA and ultra-wideband communications.

APPENDIX

If the i.i.d random variables (RVs) $\gamma_1, \gamma_2, \ldots, \gamma_L$, each with PDF $p(x_k)$ and CDF $F(x_k)$, are arranged in a descending order of magnitude and then written as $\gamma_{1:L} \geq \gamma_{2:L} \geq \ldots \geq \gamma_{L:L}$, we refer $\underset{M}{\gamma_{k:L}} \equiv \gamma_{(k)}$ as the k-th order statistic. Recognizing that the knowledge of MGF of $\gamma = \sum_{k=1}^{M} \gamma_{k:L}$ can be used to unify the performance analysis of digital communication systems over fading channels, in this appendix, we will develop a general procedure for deriving $\phi_\gamma(s)$ for any $1 \leq M \leq L$ and also without imposing any restrictions on the fade distribution.

From (4.2), we have

$$\phi_\gamma(s) = M!\binom{L}{M}\int_0^\infty e^{-sx_M} p(x_M)[F(x_M)]^{L-M} \int_{x_M}^\infty e^{-sx_{M-1}} p(x_{M-1}) \ldots \int_{x_2}^\infty e^{-s\gamma_1} p(x_1)dx_1 \ldots dx_{M-1}dx_M \quad \text{(A.1)}$$

Now let us consider several special cases. For $M = 1$ (SC), (A.1) reduces to

$$\phi_\gamma(s) = L\int_0^\infty e^{-sx_1} p(x_1)[F(x_1)]^{L-1} dx_1 \quad \text{(A.2)}$$

For $M = 2$, (A.1) simplifies into

$$\begin{aligned} \phi_\gamma(s) &= 2\binom{L}{2}\int_0^\infty e^{-sx_2} p(x_2)[F(x_2)]^{L-2} \left\{ \int_{\gamma_2}^\infty e^{-sx_1} p(x_1)dx_1 \right\} dx_2 \\ &= 2\binom{L}{2}\int_0^\infty e^{-sx_2} p(x_2)[F(x_2)]^{L-2} \phi(s, x_2)dx_2 \end{aligned} \quad \text{(A.3)}$$

where $\phi(s, z) = \int_z^\infty e^{-sx_k} p(x_k)dx_k$ is the marginal MGF of RV γ_k and $k \in \{1, 2, \ldots, L\}$.

Letting $M = 3$ in (A.1), we obtain

$$\phi_\gamma(s) = 6\binom{L}{3}\int_0^\infty e^{-sx_3} p(x_3)[F(x_3)]^{L-3} \left\{ \int_{x_3}^\infty e^{-sx_2} p(x_2)\phi(s, x_2)dx_2 \right\} dx_3 \quad \text{(A.4)}$$

Using variable substitution $u = \phi(s, x_2)$ in the inner integral of (A.4), and after simplifications, we obtain

$$\phi_\gamma(s) = 3\binom{L}{3}\int_0^\infty e^{-sx_3} p(x_3)[F(x_3)]^{L-3}[\phi(s, x_3)]^2 dx_3 \quad \text{(A.5)}$$

with the aid of the integral identity

$$\int_a^b [g(x)]^n g'(x)dx = \frac{[g(b)]^{n+1} - [g(a)]^{n+1}}{n+1} \quad \text{(A.6)}$$

and recognizing that $du = -e^{-sx_2}p(x_2)dx_2$.

Using the procedure described above, it is straight-forward to show that for $M = 4$, (A.1) reduces to

$$\phi_\gamma(s) = 4\binom{L}{4}\int_0^\infty e^{-sx_4}p(x_4)[F(x_4)]^{L-4}[\phi(s,x_4)]^3 dx_4 \tag{A.7}$$

In summary, we can show that the $(M-1)$-fold nested integral in (A.1) may be replaced by a product of $(M-1)$ integrals by applying (A.6) repetitively, viz.,

$$\int_{x_M}^\infty e^{-sx_{M-1}}p(x_{M-1})\ldots\int_{x_2}^\infty e^{-sx_1}p(x_1)dx_1\ldots dx_{M-1} = \frac{[\phi(s,x_M)]^{M-1}}{(M-1)!} \tag{A.8}$$

Substituting (A.8) into (A.1), we obtain an elegant formula for the MGF of GSC output SNR:

$$\phi_\gamma(s) = M\binom{L}{M}\int_0^\infty e^{-sx_M}p(x_M)[F(x_M)]^{L-M}[\phi(s,x_M)]^{M-1}dx_M \tag{A.9}$$

which is valid for all combinations of L and $M \le L$ as well as for different fading environments.

At this juncture, it is instructive to examine $\phi_\gamma(.)$ for the two limiting cases of interest. When $M = 1$, (A.9) is in agreement with (A.2). On the other extreme with $M = L$, we get (using (A.6))

$$\phi_\gamma(s) = L\int_0^\infty e^{-sx_L}p(x_L)[\phi(s,x_L)]^{L-1}dx_L = [\phi(s)]^L \tag{A.10}$$

as expected (note: $\phi(s,0) = \phi(s)$ corresponds to the MGF of SNR in the no-diversity case).

It is also not very difficult to demonstrate that (A.9) collapses into a single integral expression with finite integration limits (see (4.4)) while the fading signal amplitudes follow either the Rician, or the Nakagami-m (real $m \ge 0.5$), or the Nakagami-q distribution. This is attributed to the availability of closed-form solutions for the marginal MGF $\phi(s,x_k)$ in the above cases. Moreover, if $\gamma_1, \gamma_2, \ldots, \gamma_L$ are i.i.d exponential or Gamma variates, (A.9) can also be evaluated in closed-form [42].

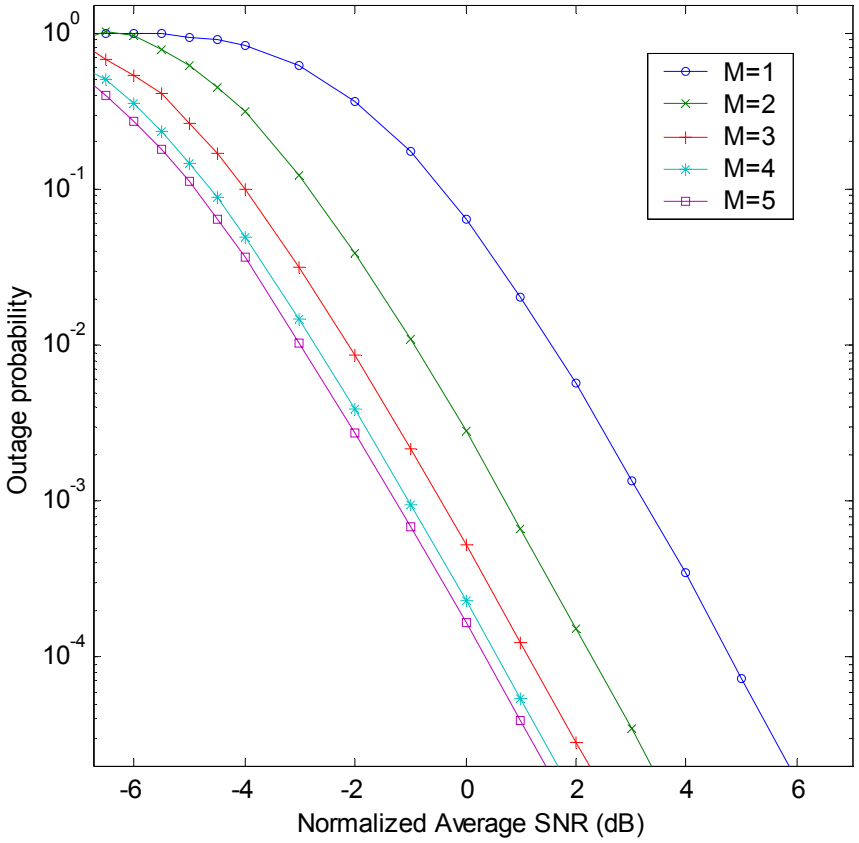

Figure 4.2 Outage probability $F_{\gamma}(\gamma^*)$ versus the normalized average SNR Ω/γ^* for $\mathrm{GSC}(M, 5)$ receiver on a Rician channel with $K = 3$.

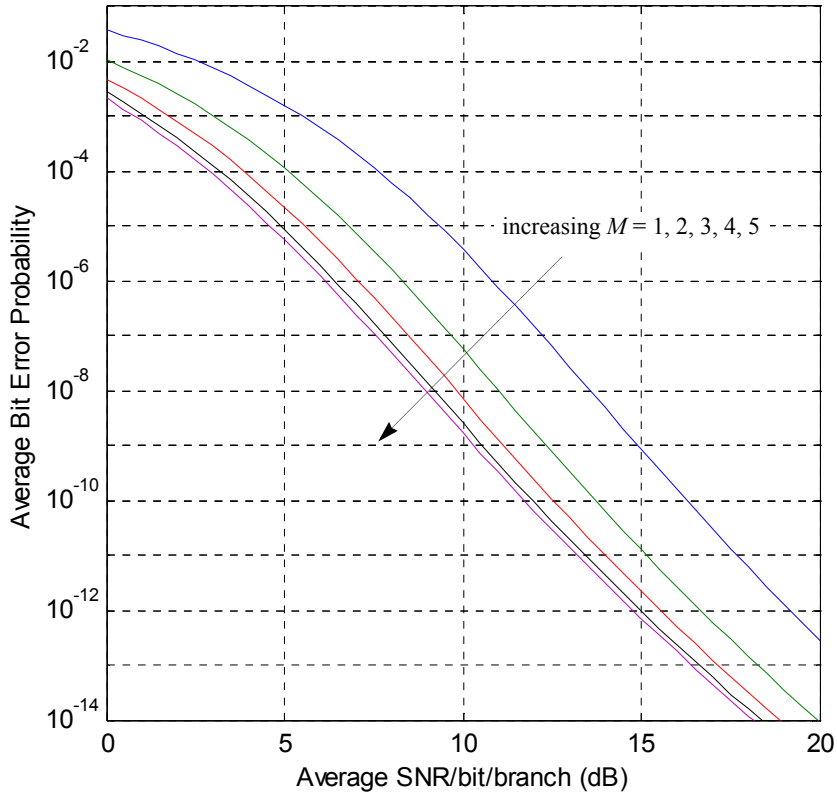

Figure 4.3 Average bit error rate performance of BPSK with $\mathrm{GSC}(M, 5)$ receiver in a Rician fading environment with $K = 3.5$.

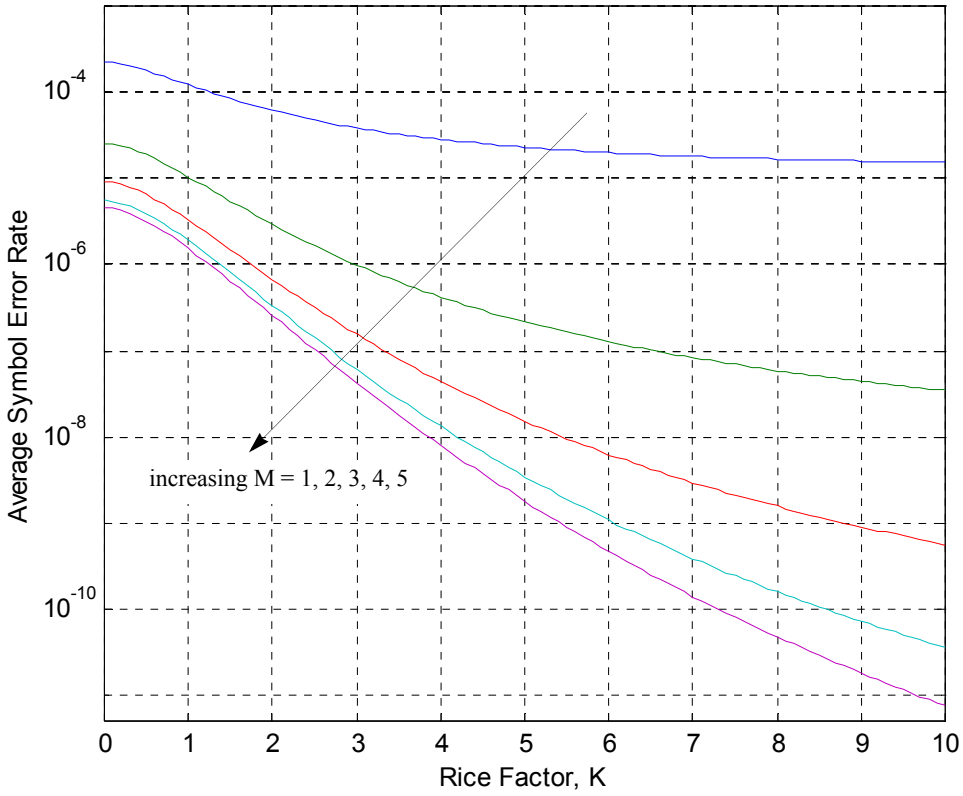

Figure 4.4 Average symbol error rate of QPSK as a function of Rice factor K for $\mathrm{GSC}(M, 5)$ receiver and average SNR/symbol/branch $\Omega = 12$ dB.

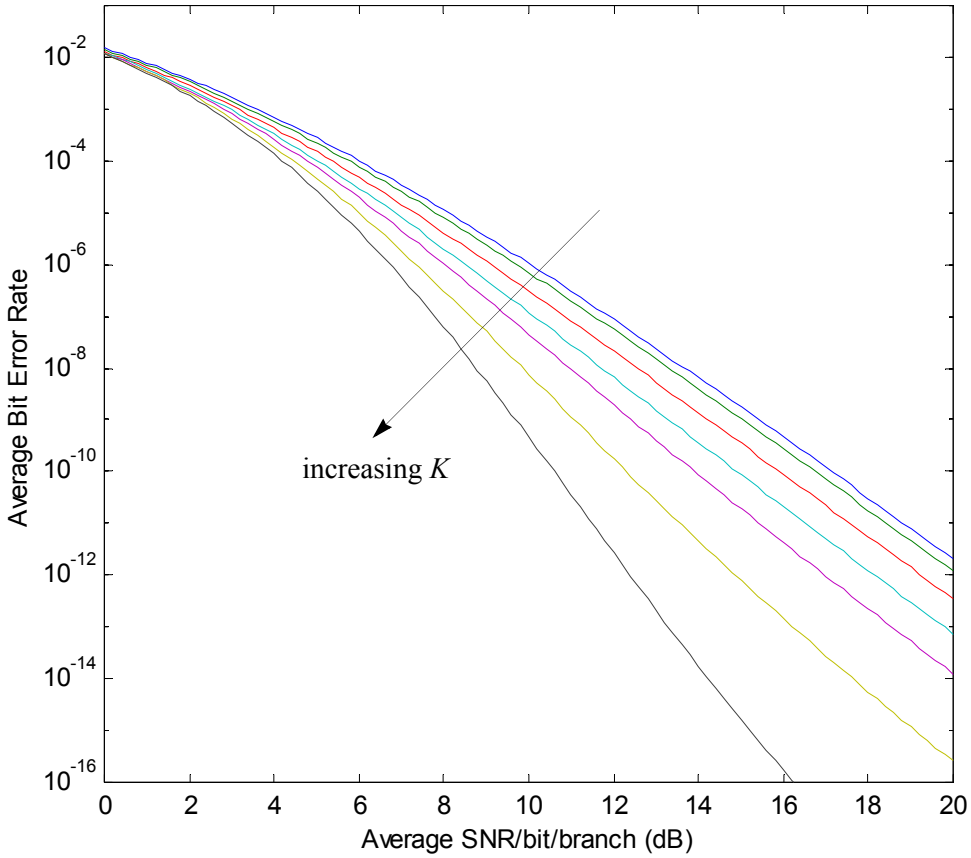

Figure 4.5 Average bit error rate of DPSK with coherent $\mathrm{GSC}(3, 6)$ receiver for different Rice factors $K \in \{0, 0.5, 1, 1.5, 2, 3, 5\}$.

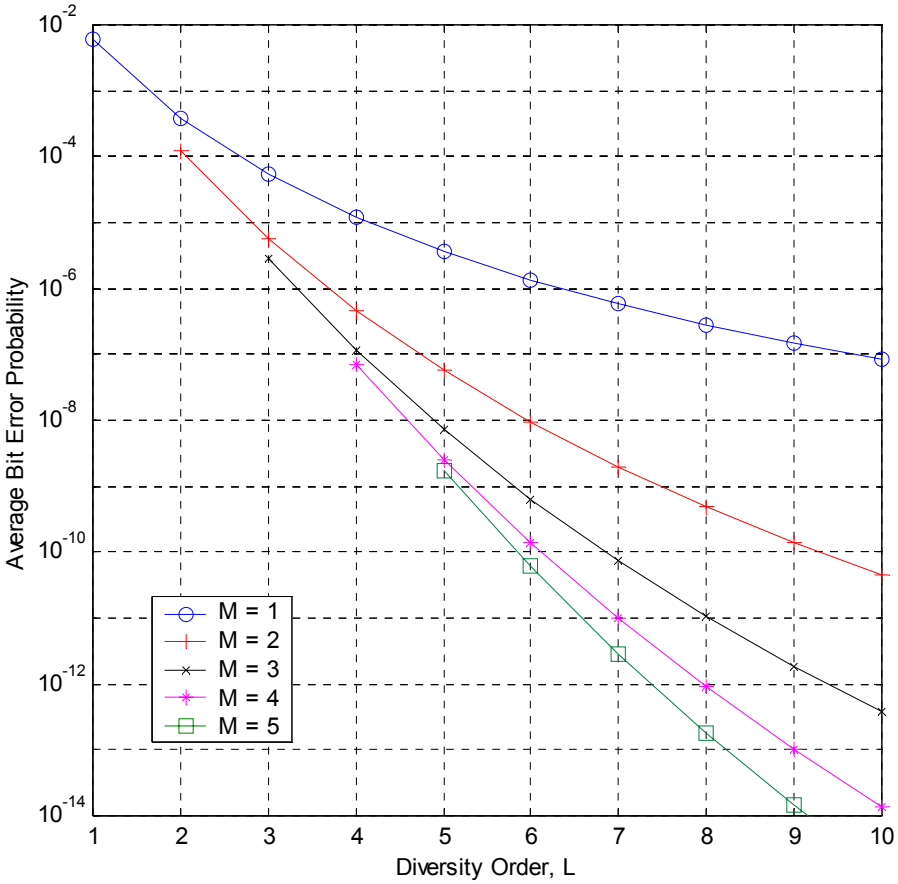

Figure 4.6 Average bit error rate of BPSK versus diversity order L for different M values in a Rician channel with $K = 3.5$ and mean SNR/bit/branch $\Omega = 10$ dB.

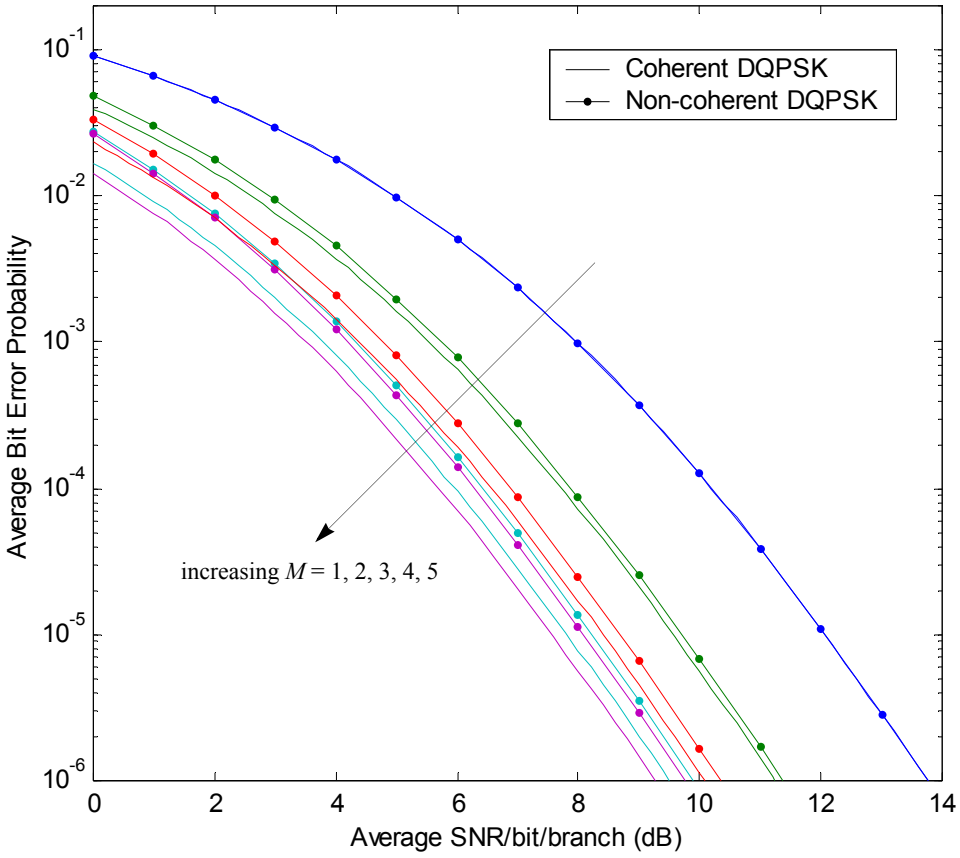

Figure 4.7 Average bit error rate performance of π/4-DQPSK with coherent and noncoherent $\mathrm{GSC}(M, 5)$ receiver structures in a Rician fading environment ($K = 2.5$).

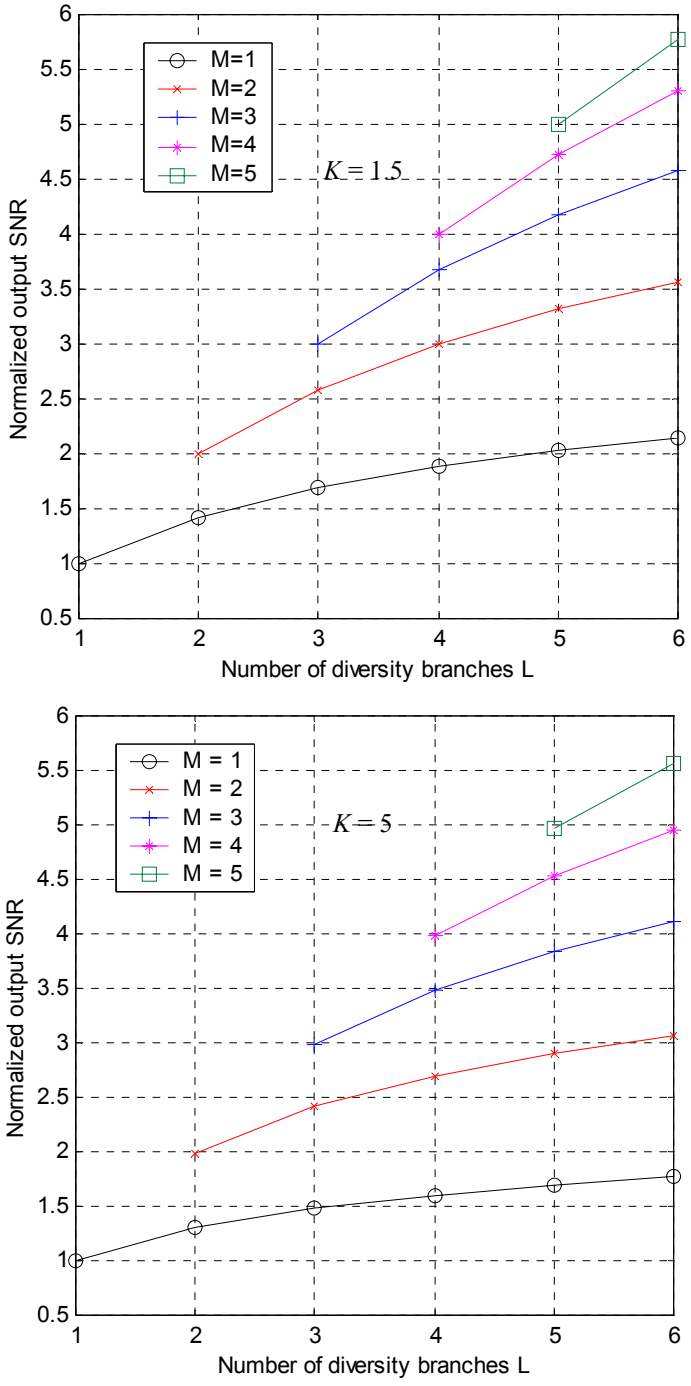

Figure 4.8 The normalized mean GSC output SNR $\bar{\gamma}_{gsc}/\Omega$ versus the total number of diversity branches L for various M values in a Rician channel with $K = 1.5$ and $K = 5$.

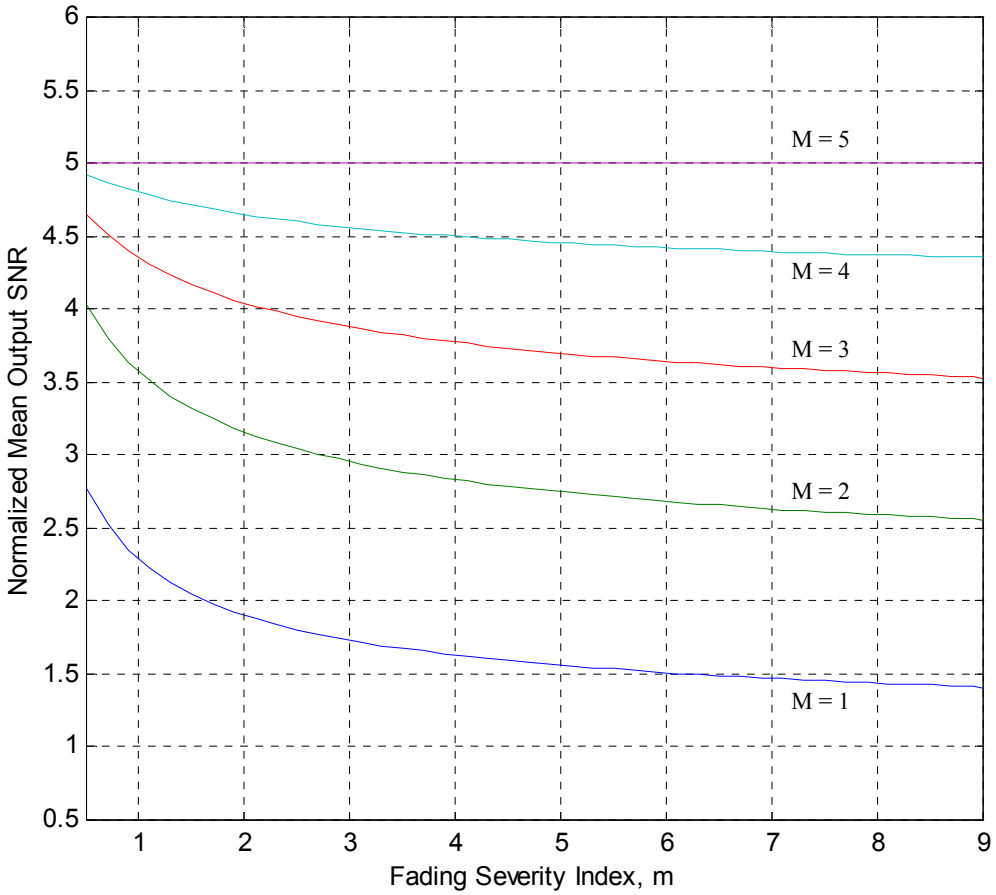

Figure 4.9 The normalized mean GSC(M, 5) output SNR versus the fading severity index of Nakagami-m channel for various selection of M.

Chapter 5

Generalized Selection Combining for i.i.d. Channels using Threshold Criterion

5.1 Introduction

The framework developed for GSC(M, L) receivers in i.i.d. channels in Chapter 4 can be further extended to formulate the Threshold GSC (T-GSC) receiver which overcomes the disadvantages of the GSC(M, L) receivers. In a severly faded channel, all the M branches in a GSC(M, L) receiver need not have high SNRs. Thus, it is possible to discard some of the M branches which do not significantly contribute to the total energy at the output of the combiner. Similarly, in an extremely good channel, combining only the first M paths with the highest SNRs may result in the exclusion of the L-M branches which may contribute significant energy to the output. The idea for a threshold based GSC receiver was first proposed in [44] by Suleman and Kousa. The major thrust of this approach was to do away with the idea of fixing the M number of branches which are combined in a GSC(M, L) receiver. Thus, depending on the channel conditions, a T-GSC receiver has the capability to increase or decrease the number of branches which need to be combined. The decision on the number of branches to be combined is based on the threshold factor μ, where $0 \leq \mu \leq 1$. Only those branches which have a normalized SNR (ratio of the instantaneous SNR of each branch to the max SNR from all the branches) higher than μ are used by the combiner.

Reviewing the literature presented on this topic over the past few years, the analytical results of T-GSC receiver presented in [45] dealt with only Rayleigh fading channels. In [44], the simulation results for T-GSC in Rayleigh and Nakagami-m fading channels were presented. However, a generalized approach applicable to all the common fading

channels has not yet been presented. In this chapter, we develop a mathematical framework for analyzing the performance of coherent and noncoherent T-GSC receivers in a variety of fading channels. The results presented in this chapter make heavy use of the MGF expressions developed in chapter 4. The combiner output statistics of T-GSC are discussed in Section 5.2. Two methods, both resulting in the same expression, have been presented for obtaining the T-GSC performance curves. The results for T-GSC are presented in Section 5.3 and the chapter concludes with Section 5.4.

5.2 T-GSC Combiner Output Statistics

The i.i.d. random variables $\gamma_1, \gamma_2, \ldots, \gamma_L$ representing the individual SNR per branch are again ordered such that $\gamma_1 \le \gamma_2 \le \ldots \le \gamma_L$. It is important to note that while γ_1 represented the branch with the highest SNR in the GSC(M, L) problem formulation in chapter 4, it denotes the lowest SNR branch for T-GSC. The re-ordering is just a matter of terminology and helps in making the problem mathematically tractable.

Since the number of combined branches for T-GSC is determined by the threshold factor μ, the instantaneous T-GSC(μ, L) output SNR can be given as follows.

$$\gamma_{Tgsc} = \sum_{k=1}^{L} w_k \gamma_{gsc} \tag{5.1}$$

where, $w_k = \begin{cases} 1 & \text{if } (\gamma_k \ge \mu\gamma_L) \\ 0 & \text{otherwise} \end{cases}$. Thus only those branches which have a branch SNR higher than a fraction μ of the maximum SNR are included in the combiner. The GSC(M, L) combiner output SNR γ_{gsc} is slightly modified from chapter 4 and is given as $\gamma_{gsc} = \sum_{k=L-M+1}^{L} \gamma_k$.

The sum $M = \sum_{k=1}^{L} w_k$ is a random variable with $1 \le M \le L$. As such, the scheme may be viewed as a conventional GSC(M, L) receiver whose number of paths being combined M is random rather than fixed. Recognizing this, it is apparent that by using a weighted sum of the GSC(k, L) combiner output statisics with the probability of selecting k number of branches, the PDF, CDF and MGF of the T-GSC(μ, L) receiver can be easily obtained. The MGF for the T-GSC(μ, L) can therefore be given as follows.

$$\phi_{\gamma_{Tgsc}} = \sum_{k=1}^{L} Pr(M = k)\phi_{\gamma_{gsc}}(s, k, L) \tag{5.2}$$

Once the MGF for T-GSC is obtained, it is trivial to obtain the error rate, mean SNR and outage probability performances. For instance, the average symbol error probability can

be given as

$$\bar{P}_{s_{Tgsc}}(\mu, L) = \sum_{k=1}^{L} Pr(M = k)\bar{P}_{s_{gsc}}(M = k, L) \tag{5.3}$$

The expressions for $\phi_{\gamma_{gsc}}(s, k, L)$ and $\bar{P}_{s_{gsc}}(k, L)$ can be easily obtained from the developments in Chapter 4.

The solution of Eq (5.2) and Eq (5.3) therefore depends on the solution for $Pr(M = k)$. The selection of the number of paths M can be expressed in the form of following cases:

(a) If $\gamma_1 \geq \mu\gamma_L$, then $M = L$,

(b) If $\gamma_2 \geq \mu\gamma_L$, then $M = L$-1,

(c) In general, if $\gamma_{L-k+1} \geq \mu\gamma_L$ and $\gamma_{L-k} < \mu\gamma_L$, then $M = k$. (5.4)

The representations as stated in Eq (5.4) are essential to the solution of the T-GSC combiner statistics. It is noted that T-GSC(0, L)and T-GSC(1, L) correspond to the classical MRC and selection combining schemes respectively. The following sub-sections present the two possible methods for evaluating $Pr(M = k)$.

5.2.1 Method I: Using First Principles

Using the relations in Eq (5.4), the probability $Pr(M = k)$ can be expressed as follows.

$$Pr(M = k) = L!\int_0^{\infty} f(x_L) \int_{\mu x_L}^{x_L} f(x_{L-1}) \int_{\mu x_L}^{x_{L-1}} f(x_{L-2}) \ldots \int_{\mu x_L}^{x_{L-k+2}} f(x_{L-k+1})$$

$$\text{X} \left[\int_0^{\mu x_L} f(x_{L-k}) \int_0^{x_{L-k}} f(x_{L-k-1}) \ldots \int_0^{x_2} f(x_1) dx_1 \ldots dx_{L-k} \right] dx_{L-k+1} \ldots dx_L \tag{5.5}$$

Recognizing that the multivariate integral can be transformed into a product of univariate integrals and using the result (A.1) from the Appendix, we have,

$$Pr(M = k) = L!\int_0^{\infty} f(x_L) \int_{\mu x_L}^{x_L} f(x_{L-1}) \int_{\mu x_L}^{x_{L-1}} f(x_{L-2}) \ldots \int_{\mu x_L}^{x_{L-k+2}} f(x_{L-k+1}) \frac{[F(\mu x_L)]^{L-k}}{(L-k)!} dx_{L-k+1} \ldots dx_L$$

$$Pr(M = k) = \frac{L!}{(L-k)!} \int_0^{\infty} f(x_L)[F(\mu x_L)]^{L-k} \left[\int_{\mu x_L}^{x_L} f(x_{L-1}) \ldots \int_{\mu x_L}^{x_{L-k+2}} f(x_{L-k+1}) \right] dx_{L-k+1} \ldots dx_L$$

Again utilizing result (A.1), we finally obtain

$$Pr(M = k) = k\binom{L}{k}\int_0^{\infty}[F(\mu x_L)]^{L-k}[F(x_L) - F(\mu x_L)]^{L-1} f(x_L)dx_L \tag{5.6}$$

5.2.2 Method II: Using results from Order Statistics

Considering the joint PDF of $\gamma_{L-k}, \gamma_{L-k+1}$ and γ_L in Eq (5.4) as $f(x, y, z)$, where $x = \gamma_{L-k}, y = \gamma_{L-k+1}, z = \gamma_L$, $Pr(M = k)$ can be evaluated as

$$Pr(M = k) = \int_{(z=0)}^{(z=\infty)} \int_{(y=\mu z)}^{(y=z)} \int_{(x=0)}^{(x=\mu z)} f(x, y, z)dxdydz \tag{5.7}$$

From [46], we get the identity

$$f(x, y, z) = \frac{L!}{(L-1-k)!(k-z)!}[F(x)]^{L-k-1}[F(z) - F(y)]^{k-z} f(x)f(y)f(z) \tag{5.8}$$

where $0 < x < y < z < \infty$, *f(.)* and *F(.)* being the PDF and CDF respectively.

Using Eq (5.8) and the noting that $\frac{dF(x)}{dx} = f(x)$, we can simplify the above equation as

$$Pr(M = k) = \frac{L!}{(L-k)!(k-z)!}\int_0^{\infty}\int_{\mu z}^{z}[F(\mu z)]^{L-k}[F(z) - F(y)]^{k-z} f(y)f(z)(dy)(dz) \tag{5.9}$$

Using the variable substitution *F(z) - F(y) = t,* we can simplify the above expression as follows:

Let $I = \int_{\mu z}^{z}[F(z) - F(y)]^{k-z} f(y)dy$,

$$\therefore I = \int_0^{(F(z)-F(y))} t^{k-z}dt = \frac{[F(z) - F(\mu z)]^{k-1}}{k-1}$$

Substituting the above result in Eq (5.9), we finally get,

$$Pr(M = k) = \frac{L!}{(L-k)!(k-1)!}\int_0^{\infty}[F(\mu z)]^{L-k}[F(z) - F(\mu z)]^{k-1} f(z)dz \tag{5.10}$$

$$Pr(M = k) = k\binom{L}{k}\int_0^{\infty}[F(\mu z)]^{L-k}[F(z) - F(\mu z)]^{k-1} f(z)dz \tag{5.11}$$

Replacing z with γ_L, we obtain $Pr(M = k) = k\binom{L}{k}\int_0^{\infty}[F(\mu\gamma_L)]^{L-k}[F(\gamma_L) - F(\mu\gamma_L)]^{k-1} f(\gamma_L)d\gamma_L$.

We note that Eq (5.6) and Eq (5.11) are similar.

Eq (5.3) along with Eq (5.11) can therefore be used to obtain the error performance

curves for T-GSC(μ, L) receivers for different modulation schemes and in different fading channels.

5.3 Results for Threshold GSC

Figure 5.1 and Figure 5.2 illustrate the error probabilities for different threshold levels in Rician and Nakagami-m fading channels using the T-GSC receiver with BPSK and QPSK modulation schemes respectively. All the BER plots are constricted between the threshold values of 1 and 0, which represent the conditions of Selection Combining (SC) and Maximum Ratio Combining (MRC) respectively. For a fixed value of ASNR/symbol/branch, as the threshold level (μ) decreases, the probability of including an additional diversity increases and hence a decrease in the error probabilities is observed. For an ABER of 10^{-6} in Figure 5.1, the diversity gains obtained with respect to selection combining for $\mu = 0.5$ and $\mu = 0.25$ are found to be 1.2 dB and 3 dB respectively.

The performance improvement obtained with increasing ASNR/symbol/branch is more at lower threshold values as compared to the higher threshold values. We note from Figure 5.2 that for an increase in ASNR/symbol/branch from 5 dB to 10 dB, the rate of decrease in the error probabilities is higher for the threshold values of $\mu = 0, 0.2$ compared to $\mu = 0.8, 1$. In T-GSC, the number of branches that are combined for a given threshold value are variable and depend on the channel conditions. At lower threshold levels, increasing the ASNR/bit/branch increases the number of branches which have signals levels greater than μ. However, increasing the ASNR/bit/symbol at higher threshold levels does not give as high a performance improvement because the threshold values are already so high that even increasing the ASNR/bit/branch does not overcome the high threshold.

Figure 5.3 shows the variation of average symbol error probability in Rician faded channels for a T-GSC, QPSK modulated receiver with a fixed value of ASNR/symbol/branch = 10 dB. The plots for $\mu = 1$ and 0 coincide with the plots for SC and MRC respectively and bound the plots for other threshold values. Not only does the symbol error probability decrease as the channel improves, but the slope of the decreasing error probability also increases with decreasing threshold levels. Though lowering of threshold levels in severely faded channels does improve the error performance, the improvement is not as high as the improvement observed at higher values of K. For example, as the threshold changes from $\mu = 0.7$ to $\mu = 0.15$, the ASER decreases from 3×10^{-5} to 5×10^{-7}

(by an order of 10^{-2}) at K = 2 and from $8x10^{-6}$ to $4x10^{-9}$ (by an order of 10^{-3}) at K = 5.

Figure 5.4a, b illustrate the average bit error probability for T-GSC(μ ,5) with both, coherent and non-coherent DQPSK modulation schemes in Nakagami-m channel with a fading coefficient m = 1.75. The difference between the coherent and non-coherent curves diminishes as the average SNR/bit/branch increases. Comparison between Figure 5.4a and Figure 5.4b reveals that, depending on the threshold factor, the performance difference between the coherent and non-coherent DQPSK modulation schemes can be much less in T-GSC scheme as compared to the GSC scheme. This behavior can be attributed to the weight contribution for each of the possible diversities in T-GSC (see Figure 5.5b). We also observe that under the condition of i.i.d. diversity branches, high branch SNRs and small diversity orders, there is not much benefit realized by using coherent reception with T-GSC. For a threshold of m = 0.4 in Figure 5.4b, the error rates with coherent and non-coherent receivers are similar for ASNR/bit/branch values greater than 9 dB.

Figure 5.5a-c plot the diversity selection probabilities against the threshold factors for a given fading channel. For a zero threshold level, the probability of selecting all the branches is 1 and as the threshold factor tends to 1, only the strongest branch is selected. At higher threshold levels, the probability of combining large number of diversity paths increases with improving channel conditions. For severely faded channels (Figure 5.5a), with a fixed, high value of threshold factor, the probability of selecting higher number of branches is lesser compared to the diversity selection probability for less severely faded channels (Figure 5.5c). This is expected, because as the channel improves, the number of branches having signal levels greater than the threshold also increases and hence we can expect the probability of selecting higher number of branches at higher thresholds to be higher for less severely faded channels.

The effect of increasing the number of antenna elements on the average bit error probabilities and threshold levels for BPSK modulation (ASNR/bit/branch = 10 dB) are shown in Figure 5.6. Each additional antenna element increases the maximum available diversity and hence decreases the bit error probability. With increasing threshold, the bit error probability increases because the number of branches which fall above the threshold decrease. Therefore, the improvement obtained with each extra element is reduced at higher threshold levels. The tradeoff in setting the μ and L values can be observed in Figure . An ABER of 10^{-6} can be obtained with either T-GSC(0.1, 4), T-GSC(0.4, 5) or T-

GSC(0.6, 6).

Figure 5.7b shows the normalized output SNR variations in a Nakagami-m fading channel for different threshold levels. The figure is remarkably different from the normalized output SNR figures for GSC(M, L) (Figure 5.7a). Even though the output SNR decreases with fading coefficient m for $\mu = 0.9$, it increases for $\mu = 0.15$. This supposedly abnormal behavior can be attributed to the behavior of the weighing factors which are illustrated in Figure 5.5a-c. For high values of μ the probability of selecting large number of branches is less. However, for lower values of μ the probability of selecting large number of branches is high and hence the weighting factors are high. For higher values of fading index m, the chances of selecting all the branches at lower threshold levels are even higher. The normalized output SNR therefore increases for lower threshold levels and decreases for higher threshold levels.

Figure 5.8 depicts the outage probability plots for a T-GSC(μ, 5) receiver for a normalized ASNR (K = 3). For a minimum instantaneous SNR value of $Pe^* = 10^{-3}$, the threshold SNR for BPSK, $\gamma^* = [\text{erfc}^{-1}(2 \times 10^{-3})]^2 = 4.77$. For an outage probability of $P_{out} = 10^{-2}$, the mean SNR/symbol/branch for T-GSC(0.2, 5) is $\Omega_{0.2} = 4.77(10^{-0.23}) = 4.49$ dB, and $\Omega_{0.4} = 4.77(10^{-0.5}) = 1.79$ dB for T-GSC(0.4, 5). Thus, to achieve the same outage probability of 10^{-2} for BPSK, a T-GSC(μ,5) receiver requires 2.7 dB higher ASNR/symbol/branch at $\mu = 0.4$ compared to $\mu = 0.2$. As was the case in all other plots, the outage probability curves are also upper and lower bounded by the SC and MRC cases.

5.4 Chapter Conclusion

The T-GSC(μ, L) receiver structure can overcome the disadvantages of a GSC(M, L) receiver. In this chapter we developed the framework for the analysis of T-GSC receivers in a myriad of propagation channels and modulation schemes. It was recognized that by treating the number of paths included at the combiner as a random variable, the T-GSC performance can easily be predicted using the GSC framework. Two methods of deriving the weighting coefficients were presented in Section 5.2. The results presented in this chapter are applicable only for i.i.d. fading channels, though it may be possible to extend the results to the i.n.d. fading environments. The importance of using T-GSC scheme particularly for noncoherent GSC receivers will be glaringly visible based on the performance of noncoherent GSC receivers in i.n.d. fading channels. A detailed analysis of the GSC(M, L) receiver performance in i.n.d. fading channels follows in the next chapter.

Appendix

This appendix provides a useful identity which aids in the transformation of multivariate nested integrals that arise in the computation of $\phi_{\gamma_{gsc}}(s, k, L)$ and $Pr(M = k)$ into a product of univariate integrals.

We begin by defining the term $I_{M-1}(x_M, a)$ as follows:

$$I_{M-1}(x_M, a) = \int_a^{x_M} f(x_{M-1}) \ldots \int_a^{x_2} f(x_1) dx_1 \ldots dx_{M-1} \text{ where } M \geq 2. \tag{A.1}$$

For M = 2, $I_1(x_2, a) = \underset{x_3}{F}(x_2) - \underset{x_2}{F}(a)$

For M = 3, $I_2(x_3, a) = \int_a f(x_2) \int_a f(x_1) dx_1 dx_2$

Using the identity of integration by parts, where $\int_a^b [g(x)]^n g'(x) dx = \frac{[g(b)]^{n+1} - [g(a)]^{n+1}}{n+1}$, $I_2(x_3, a)$ can be simplified to the following expression.

$$I_2(x_3, a) = \frac{[F(x_3) - F(a)]^2}{2}$$

Generalizing for any value of M, the identity can be expressed as follows:

$$I_{M-1}(x_M, a) = \frac{[F(x_M) - F(a)]^{M-1}}{(M-1)!} \tag{A.2}$$

We try to validate the above expression using the method of induction.

Assuming Eq (A.2) holds for M = D-1, we obtain

$$I_{D-2}(x_{D-1}, a) = \frac{[F(x_{D-1}) - F(a)]^{D-2}}{(D-2)!} \tag{A.3}$$

Using the definition given in (A.1) for M = D,

$$I_{D-1}(x_D, a) = \int_a^{x_D} f(x_{D-1}) \frac{[F(x_{D-1}) - F(a)]^{D-2}}{(D-2)!} dx_{MD-1} \tag{A.4}$$

$$\therefore I_{D-1}(x_D, a) = \frac{[F(x_D) - F(a)]^{D-1}}{(D-1)!}$$

thereby implying that Eq (A.2) holds true for any $M = D \geq 2$.

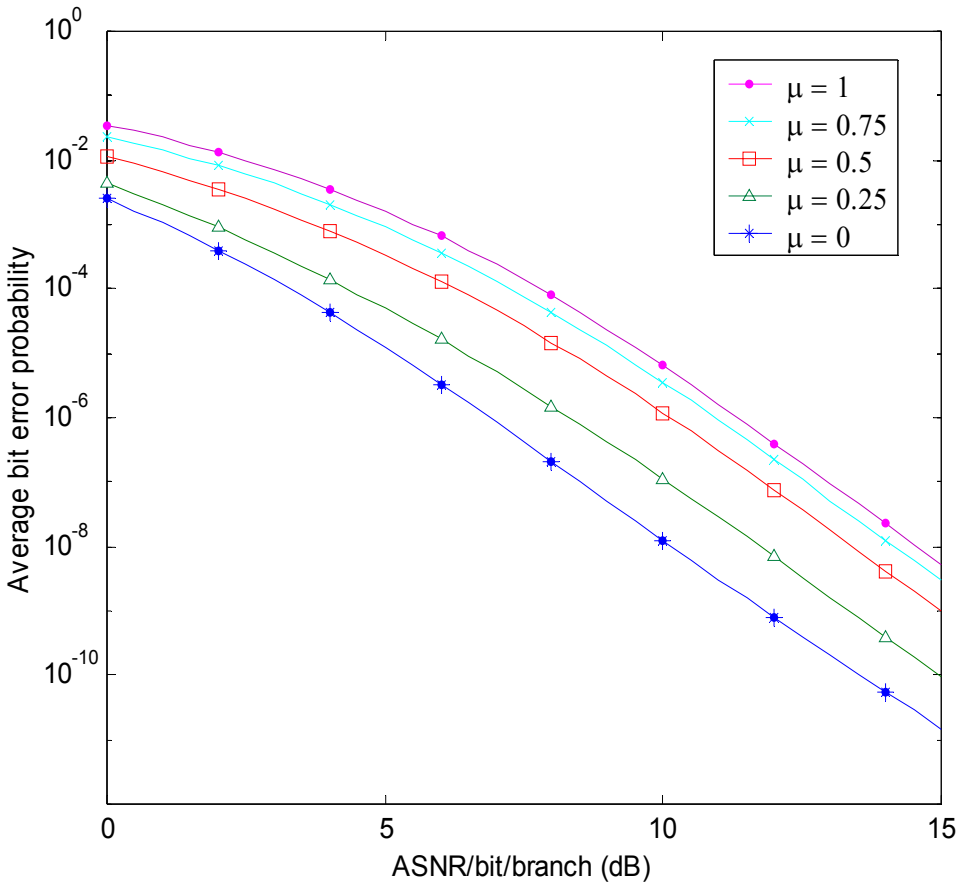

Figure 5.1 Average bit error probability versus ASNR/bit/branch for BPSK modulation with T-GSC(μ ,5) scheme in a Rician fading channel, K = 2.5.

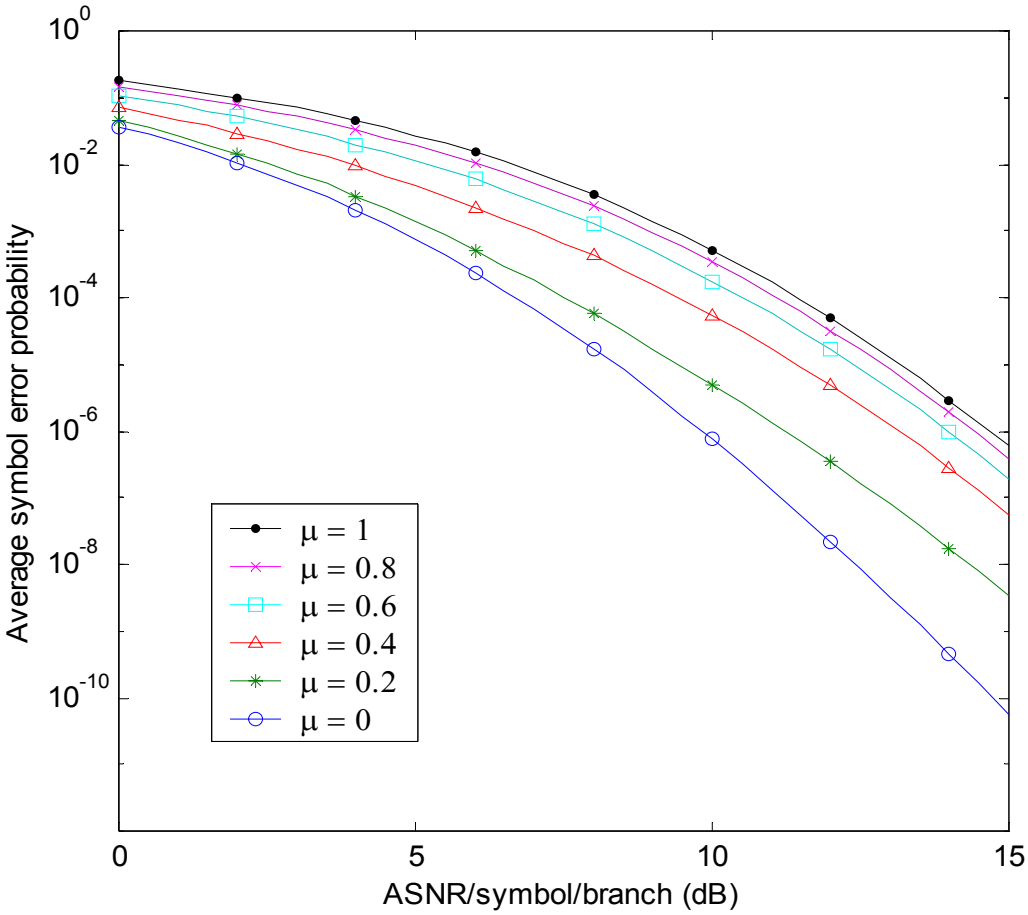

Figure 5.2 Average symbol error probability versus ASNR/symbol/branch for QPSK modulation with T-GSC(μ, 5) scheme in a Nakagami-m fading channel, m = 2.

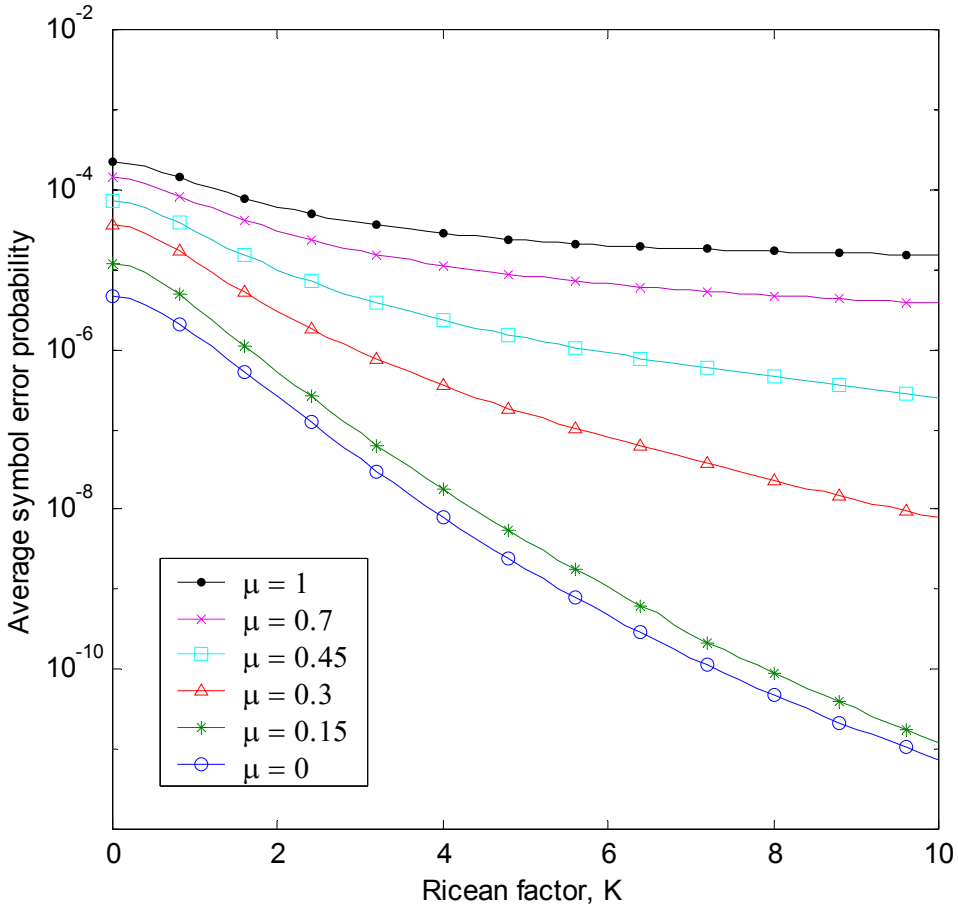

Figure 5.3 Average symbol error probability versus the Rician factor K for QPSK modulation with T-GSC(μ, 5), ASNR/symbol/branch = 10 dB.

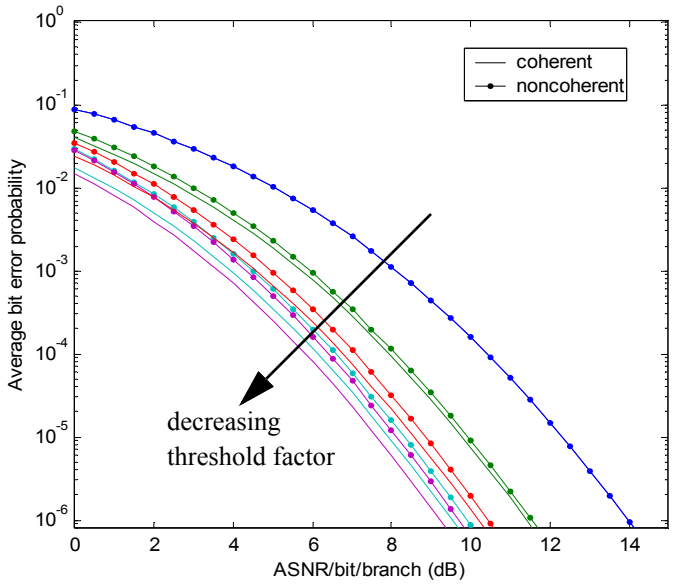

(a)

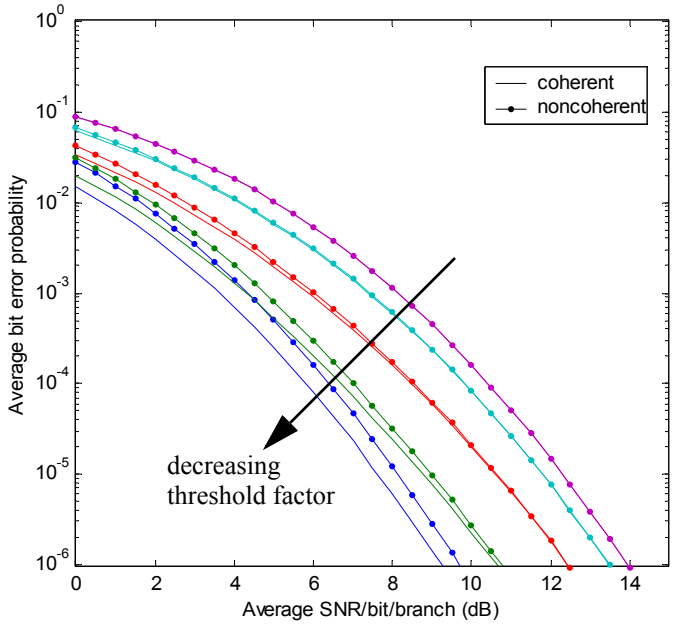

(b)

Figure 5.4 Average bit error probability versus the Average SNR/bit/branch with DQPSK modulation in a Nakagami-m fading channel, m = 1.75 for (a) GSC(M,5) scheme and, (b) T- GSC(μ, L) scheme μ = 0, 0.2, 0.4, 0.7, 1.

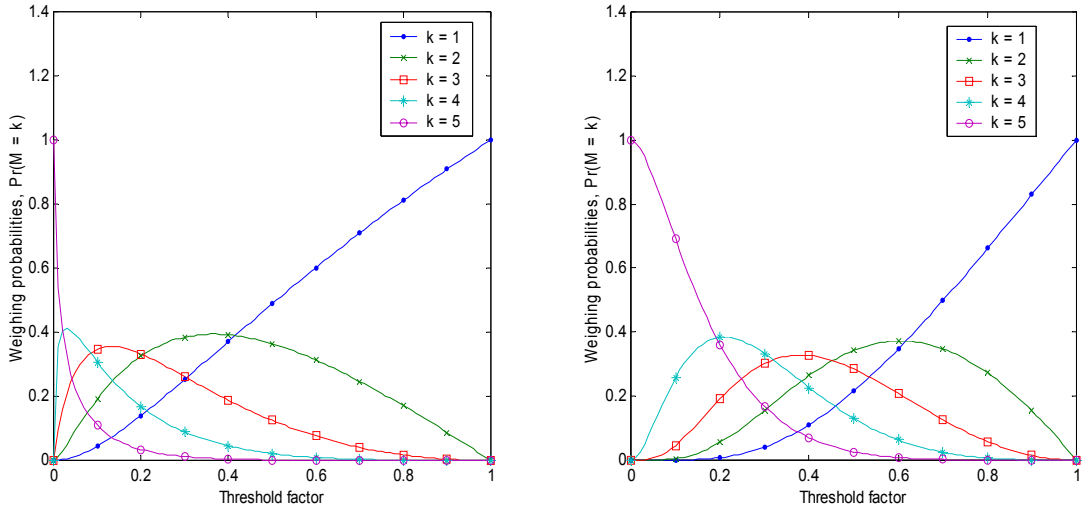

(a) (b)

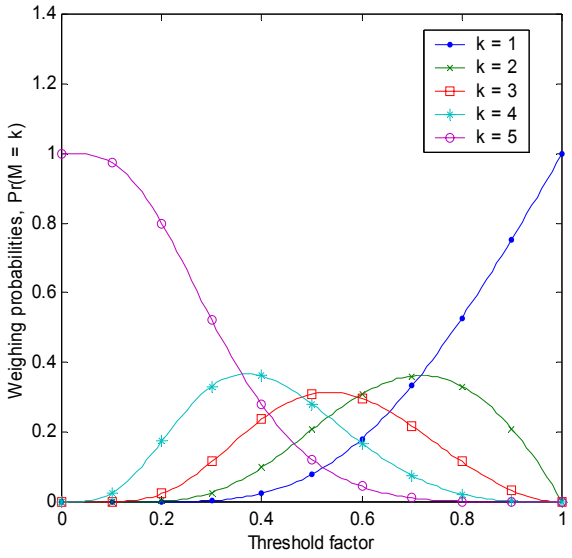

(c)

Figure 5.5 Variation of diversity selection probability with the threshold factors for different Nakagami-m fading channels for (a) m = 0.5, (b) m = 1.75, (c) m = 4.

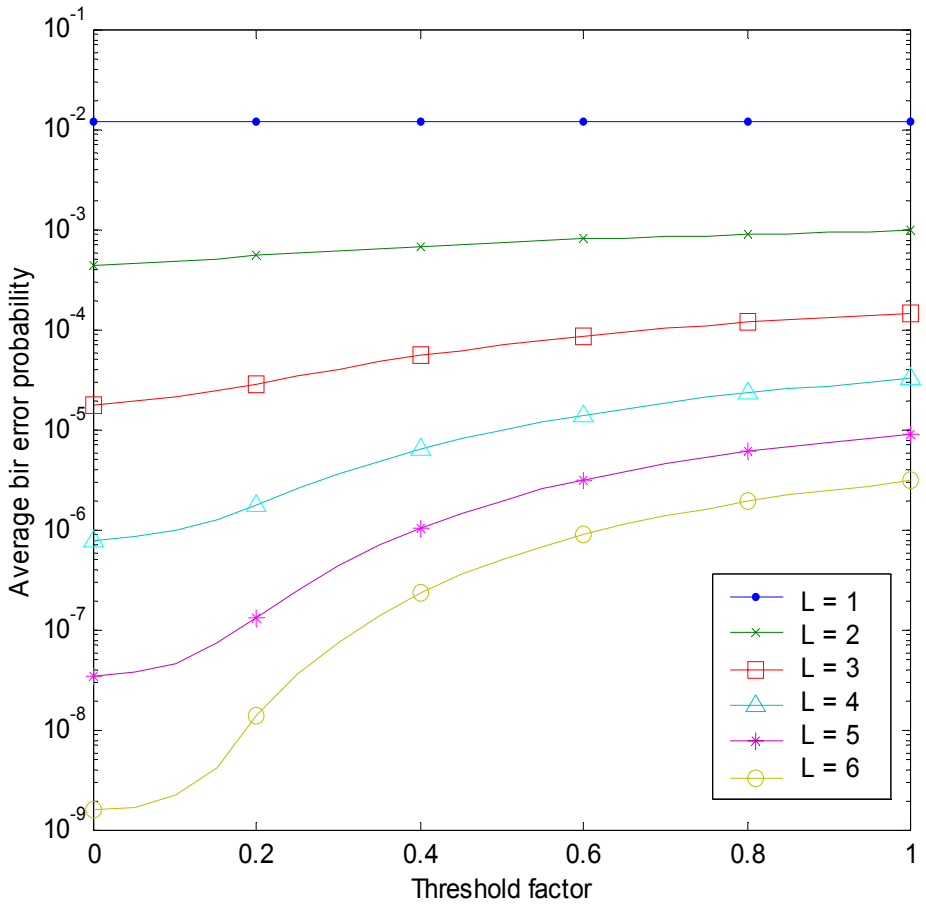

Figure 5.6 Average bit error probability versus threshold factor for a T-GSC scheme, in a Rician fading channel (K = 2), with BPSK modulation. ASNR/bit/branch = 10 dB, L = 1, 2, 3, 4, 5, 6.

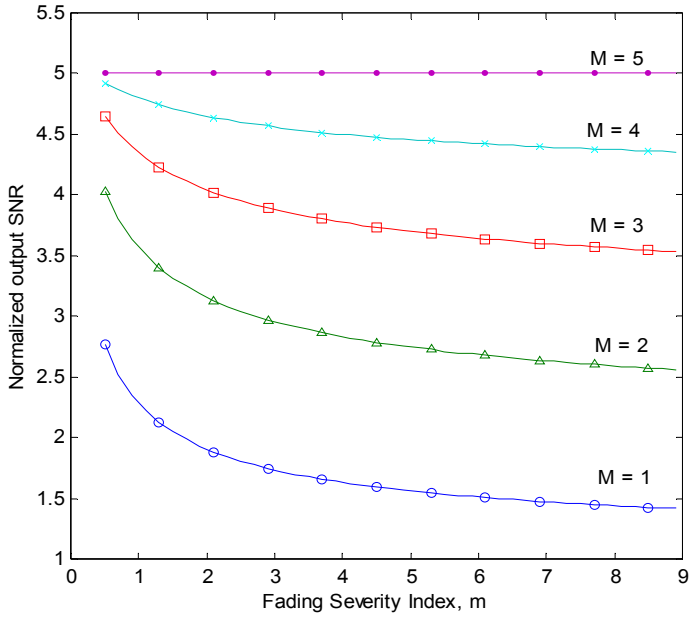

(a)

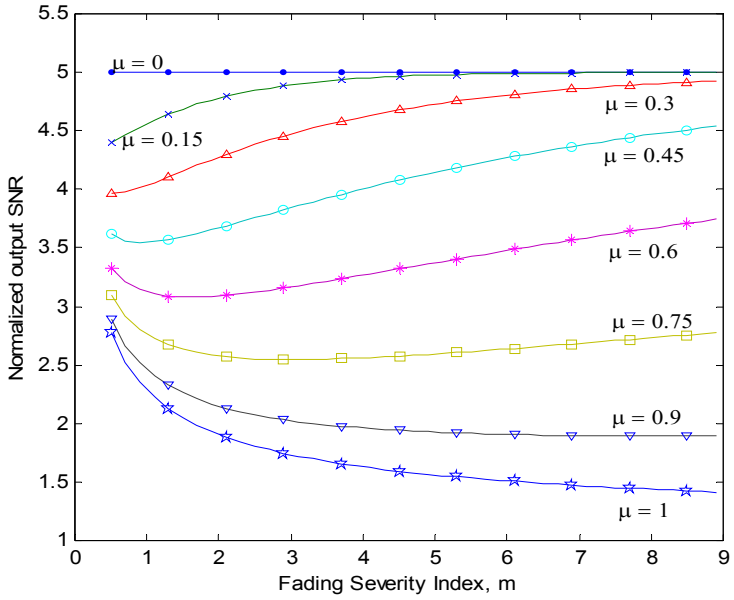

(b)

Figure 5.7 Normalized output SNR versus fading coefficient m in a Nakagami-m fading channel for (a) GSC(M,5) scheme and (b) T-GSC(μ ,5) scheme, μ = 0, 0.15, 0.3, 0.45, 0.6, 0.75, 0.9, 1.

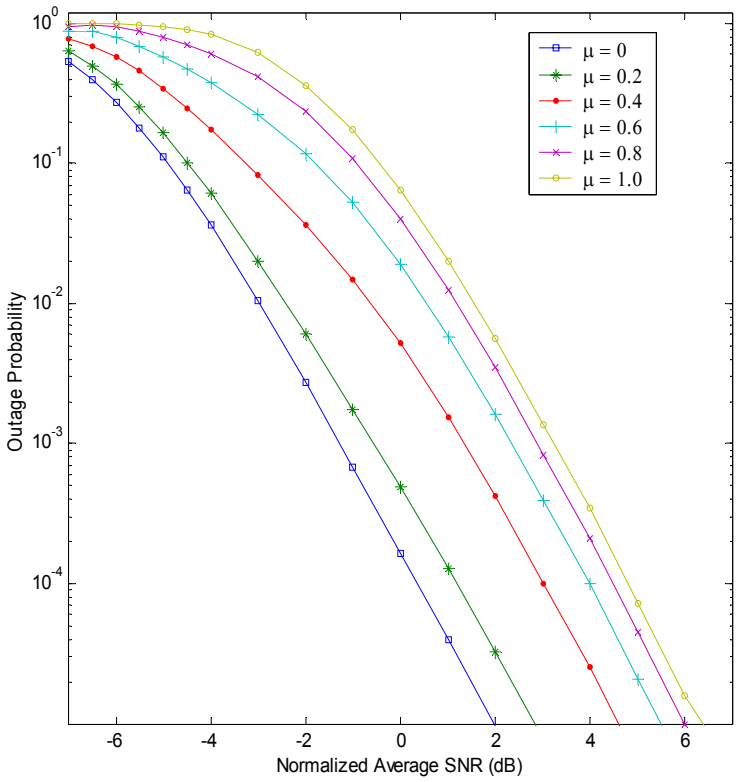

Figure 5.8 Outage probability versus the normalized average SNR for T-GSC(μ, 5) receiver on a Rician channel with K = 3.

Chapter 6

Performance of Generalized Selection Combining Schemes in i.n.d. Channels

6.1 Introduction

In Chapters 4 and 5 we studied the performance of the $\mathrm{GSC}(M, L)$ and T-GSC receivers under various fading conditions and modulation schemes. The analysis was however applicable only for i.i.d. fading channels. Expecting the channel conditions to be identical over the different signal paths is too optimistic and unrealistic in the real world. This chapter therefore develops a framework for the performance of $\mathrm{GSC}(M, L)$ in independent but non-identical (i.n.d.) channels conditions, a more realistic scenario in the real-world.

Though the literature on $\mathrm{GSC}(M, L)$ has been quite extensive, only a few of these contributions have examined the effects of i.n.d fading statistics on the receiver performance. In [20], a general formula for the Moment Generating Function (MGF) of $\mathrm{GSC}(M, L)$ output SNR is derived for the i.n.d Rayleigh fading case. The joint Probability Density Function (PDF) of the ordered instantaneous SNRs in descending order of magnitude, derived in [18], is used for studying the average output SNR and average error rates for a number of different modulation/detection schemes in i.n.d Rayleigh [23][25] and Nakagami-m [27][28][31] channels. In [28], the specific cases of $\mathrm{GSC}(2, 3)$ and $\mathrm{GSC}(2, 4)$ in conjunction with BPSK modulation scheme are treated for i.n.d Nakagami-m fading channels. In [27] and [31], the MGF of $\mathrm{GSC}(M, L)$ output SNR in i.n.d Nakagami-m fading channels is computed via an M-fold nested integral. This

approach, however, is not desirable for numerical computation when M gets large. This motivates us to derive a general yet simple-to-evaluate formula for the MGF similar to [33]-[39], but for the i.n.d case (including the mixed-fading scenario). Such an analysis is important in view of the practical statistical channel models [47]-[48], developed from the empirical data (field measurements), which indicate that the different multi-paths in the ultra-wideband and UMTS channels have i.n.d fading statistics.

In this chapter, we develop a novel mathematical framework for analyzing both coherent and noncoherent $\mathrm{GSC}(M, L)$ receiver performance over i.n.d generalized fading channels. The key to our solution is the transformation of a multivariate nested integral that arise in the computation of MGF of SNR into a product form of univariate integrals. We exploit this result to obtain computationally efficient formulas for the MGF, PDF and the CDF of $\mathrm{GSC}(M, L)$ output SNR, which in turn are used to characterize the average symbol error probability (ASEP) of different modulation/detection schemes, average SNR and outage probability metrics over generalized fading channels. Following the structures from the previous chapters, Section 6.2 discusses the development of the MGF for the receiver combiner output. Section 6.3 presents the results for the outage probability and the mean output SNR. The average symbol error performance of the GSC receiver in i.n.d. channels are discussed in Section 6.4. The work presented on GSC receivers in chapters 4, 5 and 6 have been integrated by using a Graphical User Interface (GUI). Section 6.5 demonstates the details of the GUI while the conclusion is presented in Section 6.6.

6.2 Derivation of the MGF of GSC(M, L) Combiner Output SNR

As in chapter 5, let $\gamma_1 \le \gamma_2 \le \ldots \le \gamma_L$ represent the order statistics obtained by arranging the instantaneous SNRs in increasing order of magnitude. We therefore have $\gamma_{\mathrm{gsc}} = \sum_{k=L-M+1}^{L} \gamma_k$ as the $\mathrm{GSC}(M, L)$ output SNR. As in previous cases, we are particularly interested in evaluating the MGF and the CDF of γ_{gsc} because the mean of $\mathrm{GSC}(M, L)$ out-

put SNR, outage probability and ASEP performance metrics of a variety of digital modulation/detection schemes can be computed using these quantities alone.

In [49], it is shown that the joint PDF of order statistics $\gamma_1 \le \gamma_2 \le \ldots \le \gamma_L$ at $x_1, x_2, \ldots, x_L$ is given by

$$f_{\gamma_{1:L}, \gamma_{2:L}, \ldots, \gamma_{L:L}}(x_1, \ldots, x_L) = \begin{vmatrix} f_1(x_1) & f_2(x_1) & \ldots & f_L(x_1) \\ f_1(x_2) & f_2(x_2) & \ldots & f_L(x_2) \\ \vdots & \vdots & \vdots & \vdots \\ f_1(x_L) & f_2(x_L) & \ldots & f_L(x_L) \end{vmatrix}^{+}, \quad 0 \le x_1 < x_2 < \ldots < x_L < \infty \tag{6.1}$$

where notation $|A|^{+}$ or $per([A])$ denotes the permanent of a square matrix A. The permanent, also known as plus determinant in the statistical literature, is computed similar to the determinant except that all signs are positive. For example, permanent of a 2×2 matrix and a 3×3 matrix are illustrated below:

$$per\left(\begin{bmatrix} a_{11} & a_{12} \\ a_{21} & a_{22} \end{bmatrix}\right) = a_{11}a_{22} + a_{12}a_{21}$$

$$per\left(\begin{bmatrix} a_{11} & a_{12} & a_{13} \\ a_{21} & a_{22} & a_{23} \\ a_{31} & a_{32} & a_{33} \end{bmatrix}\right) = a_{11}a_{22}a_{33} + a_{11}a_{23}a_{32} + a_{12}a_{21}a_{33} + a_{12}a_{23}a_{31} + a_{13}a_{21}a_{32} + a_{13}a_{22}a_{31}$$

More generally, for $n \times n$ matrix $A = [a_{ij}]$, we have [50]

$$per(A) = \sum_{\sigma \in S_n} \prod_{i=1}^{n} a_{i\sigma(i)} \tag{6.2}$$

where S_n is the set of all permutations of integers $\{1, 2, \ldots, n\}$ and $\sigma \in S_n$ denotes the specific function $\sigma = (\sigma(1), \sigma(2), \ldots, \sigma(n))$ which permutes the integers $\{1, 2, \ldots, n\}$. For example, $S_2 = \{(1, 2), (2, 1)\}$, $S_3 = \{(1, 2, 3), (1, 3, 2), (2, 1, 3), (2, 3, 1), (3, 1, 2), (3, 2, 1)\}$ and so on. The cardinality of S_n is equal to $n!$. The process of constructing all members of S_n is recursive and most mathematical packages have explicit commands for this purpose. For instance, S_n is constructed by the command *perms*([1,2,...,n]) in MATLAB.

Combining Eq. (6.1) and Eq. (6.2), we obtain a very compact representation for the joint PDF of $\gamma_1, \gamma_2, \ldots, \gamma_L$:

$$f_{\gamma_1, \ldots, \gamma_L}(x_1, \ldots, x_L) = \sum_{\sigma \in S_L} \prod_{i=1}^{L} f_{\sigma(i)}(x_i), \quad 0 \le x_1 < x_2 < \ldots < x_L < \infty \tag{6.3}$$

Recognizing that the MGF of GSC(M, L) output SNR, $\phi_{\gamma_{\text{gsc}}}(.)$, is the key to unified analysis of many modulation/detection schemes over fading channels as in the previous chapters, our immediate intention will be to derive the desired MGF first. Therefore, we are interested in computing

$$\phi_{\gamma_{\text{gsc}}}(s) = E\left[\exp\left(-s \sum_{i=L-M+1}^{L} \gamma_i\right)\right], \quad s \ge 0 \tag{6.4}$$

which can be written as

$$\phi_{\gamma_{\text{gsc}}}(s) = \sum_{\sigma \in S_L} \int_{0 \le x_1 < x_2 < \ldots < x_L < \infty} \cdots \int e^{-s \sum_{i=L-M+1}^{L} x_i} \prod_{i=1}^{L} f_{\sigma(i)}(x_i) dx_L dx_{L-1} \ldots dx_1 \tag{6.5}$$

While the unordered instantaneous SNRs are independent, the ordered γ_i's are not, as can be seen from Eq. (6.1). Therefore, the expectation operation in Eq. (6.4) generally involves complexity of $L!$ computations of L-fold nested integral as depicted in Eq. (6.5). However, it is possible to simplify and speed-up the computation of Eq. (6.5) by exploiting the integral identities (A.2) and (A.9). This directly leads to the development of two generic formulas for the MGF of γ_{gsc} over generalized fading channels (including the mixed-fading scenario):

$$\phi_{\gamma_{\text{gsc}}}(s) = \sum_{\sigma \in T_{L,M}} \int_0^{\infty} e^{-sx} f_{\sigma(L-M+1)}(x) \left[\prod_{i=1}^{L-M} F_{\sigma(i)}(x)\right] \left[\prod_{k=L-M+2}^{L} \phi_{\sigma(k)}(s, x)\right] dx, \quad 1 \le M \le L \tag{6.6}$$

$$\phi_{\gamma_{\text{gsc}}}(s) = \sum_{\sigma \in T_{L,M+1}} \int_0^{\infty} f_{\sigma(L-M)}(x) \left[\prod_{i=1}^{L-M-1} F_{\sigma(i)}(x)\right] \left[\prod_{k=L-M+1}^{L} \phi_{\sigma(k)}(s, x)\right] dx, \quad 1 \le M < L \tag{6.7}$$

where $\sum_{\sigma \in T_{L,M}} = \sum_{\substack{\sigma \in S_L, \sigma(1) < \sigma(2) < \ldots < \sigma(L-M) \\ \sigma(L-M+2) < \ldots < \sigma(L)}}$.

The construction of $T_{L,M}$ is also not difficult (i.e., it can be implemented within a few command lines in MATLAB). It should be emphasized that both Eq. (6.6) and Eq. (6.7) involve only one-dimension integration (instead of L-dimension integration as in Eq. (6.5)) because the integrand can be evaluated term by term for different x. Two exam-

ples are provided below to illustrate the developments of Eq. (6.6) and Eq. (6.7) and also to highlight the key intermediate steps in the derivation of the general case.

Example 1:

Suppose $L = 4$ and $N = 2$. Substituting these values in Eq. (6.5), we obtain

$$\begin{aligned}\phi_{\gamma_{\text{gsc}}}(s) &= \sum_{\sigma \in S_4} \int_0^{\infty} e^{-sx_4} f_{\sigma(4)}(x_4) \int_0^{x_4} e^{-sx_3} f_{\sigma(3)}(x_3) \int_0^{x_3} f_{\sigma(2)}(x_2) \int_0^{x_2} f_{\sigma(1)}(x_1) dx_1 \ldots dx_4 \\ &= \sum_{\sigma \in S_4,\, \sigma(1) < \sigma(2)} \int_0^{\infty} e^{-sx_4} f_{\sigma(4)}(x_4) \int_0^{x_4} e^{-sx_3} f_{\sigma(3)}(x_3) \prod_{i=1}^{2} F_{\sigma(i)}(x_3) dx_3 dx_4\end{aligned} \tag{6.8}$$

with the aid of identity (A.2). Rearranging the order of integration in Eq. (6.8) yields

$$\phi_{\gamma_{\text{gsc}}}(s) = \sum_{\sigma \in T_{4,2}} \int_0^{\infty} e^{-sx_3} f_{\sigma(3)}(x_3) \left[\prod_{i=1}^{2} F_{\sigma(i)}(x_3) \right] \phi_{\sigma(4)}(s, x_3) dx_3 \tag{6.9}$$

where

$T_{4,2} = \{(3,4,2,1), (2,4,3,1), (2,3,4,1), (3,4,1,2), (1,4,3,2), (1,3,4,2), (2,4,1,3), (1,4,2,3), (1,2,4,3), (2,3,1,4), (1,3,2,4), (1,2,3,4)\}$. It should be emphasized that the construction of all permutations in the group $T_{L,M}$ can be automated using only four command lines in MATLAB. The derivation for other combinations of (M, L) can also be treated in a similar fashion, and the final expression will always take the form of Eq. (6.6).

Example 2:

Let us consider the derivation of the MGF of $\text{GSC}(2, 5)$ output SNR. In this case, Eq. (6.5) simplifies into

$$\begin{aligned}\phi_{\gamma_{\text{gsc}}}(s) &= \sum_{\sigma \in S_5} \int_0 f_{\sigma(1)}(x_1) \int_{x_1} f_{\sigma(2)}(x_2) \int_{x_2} f_{\sigma(3)}(x_3) \int_{x_3} e^{-sx_4} f_{\sigma(4)}(x_4) \int_{x_4} e^{-sx_5} f_{\sigma(5)}(x_5) dx_5 \ldots dx_1 \\ &= \sum_{\sigma \in S_5,\, \sigma(4) < \sigma(5)} \int_0^{\infty} f_{\sigma(1)}(x_1) \int_{x_1}^{\infty} f_{\sigma(2)}(x_2) \int_{x_2}^{\infty} f_{\sigma(3)}(x_3) \prod_{k=4}^{5} \phi_{\sigma(k)}(s, x_3) dx_3 dx_2 dx_1 \\ &= \sum_{\sigma \in S_5,\, \sigma(4) < \sigma(5)} \int_0^{\infty} f_{\sigma(3)}(x_3) \left[\prod_{k=4}^{5} \phi_{\sigma(k)}(s, x_3) \right] \int_0^{x_3} f_{\sigma(2)}(x_2) \int_0^{x_2} f_{\sigma(1)}(x_1) dx_1 dx_2 dx_3 \\ &= \sum \int_0^{\infty} f_{\sigma(3)}(x_3) \left[\prod_{k=4}^{5} \phi_{\sigma(k)}(s, x_3) \right] \left[\prod_{i=1}^{2} F_{\sigma(i)}(x_3) \right] dx_3\end{aligned} \tag{6.10}$$

by applying (A.9) and (A.2) to get the second and fourth line of Eq. (6.10) respectively. The final expression is in agreement with Eq. (6.7). The above approach and the results can be readily extended to any $M < L$. The special case of $M = L$ can also be analyzed readily using identity (A.2), viz.,

$$\phi_{\gamma_{\text{gsc}}}(s) = \sum_{\sigma \in S_L} \int_0^{\infty} e^{-sx_1} f_{\sigma(1)}(x_1) \ldots \int_{x_{L-1}}^{\infty} e^{-sx_L} f_{\sigma(L)}(x_L) dx_L \ldots dx_1 = \prod_{k=1}^{L} \phi_k(s) \tag{6.11}$$

since $\phi_k(s, 0) = \phi_k(s)$.

Since we have two distinct general formulas for computing the MGF of γ_{gsc}, it is instructive to compare the computational complexity (or speed) associated with Eq. (6.6) and Eq. (6.7) for different combinations of L and M values. The complexity of Eq. (6.6) is mainly dictated by the time required to compute $M\binom{L}{M}$ one-dimensional integrals because the cardinality of set $T_{L,M}$ is equal to $L!/[(L-M)!(M-1)!]$. On the other hand, Eq. (6.7) involves the complexity of evaluation of $(L-M)\binom{L}{M}$ one-dimensional integrals (i.e., cardinality of set $T_{L,M+1}$ is equal to $L!/[(L-M-1)!M!]$). In Appendix B, we also derive yet another general expression (see (B.3)) for the MGF of $\text{GSC}(M, L)$ over generalized fading channels.

Table 6.2 compares the computational complexity of Eq. (6.6), Eq. (6.7) and (B.3) in terms of the number of summands (i.e., number of one-dimension integrals) for two different values of L. The computational complexity of (B.3) is identical to that of Eq. (6.6). It is also observed that the use of Eq. (6.6) (or (B.3)) is most attractive for $M \le \lfloor L/2 \rfloor$ while Eq. (6.7) outperforms Eq. (6.6) and (B.3) when $M \ge \lceil L/2 \rceil$. Based on these findings, we suggest the following efficient implementation of $\phi_{\gamma_{\text{gsc}}}(.)$ in generalized fading channels:

$$\phi_{\gamma_{\text{gsc}}}(s) = \begin{cases} \text{Eq. (6)} & \text{if } 1 \le M \le \lfloor L/2 \rfloor \\ \text{Eq. (7)} & \text{if } \lceil L/2 \rceil \le M < L \\ \text{Eq. (11)} & \text{if } M = L \end{cases} \tag{6.12}$$

It should also be pointed out that for the special case of independent and identically distributed (i.i.d) diversity paths, we have $f_{\sigma(k)}(x) = f(x)$, $F_{\sigma(k)}(x) = F(x)$ and $\phi_{\sigma(k)}(s, x) = \phi(s, x)$ for $k = 1, 2, \ldots, L$, and there are $M\binom{L}{M}$ equal terms in the sum of Eq. (6.6). Thus, Eq. (6.6) immediately reduces to

$$\phi_{\gamma_{\text{gsc}}}(s) = M\binom{L}{M}\int_0^\infty e^{-sx} f(x)[F(x)]^{L-M}[\phi(s, x)]^{M-1} dx, \quad 1 \le M \le L \tag{6.13}$$

which is indeed the previous result derived in [[33], Eq. (3)]. From Eq. (6.7), we also get a new expression for the MGF of γ_{gsc} with i.i.d diversity paths:

$$\phi_{\gamma_{\text{gsc}}}(s) = (L - M)\binom{L}{M}\int_0^\infty f(x)[F(x)]^{L-M-1}[\phi(s, x)]^{M} dx, \quad 1 \le M < L \tag{6.14}$$

The application of Eq. (6.12) for outage probability analysis is discussed in Section 6.3. In Section 6.4, Eq. (6.12) is used to facilitate ASEP analysis of both coherent and noncoherent $\text{GSC}(M, L)$ diversity systems over generalized fading channels.

6.3 GSC(M, L) Combiner Output Quality Indicators

In this section we shall derive analytical expressions for computing the outage probability performance of $\text{GSC}(M, L)$ diversity systems as well as the mean and variance of combiner output SNR. A procedure for computing several other higher-order statistics of output SNR is also presented.

6.3.1 Outage Probability

As in the previous cases, the outage probability P_{out} is defined as the probability that the instantaneous output SNR falls below a certain specified threshold SNR γ^*. Thus, the knowledge of the CDF of γ_{gsc} is of interest because the outage probability can be expressed in terms of this metric alone, viz.,

$$P_{\text{out}} = F_{\gamma_{\text{gsc}}}(\gamma^*) \tag{6.15}$$

However, recognizing that only the knowledge of $\phi_{\gamma_{\text{gsc}}}(.)$ is readily available (see Eq. (6.12)), we exploit the Laplace inversion method to compute the the desired CDF, as was explained in Section 4.2.

6.3.2 Higher-Order Statistics of GSC(M, L) Output SNR

If the marginal density of the k-th order statistic ($f_{\gamma_k}(.)$) is available, then one can easily derive several higher-order statistics of γ_{gsc} (such as the mean, variance and other performance measures that are of indication of the shape and dispersion properties of the output SNR). For example, the n-th moment of $\gamma_{\text{gsc}} = \sum_{k=L-M+1}^{L} \gamma_k$ may be evaluated as

$$\Delta_n = E[\gamma_{\text{gsc}}^n] = \sum_{k=L-M+1}^{L} \int_0^\infty x^n f_{\gamma_k}(x)dx, \text{ integer } n \geq 0 \tag{6.16}$$

The marginal density of the k-th order statistic γ_k at x is given by [49]

$$f_{\gamma_k}(x) = \frac{1}{(L-k)!(k-1)!} \begin{vmatrix} + & & + \\ F_1(x) & \dots & F_L(x) \\ \vdots & & \vdots \\ F_1(x) & \dots & F_L(x) \\ f_1(x) & \dots & f_L(x) \\ 1-F_1(x) & \dots & 1-F_L(x) \\ \vdots & & \vdots \\ 1-F_1(x) & \dots & 1-F_L(x) \end{vmatrix} \begin{matrix} \\ \\ \left.\begin{matrix} \\ \\ \end{matrix}\right\} k-1 \text{ rows} \\ \\ \left.\begin{matrix} \\ \\ \end{matrix}\right\} L-k \text{ rows} \end{matrix} \tag{6.17}$$

Combining Eq. (6.17) and Eq. (6.2), the marginal density of γ_k can be expressed neatly as

$$f_{\gamma_k}(x) = \frac{1}{(L-k)!(k-1)!} \sum_{\sigma \in S_L} f_{\sigma(k)}(x) \left[\prod_{i=1}^{k-1} F_{\sigma(i)}(x)\right] \left[\prod_{j=k+1}^{L} [1-F_{\sigma(j)}(x)]\right] \tag{6.18}$$

The above expression can be further simplified into Eq. (6.19) by noting that the actual order in which the subscripts occur in the two bracketed sets of Eq. (6.18) is irrelevant (i.e., all selections of subscripts are invariant in each of the bracketed sets):

$$f_{\gamma_k}(x) = \sum_{\substack{\sigma \in S_L, \sigma(1) < \dots < \sigma(k-1) \\ \sigma(k+1) < \dots < \sigma(L)}} f_{\sigma(k)}(x) \left[\prod_{i=1}^{k-1} F_{\sigma(i)}(x)\right] \left[\prod_{j=k+1}^{L} [1-F_{\sigma(j)}(x)]\right] \tag{6.19}$$

For the special case of i.i.d fading statistics, Eq. (6.19) simplifies into

$$f_{\gamma_k}(x) = k\binom{L}{k} f(x)[F(x)]^{k-1}[1-F(x)]^{L-k} \tag{6.20}$$

which is in agreement with [36].

Substituting Eq. (6.19) into Eq. (6.16), we immediately obtain a simple-to-evaluate yet general expression for the n-th order moment of γ_{gsc} over generalized fading channels, viz.,

$$\Delta_n = \sum_{k=L-M+1}^{L} \sum_{\sigma \in T_{L,L-k+1}} \int_0^{\infty} x^n f_{\sigma(k)}(x) \left[\prod_{i=1}^{k-1} F_{\sigma(i)}(x) \right] \left[\prod_{j=k+1}^{L} [1 - F_{\sigma(j)}(x)] \right] dx \tag{6.21}$$

Now the average SNR can be evaluated as $\bar{\gamma}_{\text{gsc}} = \Delta_1$ using Eq. (6.21). Also the variance of output SNR is given by $\mu_2 = \Delta_2 - (\Delta_1)^2$. More generally, the central moments may be computed via relation

$$\mu_n = E[(\gamma_{\text{gsc}} - \bar{\gamma}_{\text{gsc}})^n] = \sum_{k=0}^{n} \binom{n}{k} \Delta_k (-\Delta_1)^{n-k} \tag{6.22}$$

Several quality indicators of GSC(M, L) combiner output SNR can be readily computed with the aid of Eq. (6.21) and Eq. (6.22). For example, the dispersion of the combiner output SNR about its mean is given by its variance μ_2. The skewness, which is defined as $\nu = \mu_3/(\mu_2^{3/2})$, is a measure of the symmetry of a distribution. For symmetric distributions, $\nu = 0$. If $\nu > 0$, the distribution is skewed to the right.

6.3.3 Computational Results

Results for the outage probability and the mean output SNR statistics are presented in this subsection to illustrate the utility of the analytical expressions derived in the preceding subsections. To perform a comparative study of diversity receiver performance over i.n.d channels, it is plausible to introduce an exponential power decay model because a single parameter $\delta > 0$ can be used to represent the mean SNR imbalances across the diversity paths. Suppose the mean SNR of the *k*-th diversity path is $\bar{\gamma}_k = Ce^{-k\delta}\bar{\gamma}_s$ where $\bar{\gamma}_s$ denotes the average SNR/symbol and the parameter C is chosen such that the constraint $\sum_{k=1}^{L} \bar{\gamma}_k = \bar{\gamma}_s$ is satisfied, solving for C yields

$$\bar{\gamma}_k = \frac{(1 - e^{-\delta})e^{-\delta(k-1)}}{1 - e^{-L\delta}} \bar{\gamma}_s \tag{6.23}$$

The above model has also been widely used in the literature for modeling of multipath intensity profile (MIP) in frequency selective fading channels [19]. Note also that the receiver performance for i.i.d case may be evaluated from the analytical framework for i.n.d case by setting $\delta \to 0$ (i.e., $\delta = 10^{-5}$).

It should be emphasized, however, that the presented mathematical framework and analysis is applicable for not only the exponential decaying profile but for any i.n.d. channel models such as those described in [47] and [48]. The results obtained for mixed fading scenarios assumes more significance by noting that measurements in ultra-wideband (UWB) and UMTS/WCDMA propagation environments have indicated that the each of the resolvable multipaths have different fading statistics. Similarly for millimeter-wave communication systems where antenna arrays are employed, some of the antenna elements may receive line-of-sight signals with varying Rice factors, while others may subject to Rayleigh or Nakagami-m fading because these signals may take completely different (independent) propagation paths before arriving at the receiver.

Figure 6.3 illustrates the outage probability metric plotted as a function of the normalized average SNR/symbol $\bar{\gamma}_s/\gamma^*$ for a $\mathrm{GSC}(M, 5)$ receiver in a mixed fading scenario with exponentially decaying MIP ($\delta = 0.1$). As expected, the relative outage improvement declines with increasing M and thus, the law of diminishing returns prevails. In Figure 6.4, the normalized mean output SNR $\bar{\gamma}_{\mathrm{gsc}}/\bar{\gamma}_s$ is plotted against the diversity order L in i.n.d Nakagami-m channels for two different MIP. Similar analysis can not be found previously in [31]. For a fixed L, the total energy captured increases with increasing values of M, as anticipated. For a fixed value of M, however, the normalized average output SNR declines with increasing L. The rate at which $\bar{\gamma}_{\mathrm{gsc}}/\bar{\gamma}_s$ decreases with increasing L declines as δ increases because an increase in diversity order does not significantly increase the diversity gain and/or the percentage of energy captured at higher δ values.

6.4 ASEP Analysis

The ASEP is obtained by averaging the conditional error probability (CEP) over the PDF of $\mathrm{GSC}(M, L)$ output SNR, viz.,

$$\overline{P_s} = \int_0^{\infty} P_s(\gamma) f_{\gamma_{\text{gsc}}}(\gamma) d\gamma \tag{6.24}$$

Since $f_{\gamma_{\text{gsc}}}(.)$ is not readily available, we apply Parseval's theorem (frequency convolution theorem) to transform the product integral Eq. (6.24) into the frequency domain. Thus, we obtain [40]

$$\overline{P_s} = \frac{1}{2\pi}\int_{-\infty}^{\infty} G_{\gamma}(\omega)\phi_{\gamma_{\text{gsc}}}(-j\omega) d\omega = \frac{1}{\pi}\int_0^{\infty} \Re[G_{\gamma}(\omega)\phi_{\gamma_{\text{gsc}}}(-j\omega)] d\omega \tag{6.25}$$

where $G_{\gamma}(\omega) = \int_0^{\infty} P_s(\gamma) e^{-j\omega\gamma} d\gamma$ can be evaluated in closed-form for a broad range of digital modulation/detection schemes, and they are summarized in [[40], Table 2]. Three examples are provided next to highlight the utility of $\phi_{\gamma_{\text{gsc}}}(.)$ in the ASEP analysis of both coherent and noncoherent $\text{GSC}(M, L)$ receiver structures with nonidentical fading statistics. The expressions for the symbol error probabilities presented in section 4.2 have been applied "as is" for generating the results in this chapter, with Eq. (6.12) being the MGF for the i.n.d. channels.

Figure 6.5 shows the ASEP performance curves for QPSK in conjunction with a coherent $\text{GSC}(M, 5)$ receiver in a mixed-fading environment (which includes Rayleigh, Rician and Nakagami-m fading statistics) and $\delta = 0.1$. It is apparent that $\text{GSC}(4, 5)$ or even $\text{GSC}(3, 5)$ has performance comparable to the MRC receiver. The performance improvement in i.n.d fading also depends on the fading parameter (i.e., amount of fading) for each diversity path in addition to a larger choice of M.

Figure 6.6 illustrates the ABEP performance of BPSK with a coherent $\text{GSC}(3, 5)$ receiver for varying δ values. The relative diversity improvement declines with increasing δ because the channel becomes less dispersive. When δ is small, the inclusion of the third 'strongest' multipath reduces the ABEP appreciably compared to a heavily decayed MIP scenario where most of the signal energy is contained only in the first or second path. We also found that the gap between the curves for $\text{GSC}(3, 5)$ and $\text{GSC}(5, 5)$ gets closer as δ increases. This trend further highlights the benefits of $\text{GSC}(M, L)$ design in practical wireless channels.

Comparison between the performance of coherent and noncoherent $\text{GSC}(3, 5)$

receiver for DQPSK modulation is depicted in Figure 6.7. While the coherent receiver always performs better than noncoherent receiver, the difference in their performances decreases at higher average SNR/bit. In Figure 6.8, the efficacy of $\mathrm{GSC}(M, 6)$ receiver in the UMTS Vehicular A channel model (see Table 6.3) is examined. It is observed that significant performance improvement over classical selection diversity can be realized by combining just a few additional multipaths. In fact, $\mathrm{GSC}(4, 6)$ provides performance almost identical to the MRC receiver. However, increasing M beyond 4 does not significantly improve the ABEP performance of BPSK owing to the large power imbalances across the multipaths.

Finally in Figure 6.9, we investigate the trade-off between the diversity gain and noncoherent combining loss for 4-DPSK in a mixed fading environment. When $\delta = 1.5$, we observe that $\mathrm{GSC}(3, 5)$ provides better performance than post-detection equal-gain combining (EGC) for average SNR/bit less than 19 dB owing to the noncoherent combination loss phenomenon. Comparison between the curves corresponding to $\mathrm{GSC}(1, 5)$ reveals that statistical diversity gain has a stronger influence on the ABEP performance of DQPSK at higher average SNR/bit but the amount of energy captured is more critical at the lower average SNR/bit region.

6.5 GUI as a Simulation Tool - The Integration of all the Mathematical Framework into one

The mathematical framework developed in chapters 4-6 are quite involving. The analysis is comprehensive in the sense that it can provide the GSC receiver performance metrics (outage probability, mean output SNR, symbol error rates) for most of the commonly used modulation schemes, for any of the fading channels (either in i.i.d. or i.n.d. conditions), and for any values of M, L. The parameter specification and the generation of results has been made easier by incorporating all the frameworks in a single Graphical User Interface (GUI).

The user can select the type of receiver ($\mathrm{GSC}(M, L)$ or $T - GSC(\mu, L)$), and choose the type of fading channels and the modulation scheme. The front-end for the GUI has been developed using Microsoft Foundation Classes (MFCs) and has been linked to Matlab, which does all the backend processing. Figure 6.1 is the primary dialog window for

the simulation tool.

Once the receiver and the channel structure has been specified, the user needs to "set the simulation parameters" and further specify the simulation conditions using dialog boxes similar to the one shown in Figure 6.2.

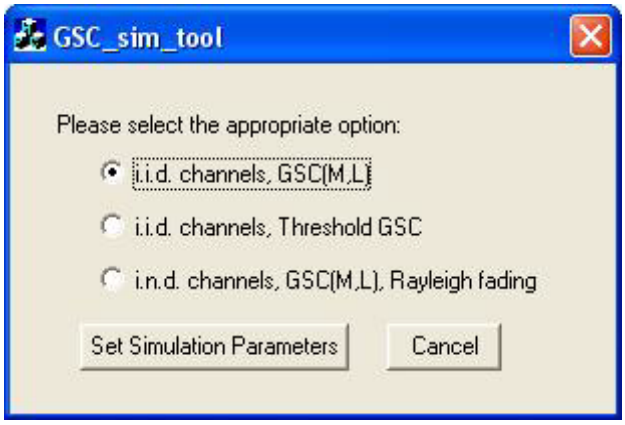

Figure 6.1 Dialog for selecting the receiver structure (GSC or T-GSC) and the fading channel conditions (i.i.d. or i.n.d.).

The simulation tool can therefore be used as a comprehensive aid for performance analysis of GSC receivers in vastly different conditions. It can also serve as a useful teaching tool which can effectively demonstrate the tradeoffs in using sub-optimal GSC receivers.

6.6 Chapter Conclusion

This part of the thesis investigates the performance of both coherent and noncoherent $\mathrm{GSC}(M, L)$ receiver over generalized i.n.d. fading channels. The MGF of γ_{gsc} is used to unify the performance evaluation of different modulation/detection schemes while the outage probability performance is predicted from the CDF expression. Concise analytical formulas for the higher order moments and central moments are also derived. Our mathematical framework can be applied to the design and analysis of several wireless systems of interest such as $\mathrm{GSC}(M, L)$ rake receiver design for wideband CDMA, ultra-wideband communications and $\mathrm{GSC}(M, L)$ antenna array design for use in millimeter-wave indoor wireless communications.

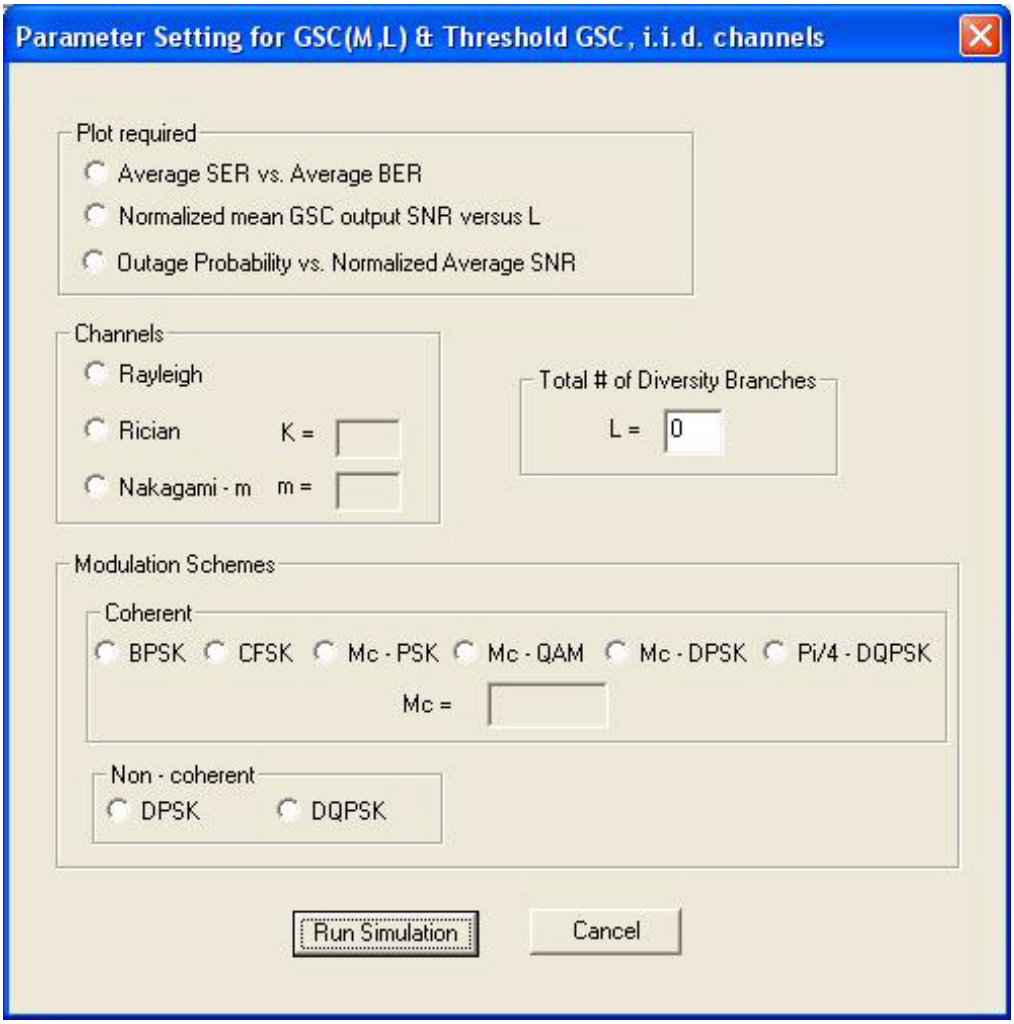

Figure 6.2 Dialog for specifying the channel conditions, modulation schemes and the type of performance metric required.

APPENDIX A

In this appendix, we show (using the principles of mathematical induction) that it is possible to transform two different multivariate nested integrals into a product of univariate integrals. These nested integrals arise in the computation of the MGF of GSC(M, L) output SNR with nonidentical fading statistics.

Define $I_{N-1}(x_M)$ as

$$I_{N-1}(x_M) = \sum_{\sigma \in S_{N-1}} \int_0^{x_N} g_{\sigma(M-1)}(x_{M-1}) \ldots \int_0^{x_3} g_{\sigma(2)}(x_2) \int_0^{x_2} g_{\sigma(1)}(x_1) dx_1 \ldots dx_{M-1}, M \geq 2 \tag{A.1}$$

where $g_{\sigma(k)}(.)$ is an arbitrary statistical function and $G_{\sigma(k)}(y) = \int_0^y g_{\sigma(k)}(x)dx$.

We will prove (using the principles of mathematical induction) that

$$I_{M-1}(x_M) = \prod_{k=1}^{M-1} G_{\sigma(k)}(x_M) \tag{A.2}$$

For $N = 2$, we have

$$I_1(x_2) = \int_0^{x_2} g_{\sigma(1)}(x_1)dx_1 = G_{\sigma(1)}(x_2) \tag{A.3}$$

implying that (A.2) holds for $N = 2$.

For $N = 3$, we obtain (using integration by parts)

$$\begin{aligned} I_2(x_3) &= \int_0^{x_3} g_{\sigma(2)}(x_2) G_{\sigma(1)}(x_2) dx_2 + \int_0^{x_3} g_{\sigma(1)}(x_2) G_{\sigma(2)}(x_2) dx_2 \\ &= 2G_{\sigma(1)}(x_3) G_{\sigma(2)}(x_3) - I_2(x_3) \end{aligned} \tag{A.4}$$

because

$$\int_0^{x_3} g_{\sigma(i)}(x_2) G_{\sigma(j)}(x_2) dx_2 = G_{\sigma(j)}(x_3) G_{\sigma(i)}(x_3) - \int_0^{x_3} G_{\sigma(i)}(x_2) g_{\sigma(j)}(x_2) dx_2 \tag{A.5}$$

Eq. (A.4) implies that (A.2) also holds for $M = 3$.

Assume (A.2) holds for $M = D - 1$. This implies

$$I_{D-2}(x_{D-1}) = \prod_{k=1}^{D-2} G_{\sigma(k)}(x_{D-1}) \tag{A.6}$$

Using the definition of (A.1) and the assumption of (A.6), we can write $I_{D-1}(x_D)$ as

$$
\begin{aligned}
I_{D-1}(x_D) &= \sum_{\substack{\sigma \in S_{D-1} \\ \sigma(1) < \ldots < \sigma(D-2)}} \int_0^{x_D} g_{\sigma(D-1)}(x_{D-1}) I_{D-2}(x_{D-1}) dx_{D-1} \\
&= \sum_{i=1}^{D-1} \int_0^{x_D} g_i(x_{D-1}) \prod_{k=1, k \neq i}^{D-1} G_k(x_{D-1}) dx_{D-1}
\end{aligned}
\tag{A.7}
$$

Applying integration by parts on (A.7), we get

$$
I_{D-1}(x_D) = (D-1) \prod_{k=1}^{D-1} G_{\sigma(k)}(x_D) - (D-2) I_{D-1}(x_D) \tag{A.8}
$$

implying that (A.2) holds for $M = D$. Therefore, by mathematical induction, (A.2) holds for all $M \geq 2$. This completes our proof.

In fact, (A.2) may also be deduced from selection diversity combining (SDC) and MRC analyses with i.n.d fading statistics. Let $f_{\sigma(k)}(.)$ and $F_{\sigma(k)}(.)$ denote the PDF and CDF of SNR of the $\sigma(k)$-th diversity path respectively. If we substitute $g_{\sigma(k)}(x_i) = f_{\sigma(k)}(x_i)$ in (A.1), we have an identical problem formulation for computing the CDF of SDC combiner output SNR with $M-1$ diversity paths. In this case, (A.2) is in agreement with the well-known result for SDC. Alternatively, if we substitute $g_{\sigma(k)}(x_i) = e^{-sx_i} f_{\sigma(k)}(x_i)$ and $x_M = \infty$ in (A.1), the resulting expression resembles the general problem formulation for computing the MGF of MRC output SNR with $M-1$ diversity paths. Once again, the accuracy of (A.2) is validated by comparison with the well-known result for MRC (see Eq. (6.11)).

Using the above approach, we also get another interesting integral identity

$$
\begin{aligned}
J_{M-1}(x_1) &= \sum_{\substack{\sigma \in S_{M-1} \\ N-1}} \int_{x_1}^{\infty} g_{\sigma(2)}(x_2) \int_{x_2}^{\infty} g_{\sigma(3)}(x_3) \ldots \int_{x_{N-1}}^{\infty} g_{\sigma(M)}(x_M) dx_M \ldots dx_2, M \geq 2 \\
&= \prod_{k=1}^{} H_{\sigma(M-k+1)}(x_1)
\end{aligned}
\tag{A.9}
$$

where $H_{\sigma(k)}(y) = \int_y^{\infty} g_{\sigma(k)}(x) dx$.

The accuracy of (A.2) and (A.9) have been validated numerically by letting $g_{\sigma(k)}(.) = f_{\sigma(k)}(.)$. We also found that the product form of $I_{M-1}(x_N)$ and $J_{M-1}(x_1)$ yields a

tremendous improvement in computation efficiency over their multivariate integral counterpart, specifically for large $M \geq 4$ values.

APPENDIX B

Suppose the instantaneous SNRs $\gamma_1, \gamma_2, \ldots, \gamma_L$ are arranged in descending order of magnitude such that $\gamma_{(1)} \geq \gamma_{(2)} \geq \ldots \geq \gamma_{(L)} \geq 0$, the joint PDF of ordered SNRs $[\gamma_{(1)}, \gamma_{(2)}, \ldots, \gamma_{(N)}]$ given in [18, Eq. (6)] can be written concisely as

$$f_{\gamma_{(1)}, \ldots, \gamma_{(M)}}(x_1, \ldots, x_M) = \sum_{\substack{\sigma \in S_L \\ \sigma(M+1) < \ldots < \sigma(L)}} \left[\prod_{k=1}^{M} f_{\sigma(k)}(x_k)\right]\left[\prod_{i=M+1}^{L} F_{\sigma(i)}(x_M)\right], \; 0 \leq x_M < \ldots < x_1 < \infty \qquad \text{(B.1)}$$

Notice that the sum in (B.1) consists of $M!\binom{L}{M}$ terms. Since $\gamma_{\text{gsc}} = \sum_{k=1}^{M} \gamma_{(k)}$, the MGF of $\text{GSC}(M, L)$ output SNR can be evaluated as

$$\begin{aligned}
\phi_{\gamma_{\text{gsc}}}(s) &= \int_{0 \leq x_M < \ldots < x_1 < \infty} \cdots \int e^{-s\sum_{k=1}^{M} x_k} f_{\gamma_{(1)}, \ldots, \gamma_{(M)}}(x_1, \ldots, x_M) dx_1 \ldots dx_M \\
&= \sum_{\substack{\sigma \in S_L \\ \sigma(M+1) < \ldots < \sigma(L)}} \int_0^{\infty} e^{-sx_M} f_{\sigma(M)}(x_M) \left[\prod_{i=M+1}^{L} F_{\sigma(i)}(x_M)\right] \\
&\quad \times \left\{\int_{x_M}^{\infty} e^{-sx_{M-1}} f_{\sigma(M-1)}(x_{M-1}) \ldots \int_{x_2}^{\infty} e^{-sx_1} f_{\sigma(1)}(x_1) dx_1 \ldots dx_{M-1}\right\} dx_M
\end{aligned} \qquad \text{(B.2)}$$

Recognizing that the $(M-1)$-fold multivariate integral in (B.2) can be transformed into a product of $M-1$ univariate integrals using identity (A.9), we immediately get

$$\phi_{\gamma_{\text{gsc}}}(s) = \sum_{\substack{\sigma \in S_L, \sigma(1) < \ldots < \sigma(M-1) \\ \sigma(M+1) < \ldots < \sigma(L)}} \int_0^{\infty} e^{-sx_M} f_{\sigma(M)}(x_M) \left[\prod_{i=M+1}^{L} F_{\sigma(i)}(x_M)\right]\left[\prod_{k=1}^{M-1} \phi_{\sigma(k)}(s, x_M)\right] dx_M \qquad \text{(B.3)}$$

where the marginal MGF $\phi_{\sigma(k)}(s, x_M)$ can be expressed in closed-form for several common fading channel models and they are tabulated in Table 6.1. Clearly, (B.3) is equivalent to Eq. (6.6).

Table 6.1. First-order statistics (PDF, CDF, marginal MGF) of SNR of the *k*-th diversity path for several common fading channel models.

Channel Model	PDF $f_k(x)$, CDF $F_k(x)$ and marginal MGF $\phi_k(s,x) = \int_x^\infty e^{-st} f_k(t)dt$ of SNR of the k-th diversity path
Rayleigh	$f_k(x) = \frac{1}{\bar{\gamma}_k}\exp(-x/\bar{\gamma}_k), x \geq 0$ where $\bar{\gamma}_k = E[x]$ = average SNR/symbol/path $F_k(x) = 1 - \exp(-x/\bar{\gamma}_k), x \geq 0$ $\phi_k(s,x) = \frac{\exp[-x(s+1/\bar{\gamma}_k)]}{1+s\bar{\gamma}_k}, s \geq 0$
Ricean	$f_k(x) = \frac{1+K_k}{\bar{\gamma}_k}\exp\left[-K_k - \frac{(1+K_k)x}{\bar{\gamma}_k}\right] I_0\left[2\sqrt{\frac{K_k(K_k+1)x}{\bar{\gamma}_k}}\right], x \geq 0$ $F_k(x) = 1 - Q\left(\sqrt{2K_k}, \sqrt{\frac{2(K_k+1)x}{\bar{\gamma}_k}}\right), x \geq 0$ where $K_k \geq 0$ is the Rice factor $\phi_k(s,x) = \frac{1+K_k}{s\bar{\gamma}_k + K_k + 1}\exp\left[\frac{-sK_k\bar{\gamma}_k}{s\bar{\gamma}_k + K_k + 1}\right] Q\left(\sqrt{\frac{2K_k(K_k+1)}{s\bar{\gamma}_k + K_k + 1}}, \sqrt{\frac{2(s\bar{\gamma}_k + K_k + 1)x}{\bar{\gamma}_k}}\right), s \geq 0$ where $Q(.,.)$ denotes the first-order Marcum Q-function
Nakagami-m	$f_k(x) = \frac{1}{\Gamma(m_k)}\left(\frac{m_k}{\bar{\gamma}_k}\right)^{m_k} x^{m_k-1}\exp\left(\frac{-m_k x}{\bar{\gamma}_k}\right), x \geq 0$ where $m_k \geq 0.5$ is the fading severity index $F_k(x) = 1 - \frac{\Gamma(m_k, xm_k/\bar{\gamma}_k)}{\Gamma(m_k)} = \frac{\gamma(m_k, xm_k/\bar{\gamma}_k)}{\Gamma(m_k)}, x \geq 0$ $\phi_k(s,x) = \frac{1}{\Gamma(m_k)}\left(\frac{m_k}{m_k + s\bar{\gamma}_k}\right)^{m_k} \Gamma(m_k, xs + xm_k/\bar{\gamma}_k), s \geq 0$ where $\gamma(.,.)$ and $\Gamma(.,.)$ denote the incomplete Gamma function and its complement
Nakagami-q	$f_k(x) = \frac{1}{\bar{\gamma}_k\sqrt{1-b_k^2}}\exp\left(\frac{-x}{(1-b_k^2)\bar{\gamma}_k}\right) I_0\left(\frac{b_k x}{(1-b_k^2)\bar{\gamma}_k}\right), x \geq 0$ where $-1 \leq b_k = \frac{1-q_k^2}{1+q_k^2} \leq 1$ $F_k(x) = I_e[b_k, x(1-b_k^2)\bar{\gamma}_k], x \geq 0$ where $0 \leq q_k \leq \infty$ is the fading severity index $\phi_k(s,x) = \frac{1}{\sqrt{(s\bar{\gamma}_k+1)^2 - (s\bar{\gamma}_k b_k)^2}} - \frac{1}{s(1-b_k^2)\bar{\gamma}_k + 1} I_e\left[\frac{b_k}{s(1-b_k^2)\bar{\gamma}_k + 1}, \frac{x(1-b_k^2)\bar{\gamma}_k}{s(1-b_k^2)\bar{\gamma}_k + 1}\right], s \geq 0$ where $I_e[.,.]$ denotes the Rice's I_e-function

Table 6.2. Comparison of computational complexity between (6.6), (6.7) and (B.3) for evaluating the MGF of GSC(N, L) output SNR over i.n.d generalized fading channels when L = 8 and L = 5. The metric of effectiveness is the number of summation terms (one-dimension integral evaluations).

	Total Number of Summation Terms							
	GSC(1,8)	GSC(2,8)	GSC(3,8)	GSC(4,8)	GSC(5,8)	GSC(6,8)	GSC(7,8)	GSC(8,8)
Eq. (6.6)	8	56	168	280	280	168	56	8
Eq. (6.7)	56	168	280	280	168	56	8	n/a
Eq. (B.3)	8	56	168	280	280	168	56	8

	Total Number of Summation Terms				
	GSC(1,5)	GSC(2,5)	GSC(3,5)	GSC(4,5)	GSC(5,5)
Eq. (6.6)	5	20	30	20	5
Eq. (6.7)	20	30	20	5	n/a
Eq. (B.3)	5	20	30	20	5

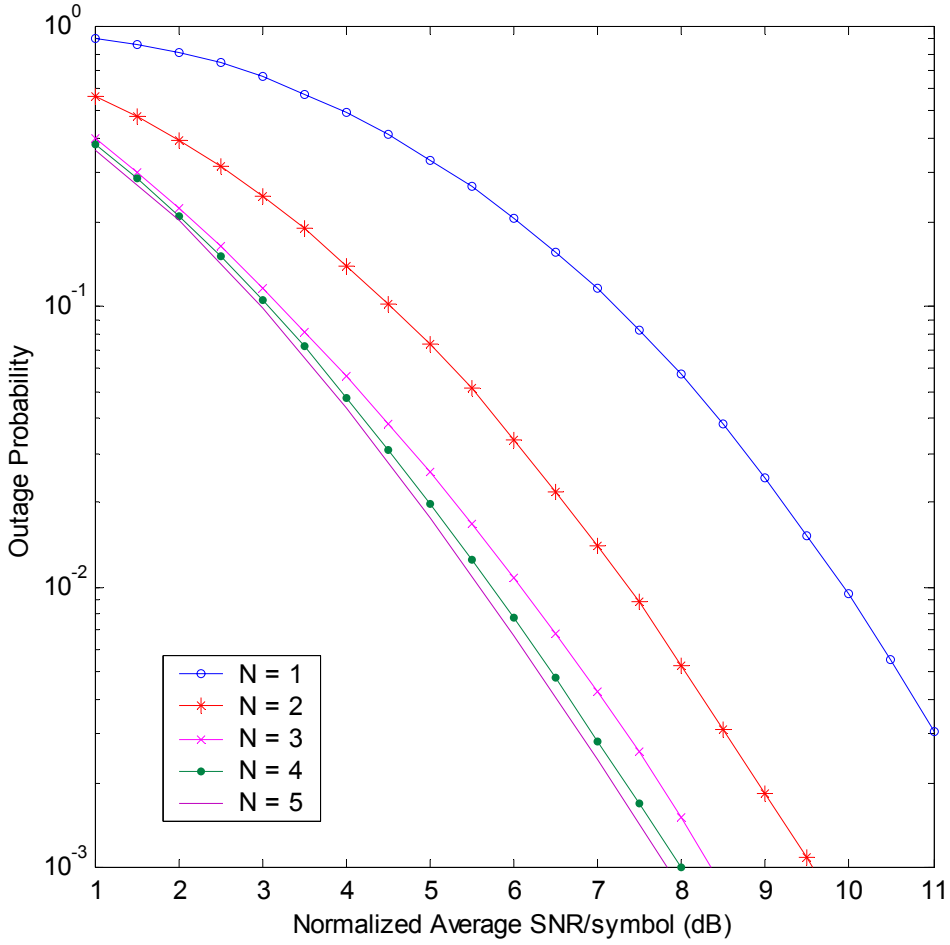

Figure 6.3 Outage probability $F_{\gamma_{gsc}}(\gamma^*)$ versus normalized average SNR/symbol $\bar{\gamma}_s/\gamma^*$ for GSC$(N, 5)$ receiver in a mixed fading $[m_1 = 0.75, m_2 = 1, K_3 = 2.5, K_4 = 1, m_5 = 1]$ and exponentially decaying MIP ($\delta = 0.1$) environment.

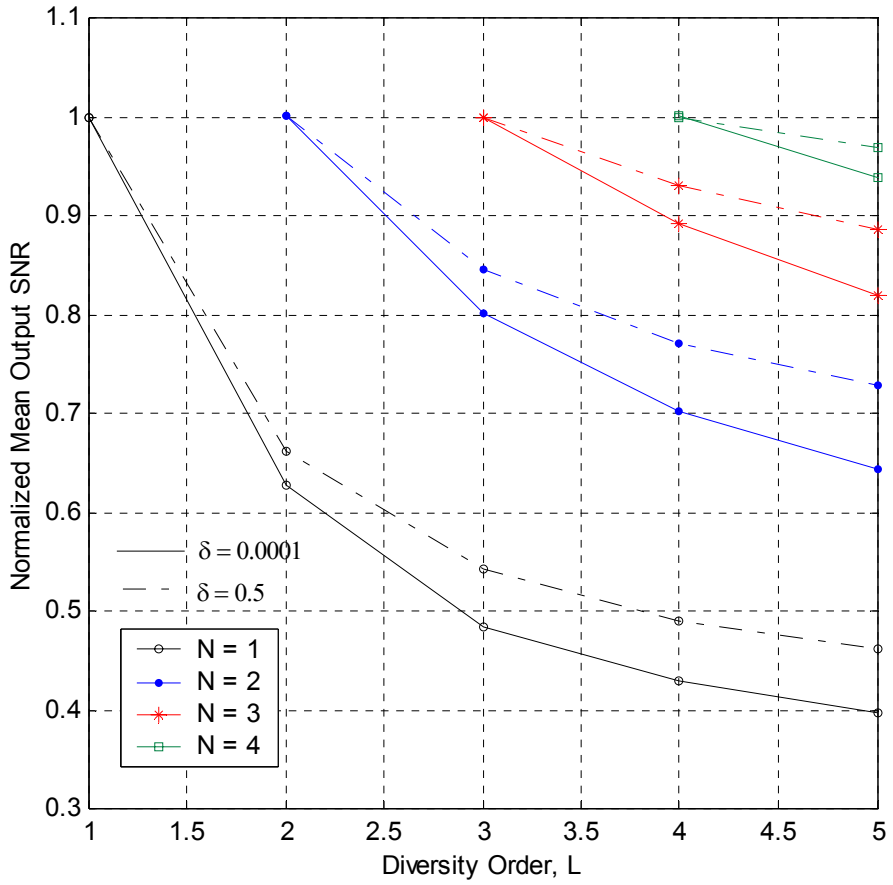

Figure 6.4 Comparison of normalized average $\mathrm{GSC}(N, L)$ output SNR versus diversity order L in i.n.d Nakagami-m channels $[m_1 = 5.5, m_2 = 4, m_3 = 2.5, m_4 = 1, m_5 = 0.75]$ for two different multipath intensity profiles ($\delta \in \{10^{-4}, 0.5\}$).

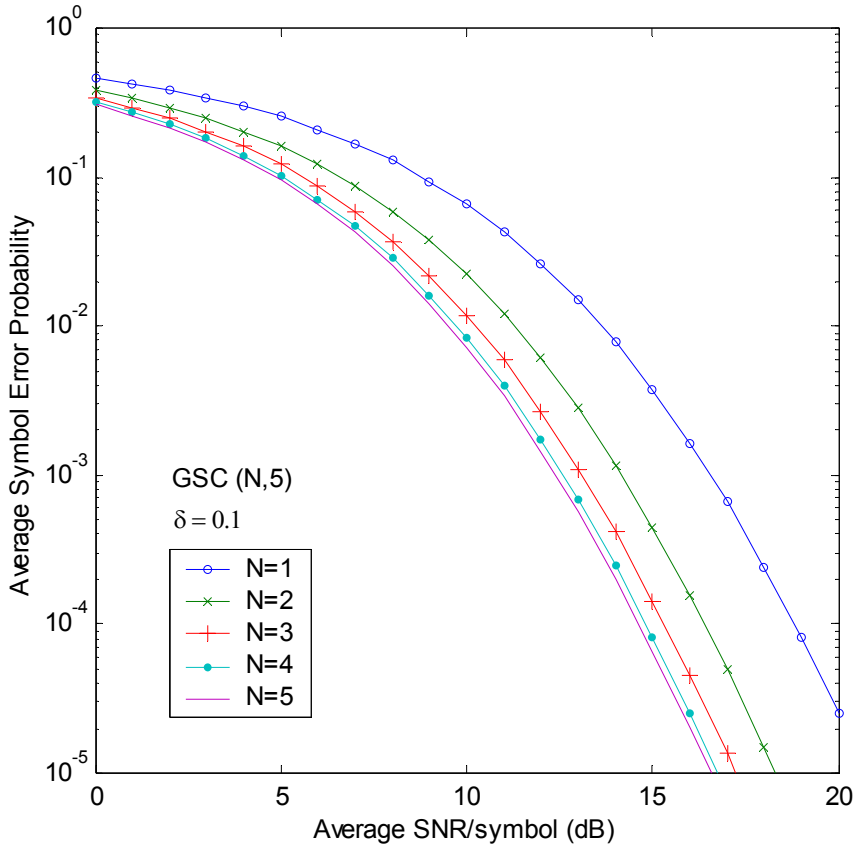

Figure 6.5 ASEP performance curves for QPSK with a coherent $\mathrm{GSC}(N, 5)$ receiver versus average SNR/symbol $\bar{\gamma}_s$ for mixed fading channel conditions $[m_1 = 0.75, m_2 = 3, K_3 = 2.5, K_4 = 1, m_5 = 1]$ and $\delta = 0.1$ (exponentially decaying MIP).

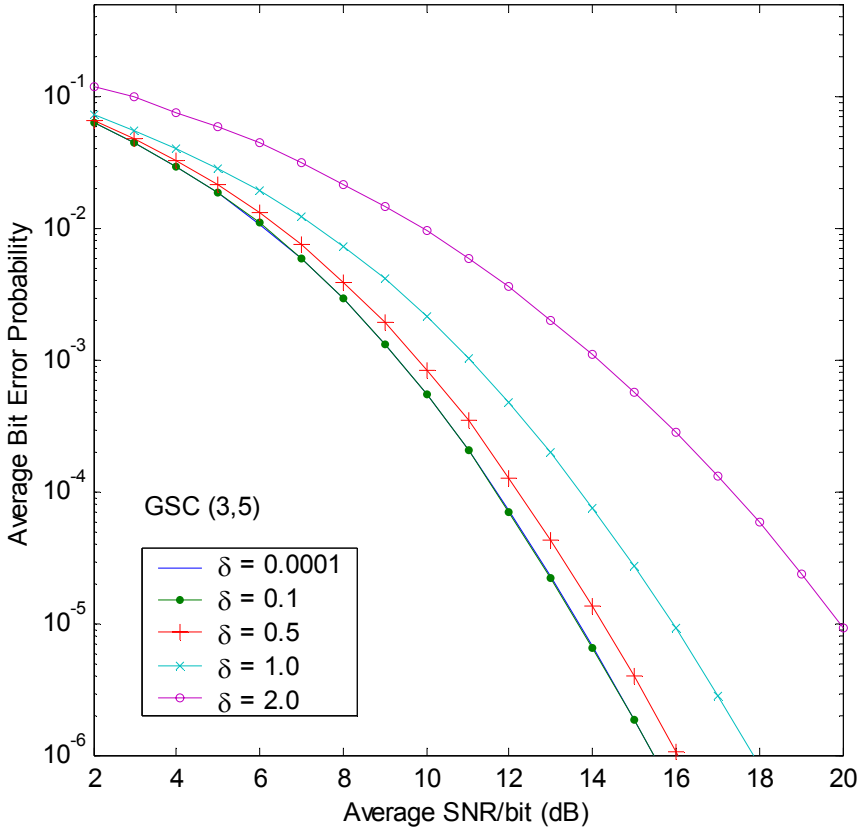

Figure 6.6 ABEP performance of BPSK versus average SNR/symbol for coherent $\mathrm{GSC}(3,5)$ receiver in different multipath intensity profiles. The fading parameters of the resolvable multipath signals are given as $[m_1 = 0.75, m_2 = 3, K_3 = 2.5, K_4 = 1, m_5 = 1]$.

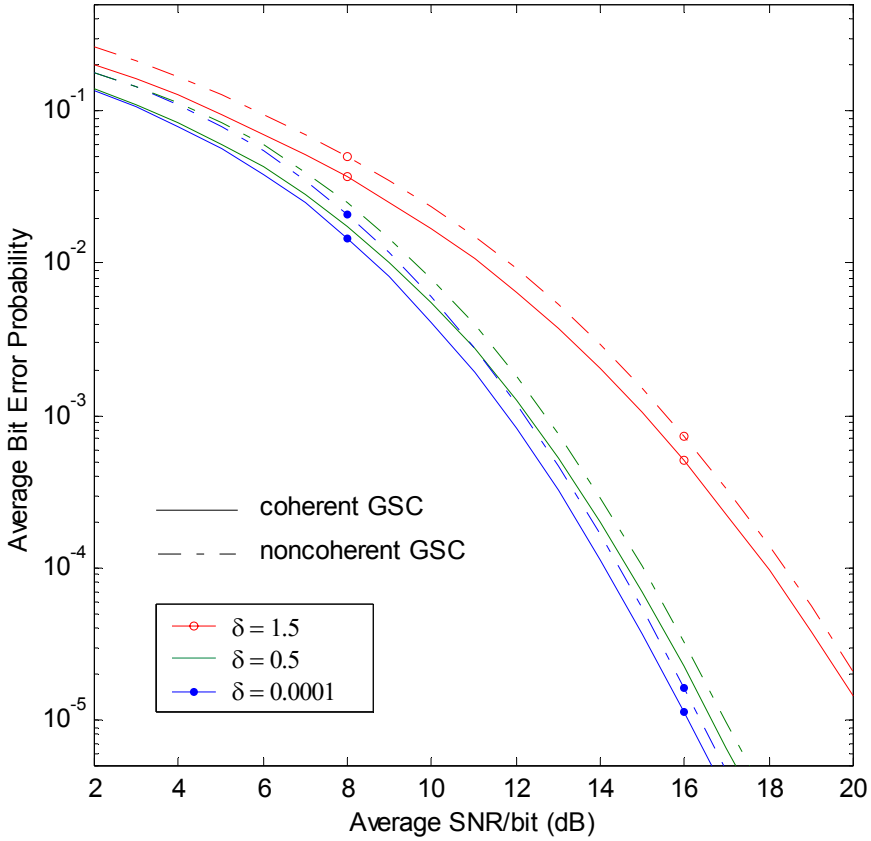

Figure 6.7 Comparison between the ABEP performance of DQPSK that employs either coherent or noncoherent $\mathrm{GSC}(3, 5)$ receiver in a mixed fading propagation environment $[m_1 = 0.75, m_2 = 3, K_3 = 2.5, K_4 = 1, m_5 = 1]$ and for varying δ.

Table 6.3. **UMTS Channel Models.**

Channel	Relative Mean Powers (dB)	Delays (μs)
Office A	0, -10, -30	0, 0.24, 0.485
Pedestrian A	0, -12.5, -25	0, 0.24, 0.485
Vehicular A	0, -1, -9, -10, -15, -20	0, 0.31, 0.71, 1.09, 1.73, 2.51

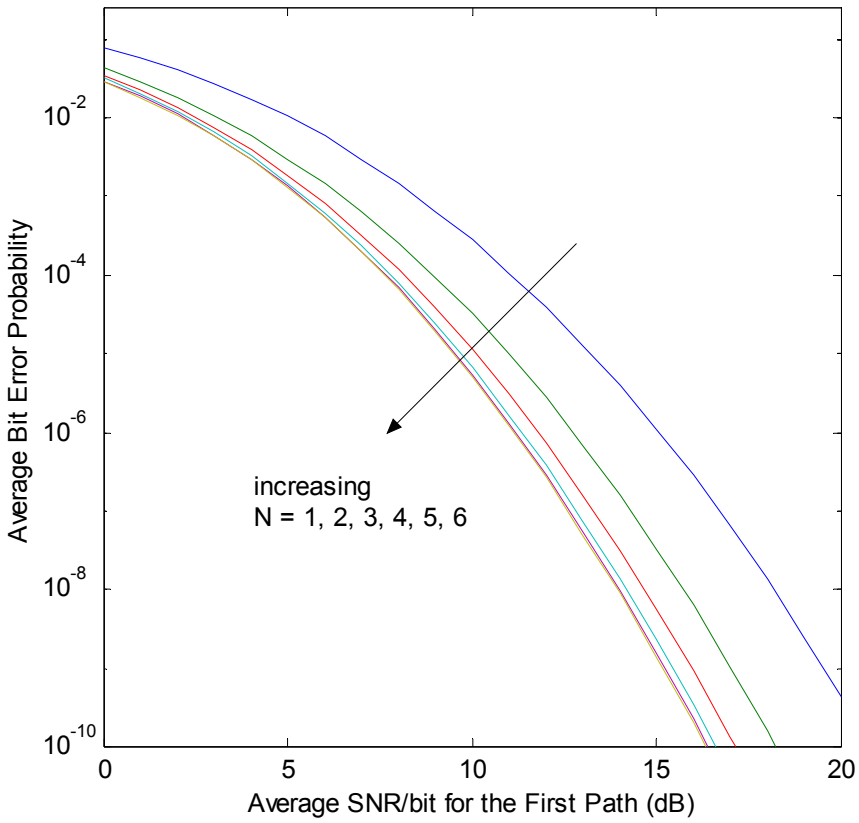

Figure 6.8 ABEP performance of BPSK with a coherent $\mathrm{GSC}(N, 6)$ receiver in a UMTS vehicular A channel model. The fading parameters of the resolvable multipaths are assumed to be $[K_1 = 3, m_2 = 4, m_3 = 3.5, K_4 = 1.5, K_5 = 0, m_6 = 0.6]$.

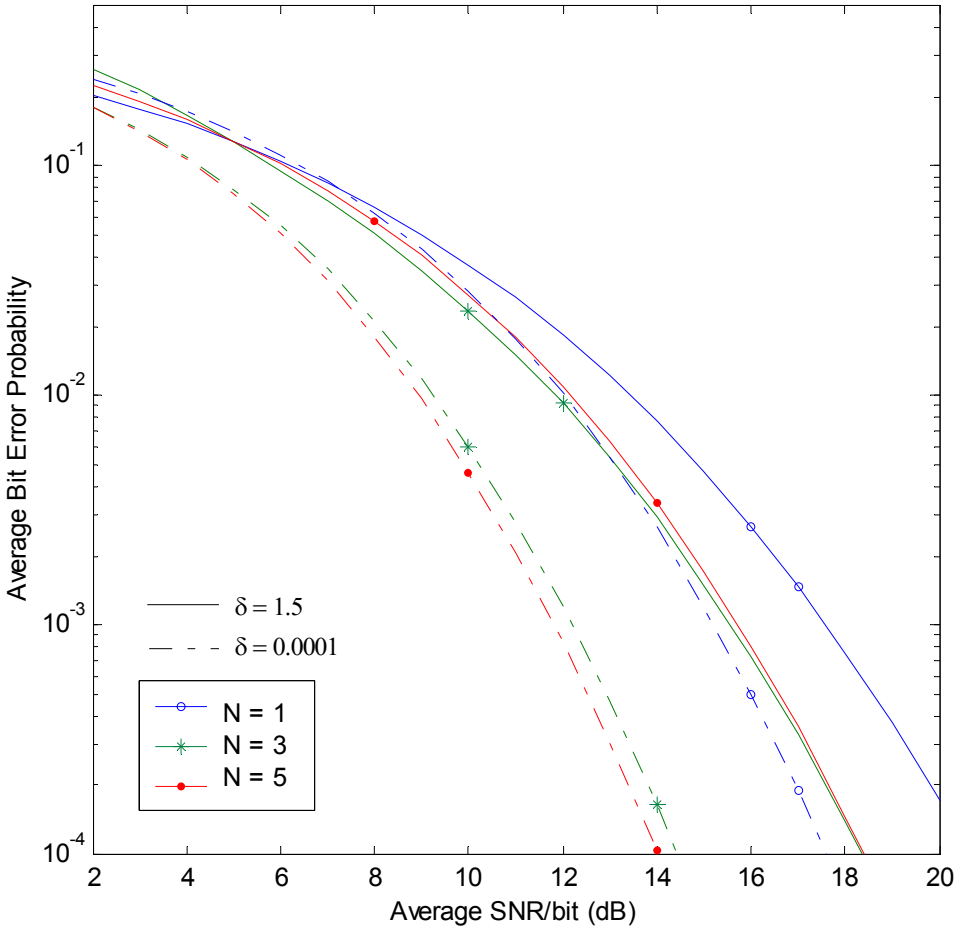

Figure 6.9 Investigation into the trade-off between diversity gain and noncoherent combining loss for DQPSK in conjunction with noncoherent GSC(N, 5) receiver in a generalized fading channel [m_1 = 0.75, m_2 = 3, K_3 = 2.5, K_4 = 1, m_5 = 1].

Chapter 7

Conclusion

7.1 Thesis Summary

In this chapter we present a summary of the work presented in this thesis. The thesis aims at developing simulation tools and new mathematical formulations to aid the design of low-complexity receiver structures for the existing and prospective wireless technologies.

Starting with the detailed description of the small scale and the large scale channel models, the performance of sub-optimal receivers are studied specifically for the SDAR, W-CDMA and UWB technologies. The SDAR simulation tool is capable of predicting the performance of the satellite digital radio receivers on a nationwide scale. The areas susceptible to below-spec performances are easily identifiable and helps the service providers in making important decisions on installment of additional terrestrial repeaters. The results for the performance of a particular practical antenna on a nationwide basis and its effect of the satellite link reliability have been presented in the form of contours over the ConUS. By providing the measured antenna patterns as inputs to the simulation tool, the possibility of using a single antenna for both the satellite signal and the terrestrial repeater signals can easily be explored.

Perhaps the most comprehensive framework for the GSC receiver performances has been developed in the latter chapters of the thesis. A generalized expression for the MGF of the GSC in i.i.d. fading channels has been developed. The computational efficiency of the expression is far greater than any of the results reported before. The MGF expression is used to evaluate the receiver performances and analyze many of the important receiver metrics such as the outage probability, error probability curves and the mean output SNR. Illustrative results for the outage probability in Rician fading channels, which have hitherto resisted a solution, have been provided. The tradeoffs of higher alphabet modulation

schemes and lower number of combiner branches on the receiver performance has been evaluated.

The performance of both coherent and noncoherent receivers has been studied with various modulation schemes and under various fading channels. The performance with selection combining and MRC encompasses all the sub-optimal receiver performances as expected. The general trend of declining relative performance improvement with higher order diversities is observed. The comparison of the error performances of coherent and noncoherent $\pi/4$-DQPSK receivers reveals the ABER performances with noncoherent GSC asymptotically approaches the ABER performance with coherent GSC receivers for a fixed M value. The mean output SNR results indicate a typical trend of selection diversity systems, viz. the rate at which the normalized mean output SNR increases declines gradually as $(L - M)$ increases.

Developing on the GSC receiver analysis, the results for the Threshold GSC (T-GSC) receivers in i.i.d. channels have been presented. Expressions for the MGF of the T-GSC receivers have been developed using two different methods. The threshold factor μ dynamically decides the number of branches to be combined at the combiner depending on the channel conditions. The special cases of $\mu = 0$ and $\mu = 1$ correspond to maximum ratio and selection combining schemes. Plots for the selection diversity probability indicate the movement of the probability curves with varying channel conditions. As the channel improves (less fading), the probability of selecting higher number of branches for combining increases. The effect of the selection diversity probability and the comparison of the mean SNR curves for GSC and T-GSC receivers are particularly interesting.

The analysis of GSC receivers in the more realistic i.n.d. channel conditions is the last topic presented in this thesis. The analysis follows a new approach of using permanents and develops MGF expressions for GSC receivers in most commonly used i.n.d. fading channels. Two separate forms have been developed for the MGF, each of which is efficient only for a selected value of M. The value of the selection diversity M thus dictates the choice of the formula to be used to obtain maximum computational efficiency. Results are presented using the exponential decaying profile to model the SNR of the non-identical branches and with non-identical (and mixed) fading scenarios. Results obtained for the case of the Vehicular A UMTS model indicates that combining only 3 branches out of 6 available branches yields performance close to that obtained for the MRC case. Results for noncoherent GSC in i.n.d. channels show that increasing the

diversity beyond a point need not necessarily improve the error performances at lower SNRs.

7.2 Suggestions for Further Work

This section presents some suggestions for extending the scope of the work presented in this thesis.

The simulation tool for SDAR currently presents only the primary statistics like the reliability of the link margin based on the large-scale propagation model. The tool can be enhanced to include the secondary statistics such as the level crossing rate and the average fade duration of the channel. It can also be possible to generate a contour for the BERs and the frame error rates if the mapping between the SNR and the BER is provided from the field measurements. The tool can be further used as a front end for presenting several performance metrics such as the audio quality which may be obtained by post-processing the output of an actual SDAR receiver.

Though the GSC scheme analysis in this thesis is pretty comprehensive, the work on GSC can also be extended in a number of research areas. Primarily, the framework needs to be extended to analyze the GSC receiver performance in correlated channel conditions. The performance of T-GSC receivers in i.n.d channels also needs to be explored. The effect of using GSC receivers on the system capacity in systems like CDMA can be studied.

Bibliography

[1] "Revision of Part 15 of FCC's rules regarding UWB transmission systems", available at www.uwb.org, April 22, 2002.

[2] T. Rappaport, *Wireless Communications,* Prentics Hall, 1999.

[3] M.T. Feeney, J. D. Parsons, "Cross-correlation between 900 MHz Signals Received on Vertically Separated Antennas in Small-Cell Mobile Radio Systems", *Communications, Speech and Vision, IEE Proceedings I* , Volume: 138 Issue: 2, April 1991.

[4] A. Turkmani, S. Mockford, J. D. Parsons, "Antenna Diversity for Mobile Radio Reception in Rural Areas", *Second International Conference on Rural Communciations*, 1990, pp: 105-110.

[5] H. Suzuki, "A Statistical Model for Urban Radio Propagation" *IEEE Transactions on Communciations,* Vol. 27, July 1977, pp.673-680.

[6] W. R. Braun and U. Dersch, "A Physical Mobile Radio Channel Model" *IEEE Transactions on Vehicular Technology*, Vol. 40, Feb. 1991, pp. 472-482.

[7] M. Nakagami, "The m-distribution - A General Formula of Intensity Distribution of Rapid Fading" *Statistical Methods of Radio Wave Propagation*, Pergamon, 1960, pp. 3-36.

[8] E. Lutz, M. Dippold, F. Dolainsky, W. Papke, "The Land Mobile Satellite Communication Channel - Recording, Statistics, and Channel Model" *IEEE Transactions on Vehicular Technology*, Vol. 40, No. 2, May 1991.

[9] T. Pratt and C. Bostian, *Satellite Communications*, John Wiley, 1986.

[10] S. J. Patsiokas, "XM satelite Radio Technology Fundamentals," *SAE 2001 World Congress*, Detroit, Michgan, 2001.

[11] R. Marino, A. Fuchs, "Dual Antenna System for Mobile SDARS Application," *SAE 2001 World Congress*, Detroit, Michgan, 2001.

[12] A. Petros, S. Licul, "Folded quadrifilar helix antenna," Antennas and Propagation Society*, IEEE International Symposium* , Vol. 4 , pp. 569-572, 2001

[13] N. Haller, "Mobile Antennas for reception of S-DARS," Antennas and Propagation Society, *IEEE International Symposium*, Vol. 1, pp. 426-429, 2001.

[14] D. Layer, "Digital Radio Takes to the Road," *IEEE Spectrum*, pp. 40-46, July 2001.

[15] www.xmradio.com, official website for XM satellite audio radio service.

[16] www.crl.go.jp/ka/control/efsat/index-e.html, website for the Communications Research Laboratory, Japan.

[17] CCIR, Report 925-1, "Factors Affecting the Choice of Antennas for Mobile Stations of the Land Mobile-Satellite Service," Recommendations and report of the CCIR, 1986, vol. VIII-3, CCIR, Geneva, Int. Telecomm. Union, 1986.

[18] N. Kong, T. Eng and L. B. Milstein, "A Selection Combining Scheme for RAKE Receivers," *Proc. 1995 Fourth IEEE International Conference on Universal Personal Communications*, pp. 426 -430.

[19] T. Eng, N. Kong and L. B. Milstein, "Comparison of Diversity Combining Techniques for Rayleigh Fading Channels," *IEEE Transactions on Communications*, Vol. 44, No. 9, pp. 1117-1129, Sept. 1996.

[20] K. J. Kim, S. Y. Kwon, E. K. Hong and K. C. Whang, "Comments on Comparison of Diversity Combining Techniques for Rayleigh Fading Channels" *IEEE Transactions on Communications*, Vol. 46, No. 9, pp. 1109-1110, Sept. 1998.

[21] T. Eng, N. Kong and L. B. Milstein, Correction to "Comparison of Diversity Combining Techniques for Rayleigh-Fading Channels," *IEEE Transactions on Communications*, Vol. 46, No. 9, pp. 1111, Sept. 1998.

[22] N. Kong and L. B. Milstein, "Average SNR of a Generalized Diversity Selection Combining Scheme," *IEEE Communications Letters*, Vol. 3, No. 3, pp. 57 -59, Mar. 1999.

[23] N. Kong and L. B. Milstein, "SNR of Generalized Diversity Selection Combining with Nonidentical Rayleigh Fading Statistics," *IEEE Transactions on Communications*, Vol. 48, pp. 1266 -1271, Aug. 2000.

[24] M. Win and J. Winters, "Analysis of Hybrid Selection/Maximal-Ratio Combining in Rayleigh Fading," *IEEE Transactions on Communications*, Vol. 47, pp. 1773-1776, Dec. 1999.

[25] M.-S. Alouini and M. K. Simon, "An MGF-Based Performance Analysis of Generalized Selection Combining over Rayleigh Fading Channels," *IEEE Transactions on Communications*, Vol. 48, pp. 401-414, Mar. 2000.

[26] A. Annamalai and C. Tellambura, "The Effects of Gaussian Weighting Errors in Hybrid SC/MRC Receivers," *Proc. IEEE Wireless Communications and Networking Conference*, pp. 211-215, Sept. 2000 (will also appear in the *IEEE Transactions on Wireless Communications*, 2002).

[27] R. Wong, A. Annamalai and V. K. Bhargava, "Evaluation of Predetection Diversity Techniques for Rake Receivers," *IEEE PACRIM'97*, pp. 227-230, Aug. 1997.

[28] M. Alouini and M. Simon, "Performance of Coherent Receivers with Hybrid SC/ MRC over Nakagami-m Fading Channels," *IEEE Transactions on Vehicular Technology*, Vol. 48, pp. 1155-1164, July 1999.

[29] M. Alouini and M. Simon, "Application of the Dirichlet Transformation to the Performance Evaluation of Generalized Selection Combining over Nakagami-m Fading Channels," *Journal of Communications and Networks*, Vol. 1, pp. 5-13, Mar. 1999.

[30] A. Annamalai and C. Tellambura, "Error Rates of Hybrid SC/MRC Diversity Systems on Nakagami-m Channels," *Proc. IEEE Wireless Communications and Networking Conference*, pp. 227-231, Sept. 2000.

[31] Y. Ma and C. Chai, "Unified Error Probability Analysis for Generalized Selection Combining in Nakagami Fading Channels," *IEEE J. Selected Areas Commun.*, Vol. 18, pp. 2198-2210, Nov. 2000.

[32] A. Annamalai and C. Tellambura, "Performance Evaluation of Generalized Selection Diversity Systems over Nakagami-m Fading Channels," to appear in the *International Journal on Wireless Communications and Mobile Computing*, Wiley, 2002.

[33] A. Annamalai and C. Tellambura, "A New Approach to Performance Evaluation of Generalized Selection Diversity Receivers in Wireless Channels," *Proc. IEEE Vehicular Technology Conference*, Oct. 2001, pp. 2309-2313.

[34] S. Stein, "Fading Channel Issues in System Engineering," *IEEE J. Selected Areas Commun.*, pp. 68-69, February 1987.

[35] M. Nakagami, "The m-distribution - A General Formula of Intensity Distribution of Rapid Fading" in *Statistical Methods of Radio wave Propagation*, Pergamon, 1960, pp. 3-36.

[36] A. Papoulis, Probability, Random Variables and Stochastic Processes, McGraw-Hill, New York: 1991.

[37] N. Beaulieu, "An Infinite Series for the Computation of the Complementary Probability Distribution Function of a Sum of Independent Random Variables and Its Application to the Sum of Rayleigh Random Variables," *IEEE Transactions on Communications*, Vol. 38, Sept. 1990, pp. 1463-1474.

[38] J. Abate, W. Whitt "Numerical Inversion of Laplace Transforms of Probability Distribution" *ORSA Journal in Computing*, Vol. 7, no. 1 1995, pp. 36-43.

[39] A. Annamalai, G. Deora and C. Tellambura, "Unified Error Probability Analysis for Generalized Selection Diversity in Rician Fading Channels," *Proc. IEEE Vehicular Technology Conference*, May 2002, pp. 2042-2046.

[40] A. Annamalai, C. Tellambura and V. K. Bhargava, "A General Method for Calculating Error Probabilities over Fading Channels," *Proc. IEEE International Conference on Communications* (Communications Theory Mini-conference), pp. 36-40, June 2000.

[41] A. Annamalai and C. Tellambura, "An MGF-Derivative Based Unified Analysis of Incoherent Diversity Reception of M-ary Orthogonal Signals in Independent and Correlated Fading Channels," provisionally accepted for publication in the *IEEE Transactions on Communications.*

[42] A. Annamalai, G. Deora and C. Tellambura, "Unified Error Probability Analysis for Generalized Selection Diversity Systems in Wireless Channels," provisionally accepted for publication in the *IEEE Transactions on Wireless Communications*.

[43] A. Annamalai and C. Tellambura, "Error Rates for Nakagami-m Fading Multichannel Reception of Binary and M-ary Signals," *IEEE Transactions on Communications*, Vol. 49, pp. 58-68, Jan. 2001.

[44] I. Sulyman and M. Kousa, "Bit Error Probability of a Generalized Selection Diversity Combining Scheme in Nakagami Fading Channels," *Proc. IEEE WCNC'00*, pp. 1080-1085.

[45] M. Simon and M.-S. Alouini, "Performance Analysis of Generalized Selection Combining with Threshold Test per Branch (T-GSC), *Proc. IEEE GLOBECOM'01*, pp. 1176-1181.

[46] H. A. David, Order Statistics, Wiley publications, New York: 1981.

[47] D. Cassioli, M. Win and A. Molisch, "A Statistical Model for the UWB Indoor Channel," *Proc. IEEE Vehicular Technology Conference*, May 2001, pp. 1159-1163.

[48] M. Sandell, "Analytical Analysis of Transmit Diversity in WCDMA on Fading Multipath Channels, *Proc. International Symposium on Personal, Indoor and Mobile Radio Communications*, 1999, pp. 1-5.

[49] R. Vaughan and W. Venables, "Permanent Expressions for Order Statistic Densities," *Royal Statistical Society Journal*, Vol. 34, No. 2, pp. 308–310, 1972.

[50] H. Minc, "Theory of permanents," *Linear and Multilinear Algebra*, Vol. 21, No. 2, pp. 109–148, 1987.

Vita

Gautam K. Deora was born in Bombay, India on August 8, 1979. He received his B. Eng. Degree (with distinction) in Electronics from Bombay University in 2000 and subsequently joined the Electrical and Computer engineering program at Virginia Polytechnic and State University starting Fall 2000.

Gautam has been a Graduate Research Assistant with the Mobile and Portable Radio Research Group (M.P.R.G.) at Virginia tech. from May 2001-July 2002 where he worked on simulation tools and mathematical model designs for low-complexity sub-optimal receivers for Satellite digital radio, CDMA and UWB technologies. Since July 2002, he has been working at Center for Remote Sensing, Fairfax, Va. on algorithm development for GPS related technologies.